

ACTA

UNIVERSITATIS OULUENSIS

Honglei Miao

CHANNEL ESTIMATION AND POSITIONING FOR MULTIPLE ANTENNA SYSTEMS

FACULTY OF TECHNOLOGY,
DEPARTMENT OF ELECTRICAL AND INFORMATION ENGINEERING,
UNIVERSITY OF OULU

C
TECHNICA



ACTA UNIVERSITATIS OULUENSIS
C Technica 270

HONGLEI MIAO

**CHANNEL ESTIMATION AND
POSITIONING FOR MULTIPLE
ANTENNA SYSTEMS**

Academic dissertation to be presented, with the assent of
the Faculty of Technology of the University of Oulu, for
public defence in Raahensali (Auditorium L10), Linnanmaa,
on May 15th, 2007, at 12 noon

OULUN YLIOPISTO, OULU 2007

Copyright © 2007
Acta Univ. Oul. C 270, 2007

Supervised by
Professor Markku Juntti

Reviewed by
Professor Markku Renfors
Professor A. Lee Swindlehurst

ISBN 978-951-42-8410-6 (Paperback)
ISBN 978-951-42-8411-3 (PDF)
<http://herkules.oulu.fi/isbn9789514284113/>
ISSN 0355-3213 (Printed)
ISSN 1796-2226 (Online)
<http://herkules.oulu.fi/issn03553213/>

Cover design
Raimo Ahonen

OULU UNIVERSITY PRESS
OULU 2007

Miao, Honglei, Channel estimation and positioning for multiple antenna systems

Faculty of Technology, University of Oulu, P.O.Box 4000, FI-90014 University of Oulu, Finland,
Department of Electrical and Information Engineering, University of Oulu, P.O.Box 4500, FI-90014 University of Oulu, Finland

Acta Univ. Oul. C 270, 2007

Oulu, Finland

Abstract

The multiple-input multiple-output (MIMO) technique, applying several transmit and receive antennas in wireless communications, has emerged as one of the most prominent technical breakthroughs of the last decade. Wideband MIMO parameter estimation and its applications to the MIMO orthogonal frequency division multiplexing (MIMO-OFDM) channel estimation and mobile positioning are studied in this thesis.

Two practical MIMO channel models, i.e., correlated-receive independent-transmit channel and correlated-transmit-receive channel, and associated space-time parameter estimation algorithms are considered. Thanks to the specified structure of the proposed training signals for multiple transmit antennas, the iterative quadrature maximum likelihood (IQML) algorithm is applied to estimate the time delay and spatial signature for the correlated-receive independent-transmit MIMO channels. For the correlated-transmit-receive MIMO channels, the spatial signature matrix corresponding to a time delay can be further decomposed in such a way that the angle of arrival (AOA) and the angle of departure (AOD) can be estimated simultaneously by the 2-D unitary ESPRIT algorithm. Therefore, the combination of the IQML algorithm and the 2-D unitary ESPRIT algorithm provides a novel solution to jointly estimate the time delay, the AOA and the AOD for the correlated-transmit-receive MIMO channels. It is demonstrated from the numerical examples that the proposed algorithms can obtain good performance at a reasonable cost.

Considering the correlated-receive independent-transmit MIMO channels, channel coefficient estimation for the MIMO-OFDM system is studied. Based on the parameters of the correlated-receive independent-transmit MIMO channels, the channel statistics in terms of the correlation matrix are developed. By virtue of the derived channel statistics, a joint spatial-temporal (JST) filtering based MMSE channel estimator is proposed which takes full advantage of the channel correlation properties. The mean square error (MSE) of the proposed channel estimator is analyzed, and its performance is also demonstrated by Monte Carlo computer simulations. It is shown that the proposed JST minimum mean square error (MMSE) channel estimator outperforms the more conventional temporal MMSE channel estimator in terms of the MSE when the signals in the receive antenna array elements are significantly correlated. The closed form bit error probability of the space-time block coded OFDM system with correlation at the receiver is also developed by taking the channel estimation errors and channel statistics, i.e., correlation at the receiver, into account.

Mobile positioning in the non-line of sight (NLOS) scenarios is studied. With the knowledge of the time delay, the AOA and the AOD associated with each NLOS propagation path, a novel geometric approach is proposed to calculate the MS's position by only exploiting two NLOS paths. On top of this, the least squares and the maximum likelihood (ML) algorithms are developed to utilize multiple NLOS paths to improve the positioning accuracy. Moreover, the ML algorithm is able to estimate the scatterers' positions as well as those of the MSs. The Cramer-Rao lower bound related to the position estimation in the NLOS scenarios is derived. It is shown both analytically and through computer simulations that the proposed algorithms are able to estimate the mobile position only by employing the NLOS paths.

Keywords: channel estimation, MIMO-OFDM, mobile positioning, NLOS, parameter estimation

Dedicated to my mother and my wife

Preface

The research related to this thesis has been carried out mostly at the Centre for Wireless Communications (CWC) of the University of Oulu, Finland. I joined the CWC in August 2002 to start my postgraduate studies after I had worked for three years in China Academy of Telecommunication Technology (CATT), Beijing, China. I wish to thank the Director of the CWC at the time of my arrival, Professor Matti Latva-aho, for giving me an opportunity to work in such a joyful and inspiring research unit. My deepest gratitude goes to my advisor, Professor Markku Juntti, without whose instruction this thesis would have not been completed. In particular, I wish to thank him for his constant encouragement and supervision during the whole year of my thesis writing period at Elektrobit and Nokia. His high research standards and technical precision will always remain in my professional life.

Most of the work presented in the thesis was conducted in the Future Radio Access (FUTURA) project. I would like to thank Professor Jari Ilnatti for his instruction in the project work. I wish to express my gratitude to my colleague Dr. Kegen Yu, the cooperation and joint work with him has proven to be very efficient and fruitful. Specifically, the positioning related research in Chapter 5 is the outcome of discussions with him. I wish to thank the reviewers of the thesis, Professor A. Lee Swindlehurst from Brigham Young University, Provo, UT, USA, and Professor Markku Renfors from Tampere University of Technology, Tampere, Finland for their insightful comments. I am also grateful to Gordon Roberts for proofreading the manuscript.

I am fortunate to work at the CWC, and would like to thank numerous members of the CWC for creating such friendly and challenging environments to pursue research. My appreciation goes to Dr. Zexian Li, Dr. Yi Wu, Mr. Marian Codreanu, Mr. Mikko Vehkaperä, Mr. Juha Karjalainen, Professor Tadashi Matsumoto, Dr. Djordje Tujkovic, Dr. Nenad Veselinovic, Mr. Jari Ylioinas, Mr. Antti Tolli, and Dr. Kari Hooli for all the lively discussions throughout my postgraduate studies at the CWC. The administrative support of Hanna Saarella, Timo Äikas, Laila Kuhalampi, Elina Kukkonen and the computer support of Jari Silanpää are gratefully acknowledged.

The financial support provided by the Academy of Finland, Elektrobit, Ltd., In-

strumentointi, Nokia, the Finnish Defense Force, the National Technology Agency of Finland as well as the Nokia Foundation enabled this work and is thus gratefully acknowledged.

I owe my deepest thanks to my friends Shufeng Zheng and Yang Qu with whom I shared unforgettable moments during my stay in Oulu. They have helped me a lot both in my profession and life itself. I am also grateful to Miao Luo, Jing Chai, Man Gu, Yi Zheng and Fei Wang for all the nice moments we have shared.

Finally, I wish to thank my mother Lanyi for all the love and support she gave me throughout my life and hard years of study. Her positive attitude towards education has been an important driving force for my later studies. Without her encouragement, it would not have been possible to start the doctoral study abroad and complete the thesis.

Most importantly, my warmest gratitude belongs to my wife Lili for all the sincere love, support and understanding she had for me throughout all these years. My gratitude to her is also for putting up with thousands of hours I spent on writing the thesis and frequently broadening my horizon beyond the scope of the thesis.

Espoo, March 10, 2007

Honglei Miao

Symbols and abbreviations

$a_{\text{T}}(\cdot)$	transmit antenna pattern
$a_{\text{R}}(\cdot)$	receive antenna pattern
$\mathbf{a}(\theta)$	array response vector (steering vector)
$\mathbf{a}_{\theta_i,j}$	receive antenna array response vector for the j th path in the i th cluster
$\mathbf{a}_{\phi_i,j}$	transmit antenna array response vector for the j th path in the i th cluster
\mathbf{A}_i	spatial signature matrix associated with the i th transmit antenna ($d_i \times N_{\text{R}}$)
$\mathbf{A}[n]$	spatial signature matrix associated with all the transmit antennas during the n transmit block ($d \times N_{\text{R}}$)
$\mathbf{A}_{\theta,i}$	receive antenna array response matrix corresponding to the i th cluster
$\dot{\mathbf{A}}_{\theta,i}$	matrix consisting of the first m rows of $\mathbf{A}_{\theta,i}$
$\ddot{\mathbf{A}}_{\theta,i}$	matrix consisting of the first $N_{\text{R}} - m$ rows of $\mathbf{A}_{\theta,i}$
$\mathbf{A}_{\phi,i}$	transmit antenna array response matrix corresponding to the i th cluster
$\mathcal{A}_i[n]$	spatial signature matrix associated with the i th cluster consisting of l_i paths ($N_{\text{T}} \times N_{\text{R}}$) during the n th block
$\mathcal{A}_i^j[n]$	matrix constructed from the j th column to the $N_{\text{R}} - m + j$ column of $\mathcal{A}[n]$
$\mathcal{A}[n]$	spatial signature matrix associated with all the clusters during the n transmit block ($N_{\text{T}}d \times N_{\text{R}}$)
$\mathbf{b}[k]$	the first row of $\mathbf{B}[k]$
b_i	the intercept of the i th possible region
$\mathbf{B}[k]$	Alamouti codes transmitted at the k th sub-carrier in two successive OFDM symbols
c	the speed of the wave
$\mathbf{c}_i[n]$	symbol sequence transmitted during the n OFDM symbol

$\mathbf{C}_i[n]$	diagonal matrix with the diagonal of $\mathbf{c}_i[n]$ at time n , ($K \times K$)
$\mathbf{C}[n]$	concatenation of all the diagonal matrix $\mathbf{C}_i[n]$, ($K \times N_T K$)
$\mathcal{C}[n]$	partial FFT transformed version of the concatenation matrix $\mathbf{C}[n]$, ($K \times LN_T$)
\mathcal{C}	concatenation matrix $\mathbf{C}[n]$ consisting of the pilot symbols, ($K \times LN_T$)
d	number of clusters in the time domain, in correlated-receive independent-transmit MIMO channels, $d = \sum_{i=1}^{N_T} d_i$; in correlated-transmit-receive MIMO channels, all the transmit antennas share d clusters
d_i	number of clusters related to the i th transmit antenna
\mathfrak{d}	distance of the propagation path
\mathbf{e}_k	the k th eigenvector of the received signal covariance matrix
$\mathbf{e}_{i,j}$	j -dimensional i th unit vector with the one at the i th entry and zeros for the others
$\mathbf{e}_{h_i}[n, l]$	estimation error vector of $\mathbf{h}_{\text{MMSE},i}[n, l]$
\mathbf{E}_N	eigenvector matrix of the noise subspace
\mathbf{E}_S	eigenvector matrix of the signal subspace
\mathbf{F}_K^L	matrix consisting of the left L columns of the K -point FFT matrix
$g(t)$	overall pulse shaping filter
$g_T(t)$	transmit pulse shaping filter
$g_R(t)$	receive pulse shaping filter
$\mathbf{h}_i[n, l]$	the l th vector tap of the vector CIR corresponding to the i th transmit antenna at time n
$\tilde{\mathbf{h}}[n]$	channel frequency response at time n
$\hat{\mathbf{h}}_{\text{ML},i}[l]$	ML based CIR estimates of the l th tap related to the i th transmit antenna during all the pilot symbol durations in the receive processing window
$\hat{\mathbf{h}}_{\text{MMSE},i}[n, l]$	JST MMSE based estimate of the l th tap of the CIR from the i transmit antenna at time n
$\mathbf{H}_i[n]$	CIR matrix related to the i th transmit antenna ($L \times N_R$) at time n
$\mathbf{H}[n]$	concatenation CIR matrix of all the transmit antennas ($N_T L \times N_R$) at time n
$\tilde{\mathbf{H}}_i[n]$	CFR matrix to the i th transmit antenna ($K \times N_R$) at time n
$\tilde{\mathbf{H}}[n]$	concatenate CFR matrix of all the transmit antennas ($N_T K \times N_R$) at time n
$\hat{\mathbf{H}}_{\text{ML},i}[n]$	ML based CIR matrix estimate related to the i th transmit antenna at time n
\mathbf{I}_L	L -dimensional identity matrix
$\mathbf{I}(\boldsymbol{\rho})$	FIM parameterized by $\boldsymbol{\rho}$

k_i	slope of the i th possible region
$\vec{k}(\cdot)$	wave vector
K	number of carriers in an OFDM symbol
l_i	number of paths in the i th cluster
L	number of paths in the space–time domain
$\mathcal{L}(\cdot)$	likelihood function
L_g	length of the CIR at the oversampling rate
m	number of antennas of the subarray used in the ESPRIT algorithm
M	number of samples of the training signal
N_D	number of data symbols within a transmit burst
N_f	number of FSs
N_{ray}	number of rays from a cluster with approximately same time delays
N_P	number of pilot symbols within a transmit burst
N_R	number of receive antennas
N_T	number of transmit antennas
$\mathcal{O}(\cdot)$	objective function of the ML based position estimation
P	number of data symbols before and after the training symbol part exploited for the channel estimation in the observation window
$\mathbf{p}(t)$	position vector of MS
p_l	average power of the l th path
$\mathbf{q}[k]$	decision statistic vector obtained by the MRC for the transmitted symbol vector of the Alamouti codes at the k th sub–carrier
r	distance from the scatterer to the FS
$\mathbf{R}[n]$	received symbol matrix at time n ($K \times N_R$)
\mathbf{R}_{TX}	transmit correlation matrix
\mathbf{R}_{RX}	receive correlation matrix
$s(t)$	continuous time transmitted signal
$s_i(t)$	continuous time training signal from the i th transmit antenna
$\mathbf{s}(t)$	continuous time transmitted signal, ($N_T \times 1$)
\mathbf{s}_i	discrete time training signal vector from the i th transmit antenna
$\mathbf{s}_i(\tau_{i,j})$	training signal of the i th transmit antenna with delay $\tau_{i,j}$
$\mathbf{S}(\boldsymbol{\tau})$	training signal matrix consisting of all the delayed training signals ($M \times N_T d$)
$\mathbf{S}_i(\boldsymbol{\tau}_i)$	training signal matrix whose columns correspond to the different delays
$\mathbf{S}(\boldsymbol{\tau})$	training signal matrix including all the delayed training signals from all the transmit antennas

$\mathcal{S}(\tau_i)$	training signal matrix whose columns correspond to the training signals of all the transmit antennas with the same delay τ_i ($M \times N_T$)
\mathcal{S}	index set of the OFDM symbols during the receive processing window
\mathcal{S}_P	index set of pilot symbols in the receive processing window
\mathcal{S}_D	index set of the data symbols in the receive processing window
\mathcal{T}	time domain correlation matrix due to the Doppler spectrum, ($N_P \times N_P$)
T_B	time duration of a transmission burst during which the channel is assumed to be constant
T_{CP}	time duration of the cyclic prefix
T_S	sample duration of the training signal
T_{syimb}	sample duration within an OFDM symbol
T_{OFDM}	time duration for one OFDM symbol
$\mathbf{w}(t)$	continuous time noise vector at the receive antenna array
\mathbf{W}	noise matrix in the received signal ($N_R \times N$)
$\mathbf{W}[n]$	noise matrix in the received signal during the n block ($M \times N_R$)
$\mathbf{W}_i[n, l]$	Wiener filtering matrix for the l th tap of the CIR of the i th transmit antenna at time n , ($N_P N_R \times N_P N_R$)
(x, y)	coordinates of the MS
$(\hat{x}_{\text{LS}}, \hat{y}_{\text{LS}})$	LS based MS's position estimate
(x_t, y_t)	coordinates of the FS
(x_s, y_s)	coordinates of the scatterer
$\mathbf{x}(t)$	continuous time received signal vector, ($N_R \times 1$)
$\vec{x}_{T,i}$	position vector of the i th transmit antenna
$\vec{x}_{R,j}$	position vector of the j th receive antenna
\mathbf{X}	received signal matrix ($N_R \times N$)
$\mathbf{X}[n]$	received signal matrix during the n th block ($M \times N_R$)
α	weight factor of the semiblind channel estimator
$\boldsymbol{\alpha}(t)$	patial signature at the receive antenna array
$\boldsymbol{\alpha}_{i,j}$	spatial signature vector of the j th cluster related to the i th transmit antenna
γ	SNR of the received signal
γ_P	SNR of the received pilot symbols
γ_D	SNR of the received data symbols
γ_l	complex gain of the l th path
$\gamma_{i,j}$	complex gain of the j th path in the i th cluster in the correlated-transmit-receive MIMO channel, or the j th spatial signature related to the i th transmit antenna in the correlated-receive independent-transmit MIMO channels

Γ	transform matrix mapping the range of $\mathcal{S}(\tau)$ to that of $\mathcal{S}(\tau)$
$\delta[\cdot]$	Dirac's delta function
Δ_R	receive antenna spacing in terms of wavelength
Δ_T	transmit antenna spacing in terms of wavelength
Δ_τ	time difference between neighbor taps
$\bar{\theta}_{R,i,j}$	mean AOA of the paths coming from the j th cluster related to the i th transmitter
$\theta_{i,j}$	the second element of the receive antenna array response vector due to the AOA $\theta_{R,i,j}$
Θ_i	diagonal matrix constructing by $\theta_{i,j}$
θ_A	azimuth of the wave
θ_E	elevation of the wave
θ_R	angle of arrival
θ_T	angle of departure
ϑ_i	parameter vector of the i th path
λ	wavelength of the propagation wave
$\xi_j[k]$	MMSE estimation error vector of the CFR vector for the k th sub-carrier at the j th receive antenna
Ξ	modulation symbol alphabet
Π_N	matrix with the reverse order of the rows of \mathbf{I}_N
$\rho[\cdot]$	temporal correlation function
ρ	vector of the actual coordinates of the MS and the scatterers
σ_N^2	variance of the noise element
$\sigma_{\theta_{R,i,j}}$	angular spread of the j th cluster related to the i th transmitter
$\sigma_{\hat{e}_h}^2$	average estimation error variance for each tap
$\Sigma_{\mathbf{a}}$	auto-correlation matrix of the vector \mathbf{a}
$\Sigma_{\mathbf{a},\mathbf{b}}$	cross covariance matrix of two random vector \mathbf{a} and \mathbf{b}
τ_l	time delay of the l th path
$\boldsymbol{\tau}_i$	time delay vector of the transmitted signal from the i th transmit antenna
$\boldsymbol{\tau}$	time delay vector associated with all the transmit antennas
$\hat{\boldsymbol{\tau}}$	estimated time delay vector
$\phi_{i,j}$	the second element of the transmit antenna array response vector due to the AOD $\theta_{T,i,j}$
Φ_i	diagonal matrix constructing from $\phi_{i,j}$
φ	vector of the actual coordinates of the MS
$\boldsymbol{\psi}$	vector of the actual coordinates of the scatterers
ω_c	carrier frequency
Ω	matrix representation of a blind estimation method
$\tilde{(\cdot)}$	Fourier transform of the argument

$\hat{(\cdot)}$	estimate of the argument
$(\cdot)^\dagger$	pseudo-inverse of the matrix (\cdot)
$(\cdot)^*$	complex conjugate of the matrix (\cdot)
$(\cdot)^\top$	the transpose of the matrix (\cdot)
$\angle(\cdot)$	the angle of the vector argument (\cdot)
$ \mathbf{A} $	the determinant of the matrix \mathbf{A}
\otimes	Kronecker product
\odot	Hadamard product
\diamond	column-wise Kronecker product
∇	the gradient operator
$*$	convolutional operator
$\mathcal{CN}(\cdot, \cdot)$	complex Gaussian distribution
$\mathcal{N}(\cdot, \cdot)$	normal distribution
$\text{diag}(\cdot)$	diagonal matrix with the argument vector on main diagonal
$\text{Im}(\cdot)$	imaginary part of the argument
$\text{Re}(\cdot)$	real part of the argument
$\text{vec}(\cdot)$	the vector stacking all the columns of the argument matrix
AMSE	analytical mean square error
AOA	angle of arrival
AOD	angle of departure
BEP	bit error probability
BER	bit error rate
CFR	channel frequency response
CIR	channel impulse response
CP	cyclic prefix
CRLB	Cramér–Rao lower bound
CSI	channel state information
DDCIR	double directional channel impulse response
DFT	discrete Fourier transform
DML	deterministic ML
EM	expectation maximization
ESPRIT	estimation of signal parameters via rotational invariance techniques
FCC	Federal Communication Commission
FFT	fast Fourier transform
FIM	Fisher information matrix
FS	fixed station
GML	Gaussian maximum likelihood
GPS	Global Positioning System
IFFT	inverse fast Fourier transform

i.i.d.	independent and identically distributed
IPC	information processing centre
IQML	iterative quadrature maximum likelihood
LDC	linear dispersion code
LS	least squares
LOS	line of sight
MIMO	multiple-input multiple-output
ML	maximum likelihood
MMSE	minimum mean square error
MODE	method of direction-of-arrival estimation
MRC	maximum ratio combiner
MS	mobile station
MSE	mean square error
MUSIC	multiple signal classification
NLLS	non-linear least square
NLOS	non-line of sight
NMSE	normalized mean square error
OFDM	orthogonal frequency division multiplexing
PDF	probability density function
PDU	protocol data unit
QOS	quality of service
QPSK	quadrature phase shift keying
RMSE	root mean square error
RNC	radio network controller
RSS	received signal strength
RP	reference point
SAGE	space-alternating generalized expected maximization
SIJADE	shift-invariance joint angle and delay estimation
SIMO	single-input multiple-output
SISO	single-input single-output
SNR	signal-to-noise ratio
STBC	space-time block code
STC	space-time code
STTC	space-time trellis code
TDD	time division duplex
FDD	frequency division duplex
TDMA	time division multiple access
TDOA	time difference of arrival
TOA	time of arrival
ULA	uniform linear array

UWB	ultra wideband
V-BLAST	Vertical Bell Labs Layered Space-Time
WiMAX	worldwide interoperability for microwave access
WLAN	wireless local area network
WMAN	wireless metropolitan area network
WSF	weighted subspace fitting

Contents

Abstract	
Preface	
Symbols and abbreviations	
Contents	
1 Introduction	19
1.1 MIMO-OFDM Systems	20
1.2 Mobile positioning	22
1.3 Aims and problem definition	23
1.4 Outline of the thesis	24
1.5 The author's contribution to the publications	25
2 Review of the literature	26
2.1 The MIMO channel model	26
2.2 MIMO channel parameter estimation	31
2.2.1 Angle of arrival estimation	32
2.2.2 Single-input-multiple-output channel parameter estimation	36
2.2.3 MIMO channel parameter estimation	37
2.3 MIMO channel estimation	38
2.3.1 Channel estimation for the single-carrier MIMO system	39
2.3.2 Channel estimation for the MIMO-OFDM system	42
2.4 Mobile positioning	45
2.4.1 Positioning algorithms	45
2.4.2 Non-line-of-sight positioning error mitigation	48
3 Space-time MIMO channel parameter estimation	50
3.1 The space-time channel model	51
3.1.1 The correlated-receive independent-transmit MIMO channel	51
3.1.2 The correlated-transmit-receive MIMO channel	53
3.2 Joint time delay and spatial signature estimation	54
3.2.1 Signal model and training signal design	54
3.2.2 Iterative quadrature maximum likelihood based time delay and spatial signature estimation	56
3.2.3 Identifiability and the Cramér-Rao lower bound	57
3.2.4 Numerical examples	58

3.3	Joint the time delay, angle of arrival and angle of departure estimation	59
3.3.1	Signal model	60
3.3.2	2-D unitary ESPRIT based joint angle of arrival and angle of departure estimation	63
3.3.3	Identifiability and the Cramér-Rao lower bound	69
3.3.4	Numerical examples	70
3.4	Conclusions	72
4	Channel estimation for a MIMO-OFDM system with spatially correlated channels	75
4.1	The correlated MIMO-OFDM system model	76
4.1.1	Frame structure	76
4.1.2	Channel statistics	77
4.2	Minimum mean square error channel estimation	79
4.2.1	Signal model	80
4.2.2	Minimum mean square error channel estimation	81
4.2.3	Mean square error analysis and examples	83
4.3	Bit error probability of STBC-OFDM with channel estimation errors	86
4.3.1	The signal model	87
4.3.2	Bit error probability analysis	88
4.3.3	Numerical examples	89
4.4	Conclusions	90
5	Positioning for non-line of sight propagation	92
5.1	System model	93
5.2	Geometric approach with two fixed stations	94
5.2.1	Algorithm derivation	94
5.2.2	Root mean square error analysis	96
5.3	Least squares algorithm with multiple fixed stations	99
5.3.1	Algorithm derivation	99
5.3.2	Root mean square error analysis	99
5.4	Maximum likelihood position estimation and the Cramér-Rao lower bound	101
5.4.1	Joint mobile station and scatterers' position estimation	101
5.4.2	The Cramér-Rao lower bound	102
5.5	Numerical examples	105
5.5.1	Least squares algorithm	106
5.5.2	The maximum likelihood algorithm and the Cramér-Rao lower bound	107
5.6	Conclusions	108
6	Conclusions	115
6.1	Summary and discussion	115
6.2	Future research directions	116
	References	118
	Appendices	

1 Introduction

The next generation of wireless networks is expected to provide subscribers with wireless multimedia services such as high speed Internet access, hand-held television and mobile computing etc. The rapidly growing demand for these services is driving communication technology towards higher data rates with even mobility, and higher quality of services (QOS). Mobile positioning in a wireless network is also growing when emergency call services become mandatory as well as with the advent of more advanced location-aware based services and mobile gaming.

The multiple-input multiple-output (MIMO) technique, applying several transmit and receive antennas, has emerged as one of the most prominent technical breakthroughs in the last decade, and has been considered as a significant technical advance for resolving the bottleneck of traffic capacity in the future Internet-intensive wireless network. The key advantages furnished by MIMO techniques include the improvements of the spectrum efficiency (data rate) and QOS, like bit error rate (BER), which can be realized by so called spatial multiplexing and space-time coding techniques, respectively. However, all these performance gains could be achieved only if the channel state information is available at the receive side or both ends of the communication link. As such, channel estimation for a MIMO system is crucial to facilitate potential succeeding processing steps, e.g., equalization and symbol detection etc. The practical MIMO systems demonstrate the significant correlation at the both ends of the link, and the correlations of the MIMO channels depend on the unknown parameters of the underlying propagation channels. Consequently these channel parameters should be capitalized to enhance the channel estimator. In addition, the estimated channel parameters can be utilized to determine the mobile's position.

This thesis focuses on the MIMO channel parameter estimation, and its utilization in enhanced channel coefficient estimation for the MIMO orthogonal frequency division multiplexing (MIMO-OFDM) system and mobile positioning in the non-line of sight scenario. In Section 1.1, a brief introduction to the MIMO-OFDM system is given. Section 1.2 briefly overviews the mobile positioning techniques. The aims and outline of the thesis are described in Section 1.3. Section 1.5 addresses the author's contributions to the original publications.

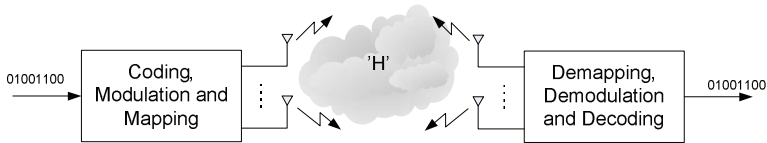


Fig. 1. A MIMO system.

1.1 MIMO–OFDM Systems

The MIMO system refers to a wireless communication system for which the transmitting end as well as the receive end is equipped with multiple antenna elements. The typical setup of the MIMO system is illustrated in Fig. 1. The core idea in MIMO systems [1] is space-time signal processing where the signals in the time domain and spatial domain inherent from the multiple spatially distributed antennas are jointly processed. As a consequence, MIMO systems can be viewed as an extension of the traditional smart antennas, where multiple antenna elements are employed at only the transmitter or the receiver. Beamforming and spatial diversity are the major powerful techniques of smart antenna systems. The beamforming enables the increase of the average signal-to-noise ratio (SNR) through focusing the energy into desired directions, in either the transmitter or the receiver. In particular, given the responses of each element to the desired signal and interference signals, it can maximize the average desired signal level and/or minimize the inference signal level. Due to the fact that the probability of losing the signal vanishes exponentially with the number of the uncorrelated antennas being used, i.e., diversity order, the spatial diversity furnished by the smart antennas can improve the link reliability or coverage range versus quality tradeoff [2]. Obviously, the MIMO system inherits all the benefits of the conventional smart antennas. More detailed treatments of smart antenna and MIMO techniques can be found in the books by Paulraj *et al.* [3], Bolcskei *et al.* [4] and Kaiser *et al.* [5].

Due to the nature of MIMO channels, i.e., a matrix channel rather than a vector channel in smart antennas, the advantage of the MIMO system is far beyond just the diversity gain or array gain. Effectively taking advantage of random fading, MIMO has the ability to increase the channel capacity significantly [6, 7]. According to Gesbert *et al.* [1], the first results hinting at the capacity gains of MIMO were given by Winters [8], and an earlier version of MIMO capacity gain was attributed to Paulraj and Kailath [9]. In particular, the spatial multiplexing technique originally referred to as the vertical Bell Labs Layered Space-Time (V-BLAST) was presented in [10, 11, 12]. It can simultaneously transmit independent $\min(N_T, N_R)$ data streams over the MIMO system with N_T transmit and N_R receive antennas, provided that the channel matrix is full rank. The separability of the MIMO channels depends on the presence of rich multipaths, therefore, MIMO techniques do exploit multipaths rather than mitigating them like conventional smart antennas. There are numerous research results on the MIMO channel capacity in the literature. With the assumption of the i.i.d. Rayleigh fading channels, the exact results

were derived in [6, 13, 14, 15, 16] for the case of the channel known at both the transmitter and the receiver, and in [6, 7] in the event of the channel known at the only receiver, but unknown at the transmitter. Some limiting results for the large system¹ were proposed in [16, 17] for the known correlated Rayleigh fading channels at the transmitter, and in [6, 18, 19] for the channels unknown at the transmitter.

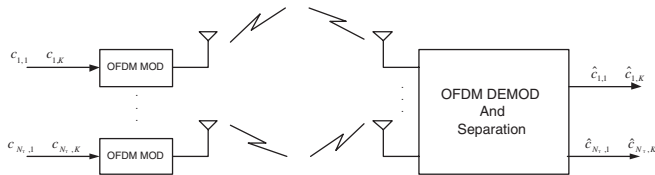
The information theoretic results published in the preceding literature only provide an upper bound on the performance realized by an algorithm or codes with unlimited complexity or latency. It is also important to develop some practical algorithms with a reasonable BER performance–complexity tradeoff. The MIMO transmission schemes typically fall into two categories: data rate maximization or diversity maximization. Inspired by the delay diversity scheme of Wittneben [20], the space-time codes (STCs) were first developed in [21]. As the key development of the STC concept, the space-time trellis code (STTC) was originally presented in [22]. In addition to the coding gain depending on the code complexity, the STTCs also show a diversity gain equal to the number of transmit antennas. To overcome the complexity of a multidimensional Viterbi algorithm required for decoding STTCs, Alamouti [23] discovered a space-time block coding (STBC) employing two transmit antennas which was generalized to an arbitrary number of antennas in [24]. By virtue of the orthogonality property, the maximum likelihood (ML) based decoding of STBCs can be achieved by only linear processing at the receiver. Due to the simplicity of the Alamouti code, it has been a part of both the W-CDMA and CDMA-2000 standards. The pure spatial multiplexing, e.g., V-BLAST [10, 12], allows an increase in data rate; however, it gives limited diversity benefit. On the other hand, STTCs and STBCs furnish the additional coding and diversity gain, while the data rate remains at the same level. It is possible to make various tradeoffs between multiplexing and diversity in [25] and [26]. In particular, the linear dispersion codes (LDCs) proposed by Hassibi and Hochwald [27], as well as Heath and Paulraj [28] unify the space-time block coding and the spatial multiplexing into a joint framework. As a result, the LDCs perform well in terms of both ergodic capacity and error probability.

All the preceding MIMO techniques have been restricted to a narrowband wireless system, i.e., a flat fading channel. However, a channel equalizer has to be used at the receiver with the space-time decoder for the broadband frequency selective channels. Using classical equalization methods along with STCs is a difficult problem. OFDM [29, 30, 31, 32] turns a frequency-selective MIMO channel into a set of parallel frequency-flat MIMO channels. This enables multi-channel equalization to be particularly simple, so that for each OFDM tone only a constant matrix has to be inverted [13, 33]. Therefore, the use of MIMO technology in combination with OFDM, i.e., MIMO-OFDM [13, 34, 35, 36, 37, 38, 39, 40, 41] has gained considerable attention recently and seems to be a very promising approach for future broadband wireless systems.

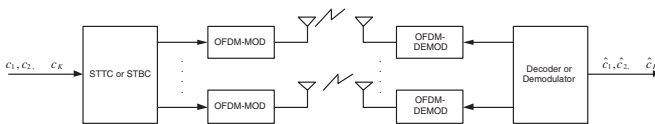
The capacity of the OFDM based MIMO system was studied in [33], and the impact of the propagation environment on the performance of the MIMO-OFDM

¹The number of antennas grows proportionally at both the transmitter and the receiver, i.e., $N_T, N_R \rightarrow \infty$ and $N_T/N_R \rightarrow c$

was presented in [42] where two types of MIMO–OFDM systems were detailed, i.e., spatial multiplexing based and space–frequency coded OFDM systems which are illustrated in Figs. 2(a) and 2(b), respectively. Moreover, MIMO–OFDM is being investigated as a core technology for the next generation wireless local area network (WLAN) standard and mobile wireless metropolitan area network (WMAN) or WiMAX, i.e., IEEE802.11n and IEEE802.16e [43].



(a) Spatial Multiplexing based OFDM System.



(b) Space–frequency Coded OFDM System.

Fig. 2. MIMO-OFDM system.

1.2 Mobile positioning

Wireless positioning has received increasing attention over the past decade [44, 45, 46, 47, 48]. Due to the different applications and the associated requirements on the equipment, e.g., the physical dimension, power consumption, the location accuracy and operating environment etc., three kinds of basic radio location systems are commonly applied, i.e., satellite positioning systems like Global Positioning System (GPS) and GALILEO, cellular and wireless local area network (WLAN) based positioning systems, as well as sensor network based positioning systems, which are often based on the ultra wideband (UWB) radio. Some applications need the combination of the above positioning systems, e.g., the cooperation of the GPS and a cellular network. The GPS system significantly improves the efficiency of fleet management, taxi and delivery drivers and intelligent transportation systems [49, 50]. Location technology in a cellular network can be employed to improve

radio resource and mobility management [51, 52, 53, 54, 55, 56, 57]. The Federal Communication Commission (FCC) has released an order in the US that mandates all wireless service providers to provide accurate subscriber location information for Enhanced-911 (E-911) services [58]. Thanks to the high accuracy, low-power and low-cost implementation, the UWB radio based positioning systems have been applied to numerous applications such as logistics, medical applications, family communications, search and rescue, control of home appliances and so on [59, 60].

The position of a mobile station (MS) can be estimated from passive measurements of the arrival times, direction of arrival, or Doppler shifts of propagation waves received at various fixed stations (FS) [61]. Sun *et al.* [62] investigated a number of positioning techniques from a system point of view. The positioning problems for cellular networks were considered in [63, 64]. The UWB radio based localization problem was investigated in [65]. Radio location can be implemented in one of two ways; either the MS transmits a signal which FSs use to determine its location or the FSs transmit signals that the MSs use to calculate their own positions, e.g., in the GPS.

There are several fundamental positioning approaches, i.e., the time-based scheme which measures the time of arrival (TOA) or time difference of arrival (TDOA) [61, 66], the angle of arrival (AOA) based scheme [61, 67] and the hybrid TDOA/AOA approach [68] which combines the TDOA measurements at the MS with the AOA measurements at the FS. A review of mobile positioning literature will be presented in Chapter 2. An overview of different positioning techniques can be found in [69].

1.3 Aims and problem definition

In spite of the major research effort invested in MIMO-OFDM channel estimation and mobile positioning techniques, several practical as well as theoretical open problems still exist in these fields. Some of them are considered in this thesis. The general aim of the thesis is to develop novel MIMO-OFDM channel estimation algorithms and mobile positioning techniques in NLOS scenarios, and to analyze their performance. Due to the fact that the channel estimation and positioning algorithm depend on the parameter estimation in nature, the MIMO channel parameter estimators are also studied in depth.

The thesis studies the MIMO channel parameter estimation and investigates the application of channel parameters in the field of MIMO-OFDM channel estimation and mobile positioning. The channel models reported in the open literature, e.g., [70], demonstrate that the significant correlations at the both ends of a MIMO system may appear in practical scenarios. Such correlations heavily depend on the channel parameters characterizing the underlying propagation channels. Several algorithms have been developed for the MIMO parameter estimation accordingly, however, some open problems such as the identifiability of the MIMO parameters and practical estimation methods for the joint time delay, angle of arrival (AOA) and angle of departure (AOD) estimation still exist in this field. Focusing on two

kinds of typical MIMO channels, i.e., the correlated-receive independent-transmit channel and the correlated-transmit-receive channel, identifiabilities of MIMO parameters are discussed and the practical parameter estimation algorithms are proposed in this thesis.

On top of the MIMO parameter estimates, the applications of these parameters to the MIMO-OFDM channel estimation and mobile positioning are examined as well. The general channel estimation schemes for MIMO and MIMO-OFDM systems in the open literature only exploit the channel properties in the time and the frequency domain. Hence, they do not take full advantage of the channel properties to improve the channel estimators. To make the discussion clearer and simpler, the thesis only considers the correlated-receive independent-transmit channel. Based on the TOA and spatial signature estimates, an enhanced joint spatial-temporal (JST) minimum mean square error (MMSE) based channel estimator for the MIMO-OFDM system is developed. Moreover, the proposed algorithm can be easily extended to the correlated-transmit-receive channel. By virtue of the channel parameters, various mobile positioning algorithms have been proposed, and some NLOS error mitigation techniques have also been documented in the open literature. However, efficiently making use of NLOS paths has not been well studied so far. With knowledge of the NLOS paths, i.e., the time delay, AOA and AOD, the thesis introduces a novel positioning algorithm which benefits from the NLOS paths rather than cancelling them. The performance of the proposed algorithms is also analyzed and the results are documented.

1.4 Outline of the thesis

Parts of the original contributions in Chapter 3-5 have been published earlier or submitted for publication [71, 72, 73, 74, 75, 76, 77, 78]. The remainder of the thesis is organized as follows.

Chapter 2 contains the literature review which presents the background knowledge for the main contributions of the thesis. The notations and mathematical models of MIMO-OFDM channel estimation and positioning algorithms utilized in the later chapters are introduced. The relevant literature on MIMO channel estimation as well as mobile positioning algorithms are reviewed.

Chapter 3, the results of which are in part included in [71, 73, 74, 76], considers MIMO channel parameter estimation. An iterative quadrature maximum likelihood (IQML) based algorithm is proposed to jointly estimate the time delay and spatial signature for the correlated MIMO channel. Moreover, by virtue of the shift-invariant structure present in the spatial signature matrix, a 2-D unitary ESPRIT algorithm is developed to estimate the AOA and AOD simultaneously. The mean squared error (MSE) of the proposed algorithms is analyzed and numerical examples are presented.

Chapter 4, the results of which are in part included in [71, 72, 73, 74, 78], considers MMSE channel estimation for the MIMO-OFDM system. In particular, a JST filtering based MMSE channel estimator is given for the MIMO-OFDM

system with correlation at the receiver side. The bit error probability (BEP) of the STBC-OFDM over the correlated MIMO channels is also studied to take the effects of channel estimation error and correlation of channels into account.

Chapter 5, the results of which are in part included in [75, 77], focuses on the mobile positioning algorithms. A novel mobile positioning algorithm in the NLOS environment is developed. With the assumption of knowledge about the time delay, the AOA and the AOD associated with each NLOS path, the proposed algorithm is capable of jointly estimating the positions of the MS and the scatterers. The root mean square error (RMSE) and Cramér-Rao lower bound (CRLB) of the position estimates are also analyzed and compared by the computer simulations.

Chapter 6 concludes the thesis. The results and conclusions are summarized and discussed. Furthermore, some open problems for future research are highlighted.

1.5 The author's contribution to the publications

The thesis is in part based on eight original publications. The author has had the main responsibility for performing the analysis and writing all the papers [71, 72, 73, 74, 75, 76, 77, 78]. The author has also implemented the software to perform the numerical analysis and computer simulations.

In papers [71, 72, 73, 74, 78], the author generated the main ideas, developed the analysis, and produced the examples. The second author provided help, ideas, and criticism during the process. In papers [73, 74, 75, 76, 77], the author developed the idea and the analysis, as well as produced the examples. The second and third authors provided help, ideas and criticism during the process. In papers [75, 77], the idea of utilizing both AOA and AOD for the positioning stems from the discussion between the author and the second author. The author developed the idea and the analysis, and produced the examples. The second and third authors provided help, ideas and criticism during the process.

2 Review of the literature

Some preliminaries and definitions necessary for analysis in the following chapters are presented in this chapter. To create a complete picture of the state of the art, a comprehensive overview of the techniques and knowledge is presented. In Section 2.1, a review of the MIMO channel models is presented. These are applied more specifically later when defining the correlated-transmit-receive MIMO channel model in Section 3.1.2. The earlier and parallel work regarding MIMO parameter and channel estimation is described in Sections 2.2 and 2.3, respectively. Therein the general channel models reviewed in Section 2.1 are also specified and specialized by several particular forms according to the problems addressed. Again a rather comprehensive review is presented to illustrate the overall picture of the state of the art in the field. The previous work about mobile positioning is reviewed in Section 2.4.

Since this is a comprehensive overview of the state of the art, some materials in this chapter may not seem to be in line with the main contribution of the thesis. To sharpen the focus of the thesis, the implicit connections of these materials with the main area of the thesis are expected. For instance, the correlated-transmit-receive MIMO channel model developed in Section 3.1.2 validates the Kronecker structure based MIMO channel model described in Section 2.1. However, the correlated-transmit-receive MIMO channel model is mainly used as a typical MIMO channel model on top of which the channel parameter estimation algorithm is developed. Validating the Kronecker structure of the MIMO channel statistics by using the correlated-transmit-receive MIMO channel model is not demonstrated in the thesis.

2.1 The MIMO channel model

Due to the fact that each channel coefficient or parameter estimation algorithm is based on a certain type of channel model, MIMO channel models that can accurately describe the propagation channels are of great importance. In addition, to design a high-performance MIMO wireless system, it is necessary to compare

the performance of different MIMO techniques, modulation schemes, tune design parameters, and to predict system performance in a fair and realistic way. As in [79], two typical examples of MIMO channel models are reviewed in this section, namely the Kronecker structure based MIMO channel model and a generic geometry based MIMO channel model with physical parameters on which all the channel models exploited in the following chapters are based.

MIMO channel modeling techniques

To set the stage for the MIMO channel models, a general overview of different channel modeling techniques is given first. Three main propagation effects must be characterized for modeling traditional wireless single-input single-output (SISO) channels, i.e., the large scale path loss, the shadow fading, and the small scale fading [80]. The path loss determines the average received power for a given transmit-receive distance. The shadowing is most often modeled statistically by a lognormal distribution, which explains the significant variation of the path loss from location to location for a fixed transmit-receive distance. The amplitude of the received signal can vary due to small scale movements of the transmitter, the receiver or the surrounding environment; this is called small scale fading. Three different distributions are mainly used to describe the statistics of the real-valued amplitude, i.e., the Rayleigh distribution for the NLOS scenarios, the Rice distribution for the LOS scenarios, and the Nakagami distribution with more degrees of freedom to fit the model to the measurement data. One of the most commonly used channel models for wideband channels is the tapped-delay-line model

$$h(\tau) = \sum_{l=1}^L \gamma_l \delta(\tau - (l-1)\Delta\tau), \quad (1)$$

where γ_l is the complex tap amplitude, L is the number of taps, $\delta(\cdot)$ is the Dirac delta function, τ is the time delay, and $\Delta\tau$ is the time spacing between neighboring taps. The average power of each tap, $E(\gamma_l \gamma_l^*)$, can be specified by the power delay profile of the channel. The absolute value of the tap amplitude, $|\gamma_l|$, is modeled by the Rayleigh or lognormal distribution [81] and the root-mean-square (RMS) delay spread is widely used to characterize the dispersion of the channel. All the preceding models are called statistical channel models since they describe the statistical properties of SISO wireless channels. Another type of model is named deterministic channel models [81] which attempt to calculate the radio propagation conditions according to the physical layout of the environment. To lower the prohibitive computation complexity of the deterministic model, ray-tracing algorithms have been proposed to serve as a simplified solution [81, 82].

MIMO channel modeling is more complicated due to the antenna array employed at the both ends of the link. Simply modeling each link, i.e., from one transmit antenna to one receive antenna, as a SISO channel and assuming they are independent and identically distributed (IID) is fairly common in many theoretical studies [7, 22]. However, this assumption is rarely true according to the practical measurements [83, 84, 70]. The spatial correlation between different links

at both ends should be taken into account when modeling MIMO channels. One kind of MIMO channel model is called the nonphysical MIMO channel model [85]. Since a complex Gaussian random vector is completely specified by its first- and second-order moments [86], it is easy to generate a MIMO channel with a specified correlation structure between the single links [87, 88]. The correlation matrix is usually obtained from the measurement data, hence the nonphysical MIMO channel model cannot separate the influence of the measurement setup from the channel itself. In contrast to the nonphysical MIMO channel model, the physical MIMO channel model [89] constructs a realistic geometric scattering environment and calculates the MIMO channel matrix as a sum of the contributions from different rays. The distribution of the scatterers depends on some important physical parameters such as AOA, AOD and time of arrival (TOA). Finding the correct statistics of these parameters is a difficult task, but the physical MIMO channel model can separate the MIMO channels from the measurement setup. These two kinds of the MIMO channel models are discussed in detail subsequently.

Statistical MIMO channel models

As mentioned previously, most statistical MIMO channel models can be categorized into nonphysical MIMO channel models and physical MIMO channel models. Below, two typical MIMO channel models corresponding to these two classes of MIMO channel models, the Kronecker structure based MIMO channel model and a generic geometry based MIMO channel model, are briefly reviewed.

For a wideband MIMO system with N_T transmit antennas and N_R receive antennas, the continuous time baseband input–output relationship can be formulated as

$$\mathbf{x}(t) = \mathbf{H}(t) * \mathbf{s}(t) + \mathbf{w}(t), \quad (2)$$

where $\mathbf{H}(t) \in \mathbb{C}^{N_R \times N_T}$ is the wideband MIMO channel impulse response, $\mathbf{x}(t) \in \mathbb{C}^{N_R}$ is the received signal vector, $\mathbf{s}(t) \in \mathbb{C}^{N_T}$ is the transmitted signal vector, $\mathbf{w}(t) \in \mathbb{C}^{N_R}$ is the noise vector at the receiver side, and $*$ denotes the convolution. Specifically,

$$\mathbf{H}(t) * \mathbf{s}(t) = \int \mathbf{H}(\tau) \mathbf{s}(t - \tau) d\tau.$$

For a narrowband flat fading MIMO system, (2) can be simplified as

$$\mathbf{x}(t) = \mathbf{H}(t) \mathbf{s}(t) + \mathbf{w}(t). \quad (3)$$

Moreover, the MIMO channel $\mathbf{H}(t)$ is assumed to be a block–fading channel, which means that the channel is constant within a block period, and varies independently from block to block. Within a block of K symbols, the n th received signal vector can be written as

$$\mathbf{x}[n] = \mathbf{H} \mathbf{s}[n] + \mathbf{w}[n], n = 1, \dots, K. \quad (4)$$

1. Kronecker structure based MIMO channel model.

The simplest nonphysical MIMO channel model is the IID MIMO channel model, which assumes that the elements of \mathbf{H} are IID zero mean complex Gaussian. The IID MIMO channel model does not consider the spatial correlation

between MIMO channel links which has been demonstrated in many MIMO measurements. To solve this problem, the MIMO channel correlation matrix $\mathbf{R}_H = \text{E}(\text{vec}(\mathbf{H})\text{vec}(\mathbf{H})^H) \in \mathbb{C}^{N_T N_R \times N_T N_R}$ is introduced, where $\text{vec}(\cdot)$ denotes the column vector stacking all the columns of the matrix, and $()^H$ defines complex conjugate transpose. The MIMO channel matrix $\mathbf{H} : \text{vec}(\mathbf{H}) \sim \mathcal{CN}(\mathbf{0}, \mathbf{R}_H)$ can be formed as

$$\text{vec}(\mathbf{H}) = \mathbf{R}_H^{1/2} \text{vec}(\mathbf{G}), \quad (5)$$

where $\mathcal{CN}(\mathbf{0}, \mathbf{R}_H)$ refers to the complex Gaussian distribution of zero mean and covariance matrix \mathbf{R}_H , $\mathbf{G} \in \mathbb{C}^{N_R \times N_T}$ is a stochastic matrix with IID $\mathcal{CN}(0, 1)$ elements, and $(\cdot)^{1/2}$ is any matrix square root such that $\mathbf{R}_H = \mathbf{R}_H^{1/2} (\mathbf{R}_H^{1/2})^H$.

The correlation between the elements of the MIMO channel matrix has been widely investigated [85, 90, 91]. In scenarios with sufficiently rich multipath scattering, it is reasonable to assume spatial stationarity¹ such that the correlation matrix of the signals as seen from the receive side will be the same no matter which of the transmit antenna is used. The receive-side correlation matrix is defined as

$$\mathbf{R}_{\text{RX}} = \frac{1}{N_T} \text{E}(\mathbf{H}\mathbf{H}^H). \quad (6)$$

Likewise, the transmit-side correlation matrix is defined as

$$\mathbf{R}_{\text{TX}} = \frac{1}{N_R} \text{E}(\mathbf{H}^H \mathbf{H}). \quad (7)$$

It is conjectured in [85] that the MIMO channel correlation matrix \mathbf{R}_H is equal to the Kronecker product of the correlation matrix \mathbf{R}_{TX} and \mathbf{R}_{RX} , i.e.,

$$\mathbf{R}_H = \mathbf{R}_{\text{TX}} \otimes \mathbf{R}_{\text{RX}}. \quad (8)$$

To verify (8), indoor MIMO channel measurements were carried out by the University of Bristol, within the European Union's IST (Information Society Technology) Program, SATURN (Smart Antenna Technology in Universal bRoadband wireless Networks) Project[88]. According to the results in [88], it is concluded that for moderate array sizes and indoor NLOS scenarios, the MIMO channel correlation matrix can be well approximated by the Kronecker product of the correlation matrices seen from both ends. For wideband MIMO channels, it has been found in [88, 92] that the Kronecker structure can be extended to each channel tap, that is,

$$\mathbf{R}_H^l = \mathbf{R}_{\text{TX}}^l \otimes \mathbf{R}_{\text{RX}}^l, \quad (9)$$

where for the l th tap, the MIMO channel correlation matrix \mathbf{R}_H^l , the transmit correlation matrix \mathbf{R}_{TX}^l , and the receive correlation matrix \mathbf{R}_{RX}^l are defined similarly as in the narrowband case.

Given that the elements of the MIMO channel matrix \mathbf{H} are zero mean complex Gaussian and that the Kronecker structure of the MIMO channel correlation

¹The correlation between the fading signals received at two antenna elements only depends on the element distance but not on the exact location.

matrix (8) holds, the narrowband MIMO channel model (5) can be rewritten as [85, 92]

$$\mathbf{H} = (\mathbf{R}_{\text{RX}})^{1/2} \mathbf{G} (\mathbf{R}_{\text{TX}})^{T/2}. \quad (10)$$

The wideband MIMO channel can be modeled by combining the Kronecker structure of the MIMO channel correlation matrix (9) with a SISO channel model (1). The channel impulse response (CIR) matrix $\mathbf{H}(t)$ can be expressed as [88]

$$\mathbf{H}(t) = \sum_{l=1}^L \sqrt{p_l} (\mathbf{R}_{\text{RX}}^l)^{1/2} \mathbf{G}_l (\mathbf{R}_{\text{TX}}^l)^{T/2} \delta(t - (l-1)\Delta\tau), \quad (11)$$

where \mathbf{G}_l is the random matrices with i.i.d. $\mathcal{CN}(0, 1)$ elements, p_l is the average power of the l th multipath component.

To reflect the underlying spatial structure of the radio environment from the Kronecker based MIMO channel models, a virtual channel representation approach has been proposed in [93]. It characterizes the MIMO channel by a virtual partitioning of the spatial domain. Combining the advantages offering by the Kronecker structure based MIMO channel model and virtual channel representation, Weichselberger *et al.* [94] recently presented a novel stochastic MIMO channel model taking into account the joint correlation of both ends of the link.

2. A generic MIMO channel model.

Most of the physical MIMO channel models are proposed to match certain scenarios or phenomena [85, 95, 90, 96]. However, they are not general enough to include all different propagation effects. In [89], a generic MIMO channel model has been proposed for outdoor macrocells and microcells. It takes into account a wide variety of propagation effects, such as a LOS component, single scattering, double scattering, far clusters, waveguiding, roof-edge diffraction, and large-scale variations.

Assuming there exist $L(t)$ multipaths between the transmitter and the receiver, the double-directional channel impulse response (DDCIR) $h(t, \tau, \theta_{\text{T}}, \theta_{\text{R}})$ can be described as [89]

$$h(t, \tau, \theta_{\text{T}}, \theta_{\text{R}}) = \sum_{l=1}^{L(t)} h_l(t, \tau_l, \theta_{\text{T},l}, \theta_{\text{R},l}), \quad (12)$$

where $h_l(\cdot)$ is the contribution from the l th multipath component (MPC), τ_l , $\theta_{\text{T},l}$, and $\theta_{\text{R},l}$ are the time delay, AOD and AOA associated with the l th MPC, respectively. Due to the movements of the scatterers, the transmitter, and the receiver, the DDCIR is time varying. The DDCIR describes the physical channel between the transmitter and the receiver.² Assume that the antenna array at both the transmitter and the receiver are small enough so that physical parameters of the MPCs do not change with the array size. Given the antenna pattern being used and the positions of the transmit and the receive arrays measured from a fixed reference point, the deterministic CIR between the i th transmit antenna and the

²It does not depend on the system setup, e.g., the antenna patterns used at the both ends of the link.

j th receive antenna can be expressed as [89]

$$H_{i,j}(t) = \sum_{l=1}^{L(t)} a_{\text{R}}(\theta_{\text{R},l}) \cdot h_l(t, \tau_l, \theta_{\text{R},l}, \theta_{\text{T},l}) \cdot a_{\text{T}}(\theta_{\text{T},l}) \cdot e^{j\langle \vec{k}(\theta_{\text{R},l}), \vec{x}_{\text{R},j} \rangle} \cdot e^{j\langle \vec{k}(\theta_{\text{T},l}), \vec{x}_{\text{T},i} \rangle}, \quad (13)$$

where $a_{\text{T}}(\cdot)$ and $a_{\text{R}}(\cdot)$ are the antenna patterns at the transmitter and the receiver, respectively. $\vec{k}(\cdot)$ is the wave vector, $\vec{x}_{\text{T},i}$ and $\vec{x}_{\text{R},j}$ are the position vectors of the i th transmit element and the j th receive element, respectively. Given the wavelength λ , the azimuth θ_{A} , the elevation θ_{E} , the definition $\theta = (\theta_{\text{A}}, \theta_{\text{E}})$, and the position vector $\vec{x} = (x, y, z)$, the operator $\langle \vec{k}(\theta_{\text{R}}) \cdot \vec{x} \rangle$ defines

$$\langle \vec{k}(\theta_{\text{R}}) \cdot \vec{x} \rangle = \frac{2\pi}{\lambda} (x \cos \theta_{\text{E}} \cos \theta_{\text{A}} + y \cos \theta_{\text{E}} \sin \theta_{\text{A}} + z \sin \theta_{\text{E}}). \quad (14)$$

The most important part of the DDCIR is to find an appropriate description of the properties of the MPCs $h_l(t, \tau_l, \theta_{\text{T},l}, \theta_{\text{R},l})$. In [89], a wide range of propagation effects have been considered to model $h_l(t, \tau_l, \theta_{\text{T},l}, \theta_{\text{R},l})$. The generic MIMO channel model gives a general framework of modeling macrocellular and microcellular MIMO channels and can be fitted to a large range of measurements; however the determination of the actual distribution of the model parameters may be a formidable task, and establishing model accuracy and reliability can be exceedingly difficult. Hence it needs to be further investigated.

In addition to the research about MIMO channel model described previously, MIMO channel modeling has also been conducted within different industrial standardization bodies. For example, MIMO channel models have been proposed by the IEEE 802.11n [97] Working Group and the 3GPP/3GPP2 Technical Specification Group [98], respectively.

2.2 MIMO channel parameter estimation

Based on the parametric channel model, i.e., the generic geometry based channel in the previous section, the relevant background literature about the channel parameter estimation, namely the time delay, AOA and AOD estimation, is discussed in this section. Such information is useful for understanding the propagation environment, and gives empirical evidence for theoretical propagation models. Moreover, they can be applied to enhance the performance of the channel impulse response estimator described in the following section, and useful for the localization of the MS in NLOS scenarios. AOA estimation is first reviewed in Section 2.2.1, it provides the fundamental methods to be used in the following sections. Section 2.2.2 considers the AOA and the time delay estimation for the single-input multiple-output (SIMO) channels. Section 2.2.3 presents the major methods for the AOA, the AOD and the time delay estimation of MIMO channels.

2.2.1 Angle of arrival estimation

AOA estimation is a rather mature research area. However, many results in this area can be easily extended to more complex cases, e.g., the joint time delay, the AOA and the AOD estimation for the MIMO channels discussed later. The AOA estimation problem is therefore first briefly reviewed in this section. Only the most influential methods are outlined, more details are available in [99, 100, 101] and the references therein.

To estimate the AOA of the received signal, antenna array must be exploited at the receiver. Assume that the time delays across the different antenna elements are much smaller than the reciprocal of the signal bandwidth, the received signals at different antennas are different phase shifted versions of the same signal. Let $s(t)$ be the complex baseband equivalent of the observed signal at a reference position. The vector-valued received signal at the receive antenna array of N_R elements can be expressed as

$$\begin{aligned}\mathbf{x}(t) &= \mathbf{a}(\theta_R)s(t) + \mathbf{w}(t), \\ \mathbf{a}(\theta_R) &= \left(e^{-j\omega_c\tau_1(\theta_R)}, e^{-j\omega_c\tau_2(\theta_R)}, \dots, e^{-j\omega_c\tau_{N_R}(\theta_R)} \right)^T,\end{aligned}\tag{15}$$

where $\mathbf{a}(\theta_R)$ is termed as the steering vector, or the array response vector, ω_c is the carrier frequency, $\tau_k(\theta_R)$, $k = 1, \dots, N_R$ denotes the time delay from the reference position to the k th element and $\mathbf{w}(t)$ defines the noise vector at the receive antenna array. Provided that the uniform linear array (ULA) is used, the first element is chosen as the reference point, and the AOA is measured with respect to the array normal, $\mathbf{a}(\theta_R)$ can be expressed as

$$\mathbf{a}(\theta_R) = \left(1, \phi, \dots, \phi^{(N_R-1)} \right)^T,\tag{16}$$

where $\phi = e^{j\frac{\omega_c\Delta_R \sin \theta_R}{c}}$, Δ_R denotes the antenna separation, c is the speed of the wave propagation. To uniquely determine θ_R , $|\angle\phi|$ must satisfy $|\angle\phi| \leq \pi$ or $\Delta \leq \lambda/2$ where λ is the wavelength. This is the well-known spatial sampling theorem.

Given that N_T different sources transmit signals $s_k(t)$, $k = 1, \dots, N_T$ to the receive antenna array simultaneously, the received signal can be formulated as

$$\mathbf{x}(t) = \sum_{k=1}^{N_T} \mathbf{a}(\theta_{R,k})s_k(t) + \mathbf{w}(t),\tag{17}$$

equivalently

$$\mathbf{x}(t) = \mathbf{A}(\theta_R)\mathbf{s}(t) + \mathbf{w}(t),\tag{18}$$

where $\mathbf{A}(\theta_R) = (\mathbf{a}(\theta_{R,1}), \dots, \mathbf{a}(\theta_{R,N_T})) \in \mathbb{C}^{N_R \times N_T}$, $\mathbf{s}(t) = (s_1(t), \dots, s_{N_T}(t))^T \in \mathbb{C}^{N_T}$, and $\mathbf{w}(t) \sim \mathcal{CN}(\mathbf{0}, \sigma^2 \mathbf{I}_{N_R})$. The classical AOA estimation problem is to determine the AOA parameters θ_{Rk} , $k = 1, \dots, N_T$ given the measurements $\mathbf{x}(t_n)$, $n = 1, \dots, N$ and the correlation matrix $\mathbf{R}_s = \mathbb{E}(\mathbf{s}(t)\mathbf{s}(t)^H)$ of the N_T -dimensional complex Gaussian vector $\mathbf{s}(t)$. In matrix form, (18) becomes

$$\mathbf{X} = \mathbf{A}(\theta_R)\mathbf{S} + \mathbf{W},\tag{19}$$

where $\mathbf{X} = (\mathbf{x}(t_1), \dots, \mathbf{x}(t_N)) \in \mathbb{C}^{N_{\text{R}} \times N}$, $\mathbf{S} = (\mathbf{s}(t_1), \dots, \mathbf{s}(t_N)) \in \mathbb{C}^{N_{\text{T}} \times N}$ and $\mathbf{W} = (\mathbf{w}(t_1), \dots, \mathbf{w}(t_N)) \in \mathbb{C}^{N_{\text{R}} \times N}$. Most AOA estimation methods use the spatial statistical covariance of the received signal

$$\mathbf{R}_{\mathbf{X}} = \text{E}(\mathbf{x}(t)\mathbf{x}^{\text{H}}(t)) = \mathbf{A}(\theta_{\text{R}})\mathbf{R}_{\text{s}}\mathbf{A}^{\text{H}}(\theta_{\text{R}}) + \sigma^2\mathbf{I}_{N_{\text{R}}}, \quad (20)$$

and the sample covariance matrix as its approximation

$$\hat{\mathbf{R}}_{\mathbf{X}} = \frac{1}{N}\mathbf{X}\mathbf{X}^{\text{H}}.$$

Beamforming techniques

The most fundamental AOA estimation method is to use conventional beamforming. The spatial spectral estimate of the received signal, referred to as conventional beamforming, takes the form

$$P_{\text{BF}}(\theta_{\text{R}}) = \frac{1}{N} \sum_{n=1}^N \frac{|\mathbf{a}^{\text{H}}(\theta_{\text{R}})\mathbf{x}(t_n)|^2}{\mathbf{a}^{\text{H}}(\theta_{\text{R}})\mathbf{a}(\theta_{\text{R}})}, \quad (21)$$

$$= \frac{\mathbf{a}^{\text{H}}(\theta_{\text{R}})\hat{\mathbf{R}}_{\mathbf{X}}\mathbf{a}(\theta_{\text{R}})}{\mathbf{a}^{\text{H}}(\theta_{\text{R}})\mathbf{a}(\theta_{\text{R}})}. \quad (22)$$

The location $\hat{\theta}_{\text{R},k}$ of the N_{T} highest peaks of $P_{\text{BF}}(\theta_{\text{R}})$ are taken as the beamforming AOA estimates. The conventional beamforming method has limited resolution determined by the array configuration. To improve the resolution of the conventional beamformer, Capon [102] proposed using the Capon spectral estimate

$$P_{\text{CAF}}(\theta_{\text{R}}) = \frac{1}{\mathbf{a}^{\text{H}}(\theta_{\text{R}})\hat{\mathbf{R}}_{\mathbf{X}}^{-1}\mathbf{a}(\theta_{\text{R}})}. \quad (23)$$

In contrast to the conventional beamformer, the resolution of the Capon beamformer improves with the SNR. However, the Capon AOA estimates still fail to take full advantage of data model (19) since the resolution does not improve with increasing N .

Subspace based methods

In the late 1970's, subspace based methods were introduced. They are based on geometry properties of the array covariance matrix. Given that $N_{\text{R}} > N_{\text{T}}$ and \mathbf{R}_{s} is full rank, the eigenvalue decomposition (EVD) of $\mathbf{R}_{\mathbf{X}}$ (20) can be partitioned into a signal subspace and a noise subspace as

$$\mathbf{R}_{\mathbf{X}} = \sum_{k=1}^{N_{\text{R}}} \lambda_k \mathbf{e}_k \mathbf{e}_k^{\text{H}} = \mathbf{E}_{\text{S}}\mathbf{\Lambda}_{\text{S}}\mathbf{E}_{\text{S}}^{\text{H}} + \mathbf{E}_{\text{N}}\mathbf{\Lambda}_{\text{N}}\mathbf{E}_{\text{N}}^{\text{H}}, \quad (24)$$

where $\lambda_1 \geq \dots \geq \lambda_{N_T} > \lambda_{N_T+1} = \dots = \lambda_{N_R} = \sigma^2$, $\mathbf{E}_S = (\mathbf{e}_1, \dots, \mathbf{e}_{N_T})$, $\mathbf{E}_N = (\mathbf{e}_{N_T+1}, \dots, \mathbf{e}_{N_R})$, $\mathbf{\Lambda}_S = \text{diag}(\lambda_1, \dots, \lambda_{N_T})$, and $\mathbf{\Lambda}_N = \sigma^2 \mathbf{I}_{N_R - N_T}$. The eigenvectors in \mathbf{E}_S span the range space of $\mathbf{A}(\boldsymbol{\theta}_R)$, which is called the signal subspace. The space spanned by the eigenvectors in \mathbf{E}_N are named the noise subspace, which is orthogonal to the range space of $\mathbf{A}(\boldsymbol{\theta}_R)$, i.e., $\mathbf{E}_N \perp \mathbf{A}(\boldsymbol{\theta}_R)$. The fundamentals of subspace methods are based on these relations.

The MUSIC (multiple signal classification) algorithm [103, 104] exploits the orthogonality relation $\mathbf{a}^H(\theta_{R,k})\mathbf{E}_N = \mathbf{0}$, $k = 1, \dots, N_T$. The noise subspace is estimated from $\hat{\mathbf{R}}_X$

$$\hat{\mathbf{E}}_X = \hat{\mathbf{E}}_S \hat{\mathbf{\Lambda}}_S \hat{\mathbf{E}}_S^H + \hat{\mathbf{E}}_N \hat{\mathbf{\Lambda}}_N \hat{\mathbf{E}}_N^H. \quad (25)$$

The MUSIC pseudospectrum is defined as

$$P_{\text{MU}}(\theta_R) = \frac{\mathbf{a}^H(\theta_R)\mathbf{a}(\theta_R)}{\mathbf{a}^H(\theta_R)\hat{\mathbf{E}}_N\hat{\mathbf{E}}_N^H\mathbf{a}(\theta_R)}. \quad (26)$$

The MUSIC algorithm calculates the AOA estimates by computing $P_{\text{MU}}(\theta_R)$ at a fine grid, and locating N_T largest local maxima. It exhibits higher resolution than the beamforming methods. However, it requires a high SNR and/or large N . Several approaches have been proposed to improve the resolution, including the min-norm algorithm [105] and the root-MUSIC algorithm [106].

The ESPRIT algorithm [107] is related to the root-MUSIC algorithm, and is computationally very efficient. It assumes that the array is composed of two identical, spatially separated subarrays. For a ULA, a popular choice is to treat the first $N_R - 1$ elements as the first subarray, and the last $N_R - 1$ elements as the second. Let \mathbf{A}_1 be the array response matrix associated with the first subarray; similarly, \mathbf{A}_2 corresponds to the second subarray. It is easy to show that

$$\mathbf{A}_2 = \mathbf{A}_1 \text{diag}(\phi_1, \dots, \phi_{N_T}). \quad (27)$$

As mentioned previously, \mathbf{E}_S spans the range space of $\mathbf{A}(\boldsymbol{\theta}_R)$ such that $\mathbf{E}_S = \mathbf{A}(\boldsymbol{\theta}_R)\mathbf{T}$ for a full rank matrix \mathbf{T} . Let \mathbf{E}_1 and \mathbf{E}_2 define the first $N_R - 1$ rows and the last $N_R - 1$ rows of \mathbf{E}_S , respectively. It follows that

$$\mathbf{E}_2 = \mathbf{E}_1 \mathbf{T} \text{diag}(\phi_1, \dots, \phi_{N_T}) \mathbf{T}^{-1}. \quad (28)$$

From (28), the ESPRIT algorithm estimates the AOAs by computing the eigenvalues of $\mathbf{E}_2 \mathbf{E}_1^\dagger$ where \mathbf{E}_1^\dagger defines the pseudoinverse of \mathbf{E}_1 . A computationally efficient implementation of the ESPRIT algorithm using only real-valued operations is proposed in [108].

Nonlinear least squares methods

The subspace methods mentioned above require that the correlation matrix \mathbf{R}_s of source signals is full rank, and the performance degrades when \mathbf{R}_s is nondiagonal.³

³However, subspace methods like the method of direction-of-arrival estimation (MODE) [109] and weighted subspace fitting (WSF) [110] work well in situations where \mathbf{R}_s is rank deficient.

Given the model (19), the straightforward approach is to use a nonlinear least-squares (NLLS) fit:

$$(\hat{\theta}_R, \hat{\mathbf{S}}) = \arg \min_{\theta_R, \mathbf{S}} \|\mathbf{X} - \mathbf{A}(\theta_R)\mathbf{S}\|^2. \quad (29)$$

This is a separable problem, the optimal solution is

$$\begin{aligned} \hat{\theta}_R &= \underset{\theta_R}{\operatorname{argmin}} \operatorname{Tr} \left(\Pi_A^\perp \hat{\mathbf{R}}_X \right), \\ \hat{\mathbf{S}} &= (\mathbf{A}^H \mathbf{A})^{-1} \mathbf{A}^H \mathbf{X}, \\ \Pi_A^\perp &= \mathbf{I} - \mathbf{A}(\mathbf{A}^H \mathbf{A})^{-1} \mathbf{A}^H. \end{aligned} \quad (30)$$

Indeed, the NLLS solution (30) coincides with the maximum likelihood (ML) estimate if the source signals are regarded as the deterministic parameters and the noise is assumed to be Gaussian. However, (30) is a d -dimensional nonlinear optimization problem which is very complex. A practical approach at a reasonable cost is to employ a relaxed optimization procedure, where AOA parameters are adjusted one at a time. A few techniques [111, 112, 113, 114] have been proposed to implement a relaxed optimization of NLLS-type criteria. The so called RELAX procedure is due to [112], it is similar to the space-alternating generalized expectation maximization (SAGE) algorithm [111] and has a simpler interpretation. In the RELAX algorithm, the "cleaned" observation matrix is defined as

$$\mathbf{X}_l = \mathbf{X} - \sum_{k \neq l} \mathbf{a}(\hat{\theta}_{R,k}) \hat{\mathbf{s}}_k, \quad (31)$$

and the relaxed criteria

$$V_l(\theta_{R,l}, \mathbf{s}_l) = \|\mathbf{X}_l - \mathbf{a}(\theta_{R,l})\mathbf{s}_l\|^2 \quad (32)$$

is minimized by

$$\hat{\theta}_{R,l} = \underset{\theta_R}{\operatorname{argmax}} \frac{\|\mathbf{a}^H(\theta_R)\mathbf{X}_l\|^2}{\|\mathbf{a}(\theta_R)\|^2}, \quad (33)$$

$$\hat{\mathbf{s}}_l = \frac{\mathbf{a}^H(\hat{\theta}_{R,l})\mathbf{X}_l}{\|\mathbf{a}(\hat{\theta}_{R,l})\|^2}. \quad (34)$$

The RELAX algorithm updates sequentially $\theta_{R,l}$ and \mathbf{s}_l for $l = 1, \dots, N_T$. At the first iteration, let $\mathbf{s}_k = 0, k > l$. The iterations continue until no significant change of the AOA parameters is observed. Such a method is usually able to rapidly yield preliminary estimates in the neighborhood of the true minimizers of the criterion function. Once sufficiently good initial estimates are available, it is preferable to switch to a Newton type local optimization method [115].

2.2.2 Single-input-multiple-output channel parameter estimation

For the AOA estimation problem considered in the preceding section, the transmitted signals are assumed to be narrowband signals; as a consequence, the MPCs can only be resolved in the space domain. When the wideband signal is transmitted, different propagation paths can also be resolved in both the space and the time domain. This section considers the simple case in which a single transmitter and multiple receivers are used, i.e., SIMO channels. The parameter estimation algorithm is based on the received signal stimulated by the known signal waveform, i.e., a training signal. Due to the significant time spread of the channels, the received signal is modeled by

$$\mathbf{x}(t) = \sum_{k=1}^d \gamma_k \mathbf{a}(\theta_{R,k}) s(t - \tau_k) + \mathbf{w}(t), \quad (35)$$

where γ_k and τ_k are the complex path gain and the time delay of the k th path, respectively.

Given samples $\mathbf{x}(t_n), n = 1, \dots, N$ from (35), and the known shape of signal $s(t)$, the parameters to be estimated in the SIMO channels are $\theta_{R,k}$, τ_k and γ_k . (35) can be written in matrix form as

$$\mathbf{X} = \sum_{k=1}^d \gamma_k \mathbf{a}(\theta_{R,k}) \mathbf{s}(\tau_k) + \mathbf{W}, \quad (36)$$

where $\mathbf{X} = (\mathbf{x}(t_1), \dots, \mathbf{x}(t_N)) \in \mathbb{C}^{N_R \times N}$, $\mathbf{s}(\tau_k) = (s(t_1 - \tau_k), \dots, s(t_N - \tau_k)) \in \mathbb{C}^{1 \times N}$ and $\mathbf{W} = (\mathbf{w}(t_1), \dots, \mathbf{w}(t_N)) \in \mathbb{C}^{N_R \times N}$. If the noise is Gaussian and spatially white, the optimal ML estimator employs the NLLS criteria

$$V(\boldsymbol{\theta}_R, \boldsymbol{\tau}, \boldsymbol{\gamma}) = \|\mathbf{X} - \sum_{k=1}^d \gamma_k \mathbf{a}(\theta_{R,k}) \mathbf{s}(\tau_k)\|_F^2. \quad (37)$$

For fixed $\boldsymbol{\theta}_R$ and $\boldsymbol{\tau}$, (37) can be easily minimized with respect to $\boldsymbol{\gamma}$. As such, $\boldsymbol{\gamma}$ can be separately optimized from $\boldsymbol{\theta}_R$ and $\boldsymbol{\tau}$. A natural approach to solve this $2d$ -NLLS problem is to apply the RELAX procedure presented in the preceding section. For example, the SAGE algorithm [116] has been applied to scenarios where also the Doppler-shifts were taken into account. In high resolution scenarios, several iterations are needed in general. The RELAX-like algorithm implies a high computational complexity. Subspace based alternatives with reduced complexities have been proposed in [117] where a computationally efficient 2D ESPRIT algorithm is exploited to determine the signal parameters based on the Fourier transform of the CIR estimate when the ULA is equipped.

2.2.3 MIMO channel parameter estimation

As discussed in Section 2.1, the MIMO transmission opens up an interesting new possibility. Besides the AOA of the incoming rays, it is also possible to find the AOD of these rays [89]. Considering the simplified DDCIR model in Section 2.1, the received signal is now modeled as

$$\mathbf{x}(t) = \sum_{k=1}^d \gamma_k \mathbf{a}_R(\theta_{R,k}) \mathbf{a}_T^T(\theta_{T,k}) \mathbf{s}(t - \tau_k) + \mathbf{w}(t), \quad (38)$$

where γ_k , $\theta_{R,k}$, $\theta_{T,k}$, and τ_k define the complex gain, the AOA, the AOD and the time delay of the k th path, respectively. $\mathbf{a}_R(\theta_{R,k}) \in \mathbb{C}^{N_R}$ and $\mathbf{a}_T(\theta_{T,k}) \in \mathbb{C}^{N_T}$ define the array response vector of the receive and the transmit antenna arrays, respectively.⁴ $\mathbf{s}(t) = \left(s_1(t), \dots, s_{N_T}(t) \right)^T \in \mathbb{C}^{N_T}$ denotes the transmitted signal.⁵ Given $\mathbf{x}(t_n)$, $n = 1, \dots, N$ and the known waveform of $\mathbf{s}(t)$, the task of the MIMO channel parameter estimation is to determine the unknown parameters γ_k , $\theta_{R,k}$, $\theta_{T,k}$ and τ_k .

The NLLS criterion in the matrix form becomes

$$V(\boldsymbol{\gamma}, \boldsymbol{\theta}_R, \boldsymbol{\theta}_T, \boldsymbol{\tau}) = \left\| \mathbf{X} - \sum_{k=1}^d \gamma_k \mathbf{a}_R(\theta_{R,k}) \mathbf{a}_T^T(\theta_{T,k}) \mathbf{S}(\tau_k) \right\|_F^2, \quad (39)$$

where $\mathbf{X} = \left(\mathbf{x}(t_1), \dots, \mathbf{x}(t_N) \right) \in \mathbb{C}^{N_R \times N}$ and $\mathbf{S}(\tau_k) = \left(\mathbf{s}(t_1 - \tau_k), \dots, \mathbf{s}(t_N - \tau_k) \right) \in \mathbb{C}^{N_T \times N}$. As mentioned in the last section, $\boldsymbol{\gamma}$ can be optimized separately from the other parameters. (39) is a 3D estimation problem. The RELAX approach applied to (39) results in the following steps. First, the clean observed matrix is calculated as

$$\mathbf{X}_l = \mathbf{X} - \sum_{k \neq l} \gamma_k \mathbf{a}_R(\theta_{R,k}) \mathbf{a}_T^T(\theta_{T,k}) \mathbf{s}(t - \tau_k). \quad (40)$$

Then, the relaxed criterion is

$$V_l(\theta_{R,l}, \theta_{T,l}, \tau_l) = \frac{|\mathbf{a}_R^H(\theta_{R,l}) \mathbf{X}_l \mathbf{S}^H(\tau_l) \mathbf{a}_T^*(\theta_{T,l})|^2}{\|\mathbf{a}_R^H(\theta_{R,l})\|^2 \|\mathbf{S}^H(\tau_l) \mathbf{a}_T^*(\theta_{T,l})\|^2}. \quad (41)$$

Once the optimum solution $(\hat{\theta}_{R,l}, \hat{\theta}_{T,l}, \hat{\tau}_l)$ has been obtained from a 3D optimization procedure, the complex path gain can be estimated as

$$\hat{\gamma}_l = \frac{\mathbf{a}_R^H(\hat{\theta}_{R,l}) \mathbf{X}_l \mathbf{S}^H(\hat{\tau}_l) \mathbf{a}_T^*(\hat{\theta}_{T,l})}{\|\mathbf{a}_R^H(\hat{\theta}_{R,l})\|^2 \|\mathbf{S}^H(\hat{\tau}_l) \mathbf{a}_T^*(\hat{\theta}_{T,l})\|^2}. \quad (42)$$

⁴(38) uses the vector representation of the MIMO channels defined in (13).

⁵The definition of $\mathbf{s}(t)$ is different from that in Section 2.2.2. Due to the focus of the thesis, if not specified, the definition in Section 2.2.3 would be used in the sequel.

An approximate solution to (39) can be found by running the above steps for $l = 1, \dots, d$ and iterating until convergence. It is obvious that the complexity of the RELAX method is very high.

Given the MIMO CIR $\mathbf{H}(t)$ which comes either from a separate estimation step or directly from the measurement data as in the channel sounder, several suboptimal methods have been proposed to reduce the complexity of the RELAX-like algorithms. The simplified DDCIR model can be written as

$$\mathbf{H}(t) = \sum_{k=1}^d \gamma_k \mathbf{a}_R(\theta_{R,k}) \mathbf{a}_T^T(\theta_{T,k}) \delta(t - \tau_k), \quad (43)$$

and the Fourier transform of (43) can be expressed as

$$\tilde{\mathbf{H}}(\omega_k) = \sum_{l=1}^d \gamma_l \mathbf{a}_R(\theta_{R,l}) \mathbf{a}_T^T(\theta_{T,l}) e^{-j\omega_k \tau_l}, \quad k = 1, \dots, M, \quad (44)$$

where M is the length of the discrete Fourier transform (DFT). In [118], the delays are first determined using the 1D ESPRIT technique, then a 2D RELAX-like approach is applied to the so called channel sample $\hat{\mathbf{H}}(\hat{\tau}_l)$. Assuming the knowledge of $\hat{\mathbf{H}}(\omega_k)$, a 3D subspace method is proposed in [119]. A novel approach which employs the IQML algorithm for the time delay estimation, and the 2D unitary ESPRIT algorithm for the joint AOA and AOD estimation will be presented in Chapter 3.

2.3 MIMO channel estimation

As stated before, all the performance gains furnished by the MIMO system are based on the assumption that all channels between the transmit antennas and the receive antennas are known. Due to complexity constraints, virtually all of today's digital wireless communication systems apply the principle of synchronized detection [120, Section 4.3.1]. This means that a channel estimate is formed and subsequently used for detection and decoding as if it were the true known channel. Channel estimation is known to be a challenging task in a wireless communication system in general, and with significant mobility in particular. Channel estimation is an extensive topic, this section only reviews several major MIMO channel estimation techniques proposed in the open literature. For a wideband MIMO system, the time dispersive or frequency selectivity due to multipath propagation is important, hence all the channels considered in this section are frequency-selective fading channels. Section 2.3.1 focuses on the single-carrier MIMO system. The MIMO-OFDM system, an important example of multicarrier MIMO system, is discussed in Section 2.3.2.

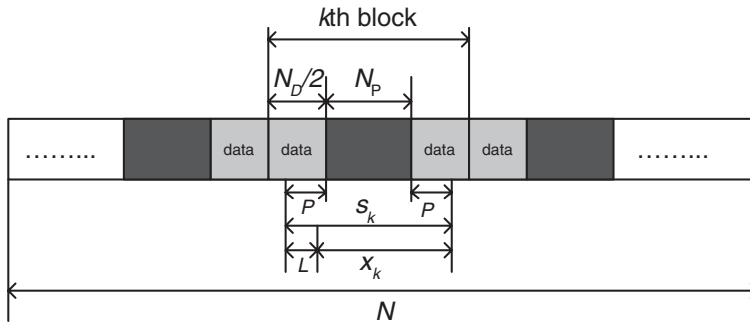


Fig. 3. Training and data symbols in a data packet.

2.3.1 Channel estimation for the single-carrier MIMO system

This section briefly reviews several important channel estimation techniques for the single-carrier MIMO system; more details are reported in [121] and references therein. In practice, the known training symbols are embedded in a data stream to facilitate the channel estimation and synchronization. As such, the training based channel estimation methods are mainly discussed. The training based channel estimation can be further improved by taking the surrounding unknown data into account, which leads to the so called enhanced training based channel estimation. The semiblind method combining the training method and pure blind methods are also briefly mentioned.

For a MIMO system with N_T transmit antennas and N_R receive antennas, the discrete time received signal sampling at the symbol rate of (2) can be modeled as

$$\mathbf{x}[n] = \sum_{l=0}^L \mathbf{H}[l] \mathbf{s}[n-l] + \mathbf{w}[n], \quad (45)$$

where $\mathbf{x}[n] \in \mathbb{C}^{N_R}$ is the received signal, $\mathbf{s}[n] \in \mathbb{C}^{N_T}$ denotes the transmitted signal, $\mathbf{H}[l]$ defines the MIMO channel matrix of order L , and $\mathbf{w}[n]$ is assumed to be zero-mean white Gaussian noise. Let $\mathbf{h}[l] = \text{vec}(\mathbf{H}[l])$, $l = 0, \dots, L$ define the column vector of stacking all the columns of $\mathbf{H}[l]$. As in [121], the simplified version of the training symbol allocation method used in [122], in which the training symbol sequence of equal length are periodically distributed within a data packet, is exploited. The placements of the training symbols within a data packet are the same for different transmit antennas. The MIMO channels are assumed to be constant during the whole data packet. We assume that the data packet consists of N symbols, in the form of K symbol blocks, where each block contains a N_P training symbol vector, surrounded at each side by $N_D/2$ unknown data symbol vectors, i.e., $N = K(N_P + N_D)$. Fig. 3 illustrates the placement of the training symbols in a data packet, and P is the number of data symbols, before and after

the training symbol part, which are exploited for the channel estimation in the observation window. Let $n_k = k(N_P + N_D) + N_D/2$ define the index of the first training symbol in the k th symbol block, and $0 \leq P \leq N_D/2$. \mathbf{s}_k and \mathbf{x}_k in Fig. 3 are defined as

$$\mathbf{s}_k = \left(\mathbf{s}^T[n_k - P], \dots, \mathbf{s}^T[n_k + N_P + P - 1] \right)^T, \quad (46)$$

$$\mathbf{x}_k = \left(\mathbf{x}^T[n_k - P + L], \dots, \mathbf{x}^T[n_k + N_P + P - 1] \right)^T, \quad (47)$$

$$\mathbf{x}_k = \mathcal{H}\mathbf{s}_k + \mathbf{w}_k, \quad (48)$$

$$\mathcal{H} = \begin{pmatrix} \mathbf{H}[L] & \cdots & \mathbf{H}[0] & & \\ & \ddots & & \ddots & \\ & & \mathbf{H}[L] & \cdots & \mathbf{H}[0] \end{pmatrix} \in \mathbb{C}^{N_R(N_P+2P-L) \times N_T(N_P+2P)}. \quad (49)$$

Define the training part of \mathbf{s}_k as

$$\mathbf{s}_{P,k} = \left(\mathbf{s}^T[n_k], \dots, \mathbf{s}^T[n_k + N_P - 1] \right)^T, \quad (50)$$

and the unknown data part as

$$\mathbf{s}_{D,k} = \left(\mathbf{s}^T[n_k - P], \dots, \mathbf{s}^T[n_k - 1], \mathbf{s}^T[n_k + N_P], \dots, \mathbf{s}^T[n_k + N_P + P - 1] \right)^T. \quad (51)$$

(48) can be split into

$$\mathbf{x}_k = \mathcal{H}_P \mathbf{s}_{P,k} + \mathcal{H}_D \mathbf{s}_{D,k} + \mathbf{w}_k, \quad (52)$$

where $\mathcal{H}_P \in \mathbb{C}^{N_R(N_P+2P-L) \times N_T N_P}$ is obtained by collecting the N_P block columns of \mathcal{H} , and $\mathcal{H}_D \in \mathbb{C}^{N_R(N_P+2P-L) \times 2N_T P}$ is obtained by collecting P left block columns and P right block columns of \mathcal{H} .

Similarly, the received signal \mathbf{x}_k can be written as a linear combination of the channel coefficient vector $\mathbf{h} = \left(\mathbf{h}^T[0], \dots, \mathbf{h}^T[L] \right)^T \in \mathbb{C}^{N_T N_R L}$. It reads

$$\mathbf{x}_k = (\mathcal{S}_k \otimes \mathbf{I}_{N_R}) \mathbf{h} + \mathbf{w}_k, \quad (53)$$

where

$$\mathcal{S}_k = \begin{pmatrix} \mathbf{s}^T[n_k - P + L] & \cdots & \mathbf{s}^T[n_k - P] \\ \vdots & \ddots & \vdots \\ \mathbf{s}^T[n_k + N_P + P - 1] & \cdots & \mathbf{s}^T[n_k + N_P + P - L - 1] \end{pmatrix}. \quad (54)$$

As in (52), (53) can also be split into a training and an unknown data part as

$$\mathbf{x}_k = (\mathcal{S}_{P,k} \otimes \mathbf{I}_{N_R}) \mathbf{h} + (\mathcal{S}_{D,k} \otimes \mathbf{I}_{N_R}) \mathbf{h} + \mathbf{w}_k, \quad (55)$$

where $\mathcal{S}_{P,k}$ and $\mathcal{S}_{D,k}$ are obtained by setting the unknown data vectors $\mathbf{s}_{D,k}$ and the training symbol vectors $\mathbf{s}_{P,k}$ to zero in \mathcal{S}_k , respectively.

Training based channel estimation

Conventional training based channel estimation methods use only those received samples that solely depend on the training symbols. Given $P = 0$, (55) results in the training based signal model

$$\mathbf{x}_k = (\mathbf{S}_{P,k} \otimes \mathbf{I}_{N_R}) \mathbf{h} + \mathbf{w}_k. \quad (56)$$

The most typical channel estimation algorithm is the ML channel estimation algorithm which exhibits good performance at a reasonable cost.

The ML channel estimate related to (56) is obtained as

$$\mathbf{h}_{\text{ML}} = \underset{\mathbf{h}}{\operatorname{argmin}} \sum_{k=0}^{K-1} \|\mathbf{x}_k - (\mathbf{S}_{P,k} \otimes \mathbf{I}_{N_R}) \mathbf{h}\|^2. \quad (57)$$

Given $K \leq N_T(L+1)/(N_P - L)$ [121], the ML channel estimate can be expressed as

$$\mathbf{h}_{\text{ML}} = \left(\left(\sum_{k=0}^{K-1} \mathbf{S}_{P,k}^H \mathbf{S}_{P,k} \right) \otimes \mathbf{I}_{N_R} \right)^{-1} \sum_{k=0}^{K-1} (\mathbf{S}_{P,k}^H \otimes \mathbf{I}_{N_R}) \mathbf{x}_k. \quad (58)$$

The MSE of the ML estimation is equal to the CRLB. It equals

$$\mathbb{E} \left((\mathbf{h}_{\text{ML}} - \mathbf{h})^H (\mathbf{h}_{\text{ML}} - \mathbf{h}) \right) = \sigma_w^2 \left(\left(\sum_{k=0}^{K-1} \mathbf{S}_{P,k}^H \mathbf{S}_{P,k} \right) \otimes \mathbf{I}_{N_R} \right)^{-1}. \quad (59)$$

Enhanced channel estimation

Conventional training based channel estimation only exploits the received samples associated with the training symbols. An enhanced channel estimate can be obtained if we also take some surrounding received data samples into account. As for Fig. 3, we consider the case where $0 < P \leq N_D/2$. Since the unknown data symbols are also involved, the estimation algorithm must estimate the unknown data symbols as well as the unknown CIR. There are two ways of coping with the unknown data symbols; one is to treat them as the deterministic parameters, the other is to assume them to be the unknown random variables with Gaussian distribution. The former results in the deterministic ML (DML) algorithm, whereas the latter leads to the Gaussian ML (GML). For the sake of simplicity, the DML is briefly reviewed in this section. More details about the GML can be found in [123]. Neither algorithm takes advantage of the finite-alphabet property of the data symbols. A method of viewing the data symbols as discrete deterministic parameters has been proposed in [124].

From (55), the enhanced ML channel estimation is obtained by solving the follow optimization problem

$$(\mathbf{h}_{\text{ML}}, \{\mathbf{s}_{D,k}\}) = \underset{(\mathbf{h}_{\text{ML}}, \{\mathbf{s}_{D,k}\})}{\operatorname{argmin}} \sum_{k=0}^{K-1} \|\mathbf{x}_k - (\mathbf{S}_{P,k} \otimes \mathbf{I}_{N_R}) \mathbf{h} - \mathcal{H}_D \mathbf{s}_{D,k}\|^2. \quad (60)$$

This can be solved by alternating minimizations between \mathbf{h} and $\{\mathbf{s}_{D,k}\}$. At the first step, assume $\hat{\mathbf{s}}_{D,k}$ to be zero. For a given estimate $\hat{\mathbf{s}}_{D,k}$, the solution of h is expressed as

$$\hat{\mathbf{h}}_{\text{ML}}(\{\hat{\mathbf{s}}_{D,k}\}) = \left(\left(\sum_{k=0}^{K-1} (\mathbf{S}_{P,k} + \hat{\mathbf{S}}_{D,k})^H (\mathbf{S}_{P,k} + \hat{\mathbf{S}}_{D,k}) \right)^{-1} \otimes \mathbf{I}_{N_R} \right) \cdot \sum_{k=0}^{K-1} \left((\mathbf{S}_{P,k} + \hat{\mathbf{S}}_{D,k})^H \otimes \mathbf{I}_{N_R} \right) \mathbf{x}_k. \quad (61)$$

The solution for $\hat{\mathbf{s}}_{D,k}$ for a given estimate $\hat{\mathbf{h}}$ is

$$\hat{\mathbf{s}}_{D,k}(\hat{\mathbf{h}}) = \mathcal{H}_D^\dagger(\mathbf{x}_k - (\mathbf{S}_{D,k} \otimes \mathbf{I}_{N_R}) \hat{\mathbf{h}}). \quad (62)$$

The procedure iterates until convergence. The CRLB and MSE of such an algorithm can be found in [121].

Semiblind channel estimation

Due to the utilization of the unknown data symbols, the enhanced channel estimation described above can be viewed as a kind of semiblind technique. However, another important semiblind channel estimation method is based on the combination of the conventional training based channel estimation algorithm with a purely blind criterion. For instance, combining the ML training based channel estimation algorithm with a quadratic blind criteria leads to a semiblind estimator

$$\hat{\mathbf{h}}_{\text{semi}} = \underset{\mathbf{h}}{\text{argmin}} \sum_{k=0}^{K-1} \|\mathbf{x}_k - (\mathbf{S}_{D,k} \otimes \mathbf{I}_{N_R}) \mathbf{h}\|^2 + \alpha \|\mathbf{\Omega} \mathbf{h}\|^2, \quad (63)$$

where $\mathbf{\Omega}$ can be obtained by some blind channel estimation methods, for example, the subspace approach [125, 126] and least-squares smoothing [127, 128]. The optimization of the weighting factor α is a well-known but essentially unsolved problem in semiblind channel estimation; an extensive discussion can be found in [129].

All the algorithms discussed above do assume no prior knowledge of the statical property of the unknown channel. Such knowledge can be applied to further improve the performance of the channel estimator; for example, the MMSE algorithm can improve the ML algorithm by optimum filtering. The details can be found in [120] and Chapter 4.

2.3.2 Channel estimation for the MIMO-OFDM system

As mentioned earlier, the frequency-selective channel can be transformed into a set of parallel frequency-flat channels in the OFDM system. As such, each subband

of the MIMO–OFDM system is a special case of a single-carrier MIMO system. However, many optimal channel estimation methods have been proposed by exploiting the OFDM structure, i.e., the dependencies between the subbands. These channel estimation algorithms are briefly reviewed in this section.

Using the frequency-domain correlation of the channel, an MMSE channel estimator for SISO–OFDM systems has been proposed in [130, 131]. In [132], the MMSE channel estimator for a SISO–OFDM system which made use of both time- and frequency-domain correlation of the frequency response of the channel has been derived. Channel estimation for single-input multiple-output (SIMO)–OFDM systems has been considered in [133]. A decision directed MMSE channel estimator has been presented for an STTC–OFDM system in [134]. A similar idea has been generalized to the MIMO–OFDM system in [135].

Signal Model

Given a MIMO–OFDM system with N_T transmit antennas and N_R receive antennas, any channel between one transmit antenna and one receive antenna is assumed to be independent of the other channels. The channel is assumed to be block-fading with a finite impulse response. It is further assumed that the successive channel snapshots correlate mutually. We also assume that the cyclic prefix (CP) duration is larger than the delay spread of the channels. The CIR vector at time n can be expressed as

$$\mathbf{h}[n] = \left(h[n, 0], h[n, 1], \dots, h[n, L-1] \right)^T, \quad (64)$$

where $L-1$ is the number of the CP samples. The channel frequency response (CFR) at time n can be expressed as

$$\tilde{\mathbf{h}}[n] = \mathbf{F}_K^L \mathbf{h}[n] \quad (65)$$

where $\mathbf{F}_K^L \in \mathbb{C}^{K \times L}$ is composed of the first left L columns of K -point FFT matrix, and K is the number of the subcarriers in one OFDM symbol.

We denote by $\mathbf{h}_{i,j}[n]$ the CIR vector and by $\tilde{\mathbf{h}}_{i,j}[n]$ the CFR vector of the forms (64) and (65) between the i th transmit antenna and the j th receive antenna during block n . Vector $\mathbf{h}_j[n] = \left(\mathbf{h}_{1,j}^T[n], \dots, \mathbf{h}_{N_T,j}^T[n] \right)^T \in \mathbb{C}^{N_T L}$ denotes a concatenation of CIR vectors from all the transmit antennas to the j th receive antenna at time n . Similarly, vector $\tilde{\mathbf{h}}_j[n] = \left(\tilde{\mathbf{h}}_{1,j}^T[n], \dots, \tilde{\mathbf{h}}_{N_T,j}^T[n] \right)^T \in \mathbb{C}^{N_T K}$ is the corresponding CFR vector concatenation. The transmitted OFDM symbol from the i th transmit antenna at time n is $\mathbf{c}_i[n] = \left(c_i[n, 1], c_i[n, 2], \dots, c_i[n, K] \right)^T \in \Xi^K$ where Ξ is the modulation symbol alphabet. Thus, at time n , the received signal block $\mathbf{r}_j[n] = \left(r_j[n, 0], r_j[n, 1], \dots, r_j[n, K-1] \right)^T \in \mathbb{C}^K$ of the j th receive antenna after FFT can be expressed as

$$\mathbf{r}_j[n] = \mathbf{C}[n] \tilde{\mathbf{h}}_j[n] + \mathbf{w}_j[n], \quad (66)$$

where

$$\begin{aligned}\mathbf{C}[n] &= \left(\mathbf{C}_1[n] \quad \mathbf{C}_2[n] \quad \dots \quad \mathbf{C}_{N_T}[n] \right) \in \Xi^{K \times N_T K}, \\ \mathbf{C}_i[n] &= \text{diag}(\mathbf{c}_i[n]) \in \Xi^{K \times K},\end{aligned}$$

$\mathbf{w}_j[n] \in \mathbb{C}^K$ is the noise vector at the j th receive antenna at time n . Noise is assumed to be white in both the time and the space domains.

Replacing CFR $\tilde{\mathbf{h}}_j[n]$ by CIR $\mathbf{h}_j[n]$ in (66) and combining the partial FFT matrix \mathbf{F}_K^L into the data matrix $\mathbf{C}[n]$, (66) can be described in terms of CIR as

$$\mathbf{r}_j[n] = \mathbf{C}[n]\mathbf{h}_j[n] + \mathbf{w}_j[n], \quad (67)$$

where

$$\mathbf{C}[n] = \left(\mathbf{C}_1[n]\mathbf{F}_K^L \quad \mathbf{C}_2[n]\mathbf{F}_K^L \quad \dots \quad \mathbf{C}_{N_T}[n]\mathbf{F}_K^L \right) \in \mathbb{C}^{K \times N_T L}.$$

The ML and MMSE Algorithm

Since the matrix $\mathbf{C}[n]$ in (67) contains the pilot symbols independent of the block index $n \in \mathcal{S}_p$, it is denoted as \mathbf{C} , and (67) can be represented as

$$\mathbf{r}_j[n] = \mathbf{C}\mathbf{h}_j[n] + \mathbf{w}_j[n], j \in \{1, 2, \dots, N_R\}. \quad (68)$$

From (68), the ML estimate of CIR $\mathbf{h}_j[n]$ becomes

$$\hat{\mathbf{h}}_{\text{ML}j}[n] = (\mathbf{C}^H \mathbf{C})^{-1} \mathbf{C}^H \mathbf{r}_j[n]. \quad (69)$$

We assume that N OFDM symbols are considered in a processing window of the MMSE channel estimator, N_p pilot symbols within the processing window, and $\{n_1, \dots, n_{N_p}\}$ defines the set of indexes of pilot symbols. We define the ML channel estimate vector as $\hat{\mathbf{h}}_{\text{ML}j} = \left(\hat{\mathbf{h}}_{\text{ML}j}^T[n_1], \dots, \hat{\mathbf{h}}_{\text{ML}j}^T[n_{N_p}] \right)^T$. It is shown in [120] that the MMSE CIR estimate $\hat{\mathbf{h}}_{\text{MMSE}j}[n]$ related to the j th receive antenna at time $n \in \mathcal{S}$ can be expressed as

$$\hat{\mathbf{h}}_{\text{MMSE}j}[n] = \mathbf{W}_j^H[n] \hat{\mathbf{h}}_{\text{ML}j}, \quad (70)$$

where $\mathbf{W}_j[n]$ is the so called Wiener filtering matrix, the calculation of which can be found in [120, 72]. The mean square error analysis of the MMSE estimator is also referred to [86, 120].

Due to the high complexity of the matrix inverse encountered in the ML and MMSE estimator, several reduced complexity channel estimation algorithms [136, 137, 138] for the MIMO-OFDM system have been proposed. Using the one-step steepest gradient method, a simplified channel estimator has been addressed in [136]. Partitioning the problem of estimating a multi-input channel into independent channel estimations, the expectation-maximization (EM) based channel estimator, which therefore avoids the matrix inversion, has been studied in [137, 138].

All the above pilot based channel estimators need the training sequences to probe the channel. The optimal training sequence for frequency offset and channel estimation in a SISO system has been considered in [139]. The training signal design for uncorrelated MIMO and correlated MIMO has been proposed in [140] and [141], respectively. Aiming at the minimum estimation error variance of the LS based estimator, the optimal pilot allocation and design for a MIMO-OFDM system has been given in [142], where also a recursive least squares (RLS) based adaptive channel estimator was addressed. Subject to the constraints of the utilization of null carriers, a preamble design method for a MIMO-OFDM system with null carriers has been studied in [143].

2.4 Mobile positioning

As mentioned in Chapter 1, most mobile positioning algorithms are based on the parameters of the LOS propagation channels, i.e., TOA, TDOA and AOA etc. Such parameters can be estimated by the algorithms reviewed in Section 2.2. Obviously, the parameter estimation errors affect the accuracy of the positioning algorithms. In particular, NLOS introduced position estimation error is the dominant error factor. Several fundamental positioning algorithms are reviewed in Section 2.4.1. Section 2.4.2 considers some proposed NLOS positioning error mitigation techniques.

2.4.1 Positioning algorithms

Various mobile positioning methods, which range from low accuracy methods based on cell identification to high accuracy methods combining wireless network information and satellite positioning, have been proposed for the different location-based services in a wireless network. These methods are typically divided into two classes, i.e., network centric methods and mobile centric methods. Network centric methods determine the positions of the MS in the network and provide the user via a specific service, whereas mobile centric methods may utilize motion models to enhance estimation accuracy. All these methods exploit measurements or estimated parameters which either explicitly or implicitly relate the MS position to the position of reference points (RP), for examples, positions of fixed stations, or to the specific behavior of the MS and its surrounding environment. For instance, the AOA gives the direction between the MS and the RP, and TOA, TDOA and received signal strength (RSS) imply the relative distance between the MS and the RP. More information about positioning in wireless networks is provided in [64, 69, 46, 62, 144].

In essence, position estimation is interpreted as a problem of solving nonlinear systems of equations. The accuracy of the solution depends on the information provided by the measurements in terms of the Fisher information matrix (FIM)

[64]. In general, the solutions are approached by applying a stochastic gradient algorithm or by numerically approximating the NLLS problem using Monte Carlo based techniques. This section presents an overview of different categories of measurements used for positioning in most wireless network and positioning algorithms associated with different measurements as in [64].

Measurements

Let $\mathbf{p}(t) = (x(t), y(t))^T$ denote the 2-D mobile position at a time t . The i th known FS position is defined by $\mathbf{p}_i(t) = (x_i(t), y_i(t))^T$. The FSs can move in time in the case of some ad-hoc networks or sensor networks. A generic measurement $y_i(t)$ obtained at the i th FS is a function $f(\mathbf{p}(t), \mathbf{p}_i(t))$ of both the MS position and the FS position, and it is contaminated by a noise item $w_i(t)$, i.e.,

$$y_i(t) = f(\mathbf{p}(t), \mathbf{p}_i(t)) + w_i(t). \quad (71)$$

Typical measurements are listed below. As in [64], all measured times are multiplied by the speed of light to get a measure in meters rather than in nanoseconds.

■ RSS:

$$y_i(t) = f_{\text{RSS}}(\|\mathbf{p}(t) - \mathbf{p}_i(t)\|) + w_i(t). \quad (72)$$

Given the transmitter and receiver powers, channel attenuation can be calculated, which is averaged over the fast fading and depends on the relative distance between the transmitter and the receiver and slow fading. According to the so called Okumura-Hata model [145], (72) becomes

$$y_i(t) = K - 10\alpha \log_{10}(\|\mathbf{p}(t) - \mathbf{p}_i(t)\|) + w_i(t), \quad (73)$$

where the standard deviation of $w_i(t)$ is 4 – 12dB depending on the environment. Alternatively, f_{RSS} of (72) can be obtained from a predicted or measured spatial digital map with the RSS values.

■ TOA:

$$\begin{aligned} y_i(t) &= f_{\text{TOA}}(\mathbf{p}(t), \mathbf{p}_i(t)) + w_i(t) \\ &= \|\mathbf{p}(t) - \mathbf{p}_i(t)\| + w_i(t). \end{aligned} \quad (74)$$

The signal's absolute travel time can be estimated in a completely synchronized network. Normally, the MS clock is not synchronized, so its clock bias is considered as a nuisance parameter. In a GSM system, the propagation time of the signal is estimated in the uplink at multiple FSs with the request of the network. The performance is determined by the synchronization accuracy, i.e., the chip rate of the system.

■ TDOA:

$$\begin{aligned} y_{i,j}(t) &= f_{\text{TDOA}}(\mathbf{p}(t), \mathbf{p}_i(t), \mathbf{p}_j(t)) + w_i(t) - w_j(t) \\ &= \|\mathbf{p}(t) - \mathbf{p}_i(t)\| - \|\mathbf{p}(t) - \mathbf{p}_j(t)\| + w_i(t) - w_j(t). \end{aligned} \quad (75)$$

The TDOA based methods eliminate the need for communicating the network synchronization to the MS, and are not affected by the MS clock bias. Therefore, it is a practical mobile measurements related to relative distance.

■ AOA:

$$\begin{aligned} y_i(t) &= f_{\text{AOA}}(\mathbf{p}(t), \mathbf{p}_i(t)) + w_i(t) \\ &= \angle(\mathbf{p}(t) - \mathbf{p}_i(t)) + w_i(t). \end{aligned} \quad (76)$$

The AOA information can be obtained from different methods ranging from low-accuracy directionally sensitive antenna, e.g., 120° for a three-sector antenna, to high-accuracy AOA estimation algorithm furnished by the antenna array.

■ Database correlation (Digital map information):

$$y_i(t) = f_{\text{MAP}}(\mathbf{p}(t)) + w_i(t). \quad (77)$$

A digital map contains, for example, RSS measurements related to the relative distance to the FS. It can be predicted or measured during the network deployment phase for the service area. Most of the shadowing is included in the maps, and the remaining shadow fading component has typically the standard deviation of 3dB. The map can also be a commercial street map for automotive terminals [146].

■ Position estimates:

$$y_i(t) = \mathbf{p}(t) + w_i(t). \quad (78)$$

A direct position estimate may be also available, e.g., from GPS, provided that a GPS receiver is equipped inside the MS.

Position Estimation

Given the measurement vector $\mathbf{y}(t) = (y_1(t), \dots, y_N(t))^T$ and associated measurement transform $\mathbf{f}(\cdot)$, and assuming that measurement noise vector $\mathbf{w}(t) = (w_1(t), \dots, w_N(t))^T \sim \mathcal{N}(\mathbf{0}, \mathbf{R}_w(t))$, where $\mathcal{N}(\mathbf{0}, \mathbf{R})$ defines the normal distribution of zero mean and autocorrelation matrix \mathbf{R} , the position estimation can be obtained by different algorithms described below.

◆ NLLS algorithm: When the measurement noise vector $\mathbf{w}(t)$ is white noise, the NLLS position estimator is an optimal approach equivalent to the ML algorithm. The NLLS based position estimate is obtained by

$$\hat{\mathbf{p}}_{\text{NLLS}}(t) = \underset{\mathbf{p}}{\operatorname{argmin}} \|\mathbf{y}(t) - \mathbf{f}(\mathbf{p}(t))\|^2. \quad (79)$$

◆ Weighted NLLS (WNLS): Provided that the $\mathbf{w}(t)$ is a colored noise vector, the NLLS estimation can be improved by the WNLS. The WNLS estimate is formulated as

$$\hat{\mathbf{p}}_{\text{WNLS}}(t) = \underset{\mathbf{p}}{\operatorname{argmin}} \left(\mathbf{y}(t) - \mathbf{f}(\mathbf{p}(t)) \right)^T \mathbf{R}_w^{-1}(t) \left(\mathbf{y}(t) - \mathbf{f}(\mathbf{p}(t)) \right). \quad (80)$$

◆ ML estimation: In a more general case, the Gaussian noise vector might be position-dependent, i.e., $\mathbf{w}(t) \sim \mathcal{N}(\mathbf{0}, \mathbf{R}_w(\mathbf{p}(t)))$, the ML estimate is formulated

as

$$\hat{\mathbf{p}}_{\text{ML}}(t) = \underset{\mathbf{p}}{\operatorname{argmin}} \left(\mathbf{y}(t) - \mathbf{f}(\mathbf{p}(t)) \right)^{\text{T}} \mathbf{R}_w^{-1}(\mathbf{p}(t)) \left(\mathbf{y}(t) - \mathbf{f}(\mathbf{p}(t)) \right) + \log \det \mathbf{R}_w(\mathbf{p}(t)), \quad (81)$$

where the term $\log \det \mathbf{R}_w(\mathbf{p}(t))$ prevents the selection of positions with large uncertainty (large $\det \mathbf{R}_w(\mathbf{p}(t))$), which could be the case with WNLS algorithm.

In general, there is no closed form solution to the algorithms above; however, numerical search methods are the natural choices, for example, steepest gradient method or Newton type methods [147, 115]. These local search algorithms require good initialization, otherwise the risk is to reach a local minima of the criteria function. It is demonstrated in [66] that a close-form solution can be obtained for the NLS problem. Further illustrations on computing the ML estimate for TDOA measurements are reported in [148, 149]. All the performance limits related to the algorithms mentioned above can be found in [64] and references therein.

2.4.2 Non-line-of-sight positioning error mitigation

All the algorithms considered in the preceding section assume that LOS propagation paths exist between the MS and the FSs. In the presence of NLOS propagation, the major positioning errors result from the measurement noise and the NLOS propagation error, which is the dominant factor [63]. In an NLOS situation, the time estimate will have a positive bias μ and probably larger variance. The PDF of the NLOS measurement error can be described by a Gaussian distribution [150] as

$$p_{\text{E}}(w_i) = \mathcal{N}(\mu, \sigma_{\text{NLOS}}^2), \quad (82)$$

where μ defines the bias introduced by the NLOS propagation, and σ_{NLOS}^2 denotes the variance of the measurement error. Detecting the NLOS paths is a difficult task in general, hence the PDF of the measurement error can be modeled by the mixture of two Gaussian distributions [150] as

$$p_{\text{E}}(w_i) = \alpha \mathcal{N}(0, \sigma_{\text{LOS}}^2) + (1 - \alpha) \mathcal{N}(\mu, \sigma_{\text{NLOS}}^2), \quad (83)$$

where α stands for the probability of measurement w_i being a result from LOS paths. To mitigate the effects of NLOS path, two methods are exploited in general. One is to use a robust error distribution as shown in (83) to design the positioning algorithm. The other is to include some searching mechanism to rule out NLOS outliers [151, 152, 153]. Approaches of the latter type have been extensively studied recently, and are briefly reviewed in this section.

Various NLOS error mitigation techniques have been proposed in the literature [151, 152, 153, 154]. Most of these techniques assume that NLOS corrupted measurements are a small portion of the total measurements. Due to the fact that NLOS corrupted measurements commonly are inconsistent with LOS expectations, they can be considered as outliers. As the GPS failure detection algorithm, measurement errors are first assumed to be Gaussian noise only, then the LS residuals

are calculated to determine if NLOS errors are present [151, 152, 153]. However, these approaches suffer from multiple NLOS measurements, because the outliers attempt to bias the final estimate to reduce the residuals. This effect can be mitigated by the use of deletion diagnostics [152, 153] where the effects of eliminating various FSs from the total set are computed and ranked. All the above-mentioned algorithms in the literature only work well with a large number of samples and a small number of outliers. However, in a practical cellular system, the number of available FSs is always limited and multiple NLOS FSs are likely to occur. It has been shown that typically only 3–6 FSs can be overheard by the MS at any time [150]. The majority of these FSs cannot be assumed to be LOS FSs. In macrocells, the propagation between an MS and its home FS is usually modeled as NLOS when the MS is far away from the FS. The home FS can only be viewed as LOS if we neglect small NLOS errors caused by local scatterers around the MS and only take the large NLOS bias into account. All other neighboring FSs can be NLOS since they are further away from the MS. In microcells, although the MS is typically modeled as being LOS with its home FS, one cannot expect the MS to be LOS with other surrounding FSs. As a consequence, only the home FS can be assumed to be LOS FS, and all other FSs should be NLOS FSs in the worst case.

Several approaches have been proposed in [63, 155, 156] to reduce estimation errors for TOA when the majority of FSs are NLOS. Since NLOS error always causes a positive bias in TOA measurements, a constrained optimization is employed to reduce the NLOS bias in [63, 156]. Generally, the distributions of NLOS errors are location dependent. When the MS is stationary or slowly moving, the NLOS error can be assumed to be static. As such, nonparametric approaches based on empirical data from various locations can be employed. For example, a pattern recognition algorithm [157] has been proposed to improve the handoff performance. Based on the statistical pattern of the received signal strength, the system can determine if a user has arrived at or is near a certain location, and if a handoff is necessary. To obtain a more accurate location estimate, other characteristics of the signal could be exploited, like a power delay profile. A mapping method utilizing a location database and a ray launch simulation tool is proposed in [158] to improve GPS positioning accuracy for the NLOS situation. These approaches give significantly better location accuracy at the cost of setting up and maintaining an empirical database.

Assuming the knowledge about the Doppler shift of each single-bounce NLOS path, the geometry based methods for mobile positioning in NLOS scenarios were presented in [159] and [160] where the scatterers and the MS is also required to be in the same straight line. Depending on how much *a priori* information is available, two approaches are proposed in [150] to mitigate NLOS errors in TDOA and TDOA/AOA location schemes: an NLOS state estimation (NSE) algorithm can be used if some prior information on NLOS errors is available from the empirical database; in the case of no knowledge about NLOS, an improved residual algorithm can be applied to detect a small number of NLOS FSs. It is demonstrated that location accuracy improvement with the methods in [150] is possible even in severe NLOS propagation conditions.

3 Space-time MIMO channel parameter estimation

The channel coefficient estimation and mobile user positioning inherently depend on the channel parameters of the underlying propagation channel, as discussed in Chapter 2. In particular, the AOAs and the AODs of the propagation paths have a significant impact on the correlation properties of the MIMO channel matrix at the receiver and the transmitter side, respectively. The variations of the channel parameters are normally slow. As will be detailed in Chapter 4, the channel coefficient estimator can be improved significantly by virtue of the correlation matrix estimated from the AOAs and the AODs. Another important application of the knowledge about the AOAs and the AODs is mobile positioning. Chapter 5 will demonstrate that the MS's position can be accurately estimated in the NLOS scenarios by capitalizing the information about both the AOAs and the AODs of the NLOS paths.

On top of the generic MIMO channel model reviewed in Section 2.1, this chapter categorizes the correlated MIMO channels into two classes, i.e., the correlated-receive independent-transmit MIMO channel and the correlated-transmit-receive MIMO channel. They correspond to two typical MIMO scenarios. Both models assume the MIMO channel contains a number of clusters consisting of waves with approximately the same time delay. The clusters related to different transmit antennas in the former model are assumed to be independent from each other, whereas the latter model assumes different transmit antennas to share a common group of clusters. The correlated-receive independent-transmit channel is characterized in terms of the time delay and the spatial signature summarizing all the contributions of the waves corresponding to the same cluster. In the correlated-transmit-receive channel model, the spatial signature can be further decomposed in terms of the AOA and the AOD of each individual path. Based on the correlated-receive independent-transmit channel, the IQML algorithm proposed in [161, 162] is extended to jointly estimate the time delay and the spatial signature of the MIMO channels. Likewise, the 2-D unitary ESPRIT algorithm in [163, 117] is applied to jointly estimate the AOAs and the AODs for the correlated-transmit-receive MIMO channel model. The CRLB and the identifiability related to these two algorithms are also presented.

The chapter is organized as follows. Section 3.1 describes two correlated MIMO channel models. The IQML based time delay and spatial signature estimation algorithm for the correlated-receive independent-transmit MIMO channels is derived in Section 3.2. Section 3.3 presents the 2-D unitary ESPRIT algorithm for jointly estimating the AOA and the AOD in the correlated-transmit-receive MIMO channels. Finally conclusions are drawn in Section 3.4.

3.1 The space-time channel model

According to the different MIMO system configurations, two types of practical space-time channel models are considered in this section. One is termed as the correlated-receive independent-transmit MIMO channels. It corresponds to the wireless MIMO systems where the structured antenna array, e.g., the ULA with antenna spacing of $\lambda/2$, is exploited at the receiver side, whereas the transmit antennas are separated far away from each other so that the MIMO channels are correlated at the receiver side and uncorrelated at the transmitter side. The other is called the correlated-transmit-receive MIMO channels. This is for those MIMO systems with the correlated antenna array equipped at both the transmitter and the receiver ends.

The correlated-receive independent-transmit MIMO channel can be considered as an intermediate channel model between the independent MIMO channel model and the correlated-transmit-receive MIMO channel model. In addition, the correlated-receive independent-transmit MIMO channel can incorporate the correlated-transmit-receive MIMO channel as a special case. Conceptually, if the transmitter is located in a rich-scattering environment, while the surroundings of the receiver have a lack of obstacles, then the correlation at the receiver will be significant, nevertheless the transmitter is assumed to be uncorrelated. Specifically, the correlated-receive independent-transmit MIMO channel characterizes several practical scenarios. For instance, when a distributed antenna array is employed at the base station, and a normal centralized antenna array is equipped at the terminal, then the forward link is a correlated-receive independent transmit MIMO channel. The dual case of such a forward link is also a correlated-receive independent-transmit MIMO channel, i.e., the reverse MIMO link where the cooperative diversity furnished by multiple terminals is employed while the normal centralized antenna array is equipped at the base station. The two types of channel models are detailed in the subsequent sections.

3.1.1 The correlated-receive independent-transmit MIMO channel

Fig. 4 illustrates the correlated-receive independent-transmit MIMO channel model. There are d_i clusters of scatterers associated with the i th transmit antenna. Con-

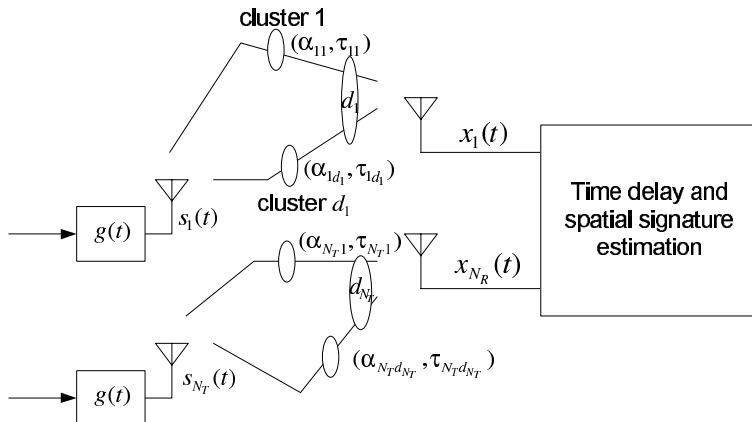


Fig. 4. Correlated–receive independent–transmit MIMO channels.

sequently $d = \sum_{i=1}^{N_T} d_i$ clusters of rays coming from N_T transmit antennas arrive at the receive antenna array¹. Each cluster of scatterers provides the receiver with several unresolvable waves with approximately the same propagation delay, the same mean AOA and the same angular spread which depends on the distribution of the scatterers within the cluster. We only consider the estimation of the time delay and the spatial signature, including the contribution of all the unresolvable waves originating from the same cluster. The estimates of the mean AOA and the angular spread could be obtained from the spatial signature estimates [161]. Thus, each cluster of waves is characterized by a pair $(\tau, \mathbf{\alpha}(t))$ where τ stands for the mean time delay of all the waves from the cluster, and $\mathbf{\alpha}(t) \in \mathbb{C}^{N_R}$ is its spatial signature vector of the form

$$\mathbf{\alpha}(t) = \sum_{i=1}^{N_{\text{ray}}} \gamma_i(t) \mathbf{a}(\theta_{R,i}),$$

where N_{ray} is the number of the rays arriving from the cluster, $\gamma_i(t)$ stands for the complex gain which is time-varying due to the Doppler spread, $\theta_{R,i}$ denotes the AOA of the i th ray which is a random variable independent of γ_i , and $\mathbf{a}(\theta_{R,i}) \in \mathbb{C}^{N_R}$ is the array response vector of the receive antenna array.

The number of the clusters and the time delay of each cluster, corresponding to a transmit antenna, change relatively slowly, and can be modelled as a constant over a reasonably long time duration. The spatial signature from each cluster is assumed to be block-fading, so that the spatial signature vector $\mathbf{\alpha}[n] = \mathbf{\alpha}(nT_B)$ during the n th transmission burst² is constant over the burst. We also assume

¹This does not imply that there are physically different d clusters along the propagation channels. In certain scenarios, some transmit antennas may share the same cluster due to the larger size of the cluster.

²It can correspond to an OFDM symbol in an OFDM system, or a time slot allocated to a

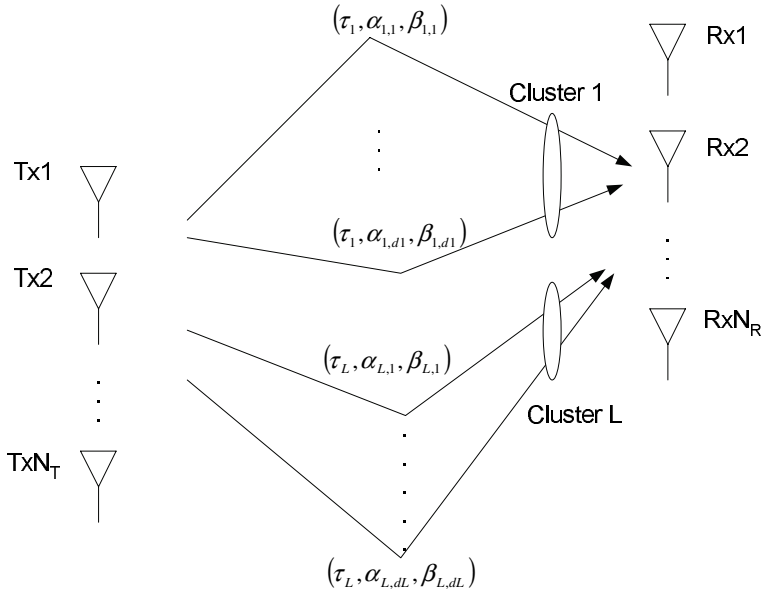


Fig. 5. Correlated-transmit-receive MIMO channels.

that the spatial signatures of different clusters are independent of each other.

3.1.2 The correlated-transmit-receive MIMO channel

When the structured antenna arrays are employed at both the transmitter and the receiver side, all the transmit antennas share the same propagation paths to the receiver, so that the MIMO channels become correlated at both the ends of the link. The correlated-transmit-receive MIMO channel model is illustrated in Fig. 5. There are d clusters of scatterers from the transmitter to the receiver. Each cluster³ provides the receiver with several propagation paths which have approximately the same time delay, but various AOAs and AODs. For instance, l_i paths with approximately the same delay are assumed to come from the i th cluster. As a result, $L = \sum_{i=1}^d l_i$ paths in the space-time domain exist between the transmitter and the receiver. As with the DDCIR model described in Section 2.1, the j th path in the i th cluster is parameterized by a four-dimensional vector $(\theta_{R,i,j}, \theta_{T,i,j}, \tau_i, \gamma_{i,j}(t))$, $i = 1, 2, \dots, d, j = 1, 2, \dots, l_i$, where $\theta_{R,i,j}$, $\theta_{T,i,j}$, $\tau_{i,j}$ and

specified user in a time division multiple access (TDMA) system. It is essential to note that one transmission burst should be shorter than the coherence time of the time varying channel during which the channel is assumed to be constant.

³Cluster herein is defined in terms of the time domain, i.e., all the unresolvable paths in the time delay domain belong to the same cluster.

$\gamma_{i,j}(t)$ stand for the AOA, the AOD, the time delay and the complex gain, respectively. We assume that L resolvable MPCs are independent of each other. As assumed in the preceding section, the number of resolvable MPCs and the parameter vector $(\theta_{R,i,j}, \theta_{T,i,j}, \tau_i)$ associated with each MPC change relatively slowly. The complex path gain $\gamma_{i,j}(t)$ is assumed to be a block-fading cyclic Gaussian random process so that $\gamma_{i,j}[n] = \gamma_{i,j}(nT_B)$ during the n th transmission burst is constant over the burst.

3.2 Joint time delay and spatial signature estimation

Based on the correlated-receive independent-transmit MIMO channel model, the estimation of the time delay and the spatial signature is considered in this section. As addressed in Section 2.2.3, ML estimation of the time delay and the spatial signature requires a multi-dimensional search which has prohibitive complexity. Several simpler algorithms based on frequency domain processing have been presented in [161]. By virtue of the specific pilot sequences with cyclic structure for the different transmitters, we extend the IQML algorithm in [161] which is applied in the SIMO environment to the MIMO channel. The performance of the proposed algorithms in terms of root mean square error (RMSE) is studied by analysis and computer simulations. The CRLB for the variance of the time delay estimate is provided as well for the benchmark of the performance comparison. In addition, the estimates of the time delay and the spatial signature obtained by the proposed algorithm can be employed as the initial searching point for the RELAX-like algorithm reviewed in Section 2.2.3.

3.2.1 Signal model and training signal design

To estimate the time delays, the training signals of a known waveform are utilized. Let T_s denote the sampling duration for the received training signal. M denotes the number of samples of the training signal⁴. Let $s_i(t)$, $1 \leq i \leq N_T$ be the continuous time training signal transmitted by the i th transmit antenna. The corresponding sampled training signal is denoted as $s_i[m] = s_i(mT_s)$, $0 \leq m \leq M-1$, $1 \leq i \leq N_T$. Let $\mathbf{s}_i = (s_i[0], s_i[1], \dots, s_i[M-1])^T \in \mathbb{C}^M$, $1 \leq i \leq N_T$ be the discrete time training signal vector transmitted by the i th transmit antenna. Vector $\boldsymbol{\tau}_i = (\tau_{i,1}, \tau_{i,2}, \dots, \tau_{i,d_i})^T \in \mathbb{R}^{d_i}$, $1 \leq i \leq N_T$ stands for the delay vector related to the transmitted signal from the i th transmit antenna whose entries denote the time delays of different clusters of scatterers.

⁴In an OFDM system, the length of the training signal can be an integer multiple of OFDM symbol duration, the optimal choice of the length of the training signal is beyond the scope of this thesis.

At the n th block, matrix $\mathbf{A}_i[n] = (\boldsymbol{\alpha}_{i,1}[n], \boldsymbol{\alpha}_{i,2}[n], \dots, \boldsymbol{\alpha}_{i,d_i}[n]) \in \mathbb{C}^{N_R \times d_i}$ defines the spatial signature matrix whose columns are the spatial signature vectors summarizing all the impinging waves through a cluster from the i th transmit antenna. Vector $\boldsymbol{\tau} = (\boldsymbol{\tau}_1^T, \boldsymbol{\tau}_2^T, \dots, \boldsymbol{\tau}_{N_T}^T)^T \in \mathbb{R}^d$ and matrix $\mathbf{A}[n] = (\mathbf{A}_1[n], \mathbf{A}_2[n], \dots, \mathbf{A}_{N_T}[n])^T \in \mathbb{C}^{d \times N_R}$ define the delay vector and the spatial signature matrix corresponding to all the transmit antennas, respectively. Vector $\mathbf{s}_i(\tau_{i,j}) = (s_i(-\tau_{i,j}), s_i(T_s - \tau_{i,j}), \dots, s_i((M-1)T_s - \tau_{i,j}))^T \in \mathbb{C}^M, 1 \leq i \leq N_T, 1 \leq j \leq d_i$ denotes the training signal of the i th transmitter with delay $\tau_{i,j}$ resulting from propagation through the j th cluster of the scatterers. Matrix $\mathbf{S}_i(\boldsymbol{\tau}_i) = (\mathbf{s}_i(\tau_{i,1}), \mathbf{s}_i(\tau_{i,2}), \dots, \mathbf{s}_i(\tau_{i,d_i})) \in \mathbb{C}^{M \times d_i}$ denotes all the delayed training signals through different clusters originating from the i th transmit antenna. At the training stage, during block n , the received signal $\mathbf{X}[n] \in \mathbb{C}^{M \times N_R}$ at the receive antenna array can be formulated as

$$\begin{aligned} \mathbf{X}[n] &= \mathbf{S}(\boldsymbol{\tau})\mathbf{A}[n] + \mathbf{W}[n], \\ \mathbf{S}(\boldsymbol{\tau}) &= (\mathbf{S}_1(\boldsymbol{\tau}_1), \mathbf{S}_2(\boldsymbol{\tau}_2), \dots, \mathbf{S}_{N_T}(\boldsymbol{\tau}_{N_T})) \in \mathbb{C}^{M \times d}, \end{aligned} \quad (84)$$

where $\mathbf{W}[n] \in \mathbb{C}^{M \times N_R}$ is the noise matrix, which is assumed to be white in both the temporal and spatial domains with variance σ_N^2 for each element.

As the basic maximum likelihood algorithm for estimating the time delay and the spatial signature requires a d -dimensional search, we are motivated to design a special training signal to reduce the complexity. With the aid of the proposed training signals, an iterative approximate ML estimator, i.e., the IQML algorithm, can be applied to the MIMO system in a similar fashion as that in [161].

The range over which the elements of $\boldsymbol{\tau}$ may vary is usually known. For instance, the maximum delay of the ETSI BRAN Channel Model A [164] is 390ns. In an OFDM system, the time delay is always assumed to be shorter than the length of the CP. We choose a cyclic shift of \mathbf{s}_1 with the shift iT_{CP} , or iT_{CP}/T_s samples, as the training signal for the i th transmit antenna $\mathbf{s}_i, i \in (2, 3, \dots, N_T)$. Fig. 6 illustrates the structure of the training signals for multiple transmit antenna in a MIMO system. The cyclic time delay shift corresponds to a phase rotation in the frequency domain. Thus, the receiver can consider multiple transmitted signals as one signal with different known delays. By means of the estimation algorithm to be described in Section 3.2.2, the estimated delay vector $\hat{\boldsymbol{\tau}}$ is $(\hat{\boldsymbol{\tau}}^1, T_{CP} + \hat{\boldsymbol{\tau}}^2, \dots, (N_T - 1)T_{CP} + \hat{\boldsymbol{\tau}}^{N_T})$, from which the real delays can be recovered. The design of an optimal training sequence \mathbf{s}_1 for the first transmit antenna is a cumbersome problem. As in [161], we use a random sequence as \mathbf{s}_1 in our simulation model.

Due to the special structure of the proposed training signals used for the time delay and spatial signature estimation, the IQML algorithm described in Section 3.2.2 assumes the known value of d . In many situations, the value of d can be found by standard detection methods as mentioned in [161, 162] and references therein. In addition, an over estimated d is a common practice in linear prediction methods. Assuming an overestimate of d , the IQML algorithm can result in an estimate of the number of clusters and the associated time delays. Given the

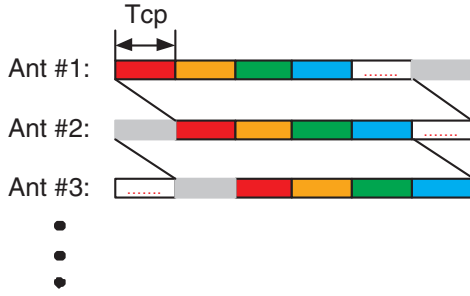


Fig. 6. Training signals for multiple transmit antennas.

estimate of d and the assumption that the time delay related to each cluster is not longer than the CP duration, the value of d_i can be found as the number of time delays which are within the interval $((i-1)T_{CP}, iT_{CP})$.

3.2.2 Iterative quadrature maximum likelihood based time delay and spatial signature estimation

As shown in [161], the ML estimation of $\boldsymbol{\tau}$ and $\mathbf{A}[n]$ requires a d -dimensional search which leads to prohibitive complexity. The IQML algorithm used earlier [161] is applied herein to reduce the complexity. The received signal in the frequency domain can be expressed as

$$\tilde{\mathbf{X}}[n] = \left(\text{diag}(\tilde{\mathbf{s}}_1)\mathbf{V}(\boldsymbol{\tau}_1), \text{diag}(\tilde{\mathbf{s}}_2)\mathbf{V}(\boldsymbol{\tau}_2), \dots, \text{diag}(\tilde{\mathbf{s}}_{N_T})\mathbf{V}(\boldsymbol{\tau}_{N_T}) \right) \mathbf{A}[n] + \tilde{\mathbf{W}}[n], \quad (85)$$

$$\mathbf{V}(\boldsymbol{\tau}_i) = \left(\mathbf{v}(\tau_{i,1}), \mathbf{v}(\tau_{i,2}), \dots, \mathbf{v}(\tau_{i,d_i}) \right) \in \mathbb{C}^{M \times d_i}, \quad (86)$$

$$\mathbf{v}(\tau_{i,k}) = \left(1, \exp(-j\frac{2\pi\tau_{i,k}}{MT_s}), \exp(-j\frac{4\pi\tau_{i,k}}{MT_s}), \dots, \exp(-j\frac{2\pi(M-1)\tau_{i,k}}{MT_s}) \right)^T. \quad (87)$$

However, this property holds for the cyclically delayed signal only. In practice, a truncated signal will be processed. Thus, (85) holds only approximately. Nevertheless, if an appropriate sampling rate is used [161], the errors in (85) can be very minor compared to the additive white noise in the received signal. Furthermore, the edge effect resulting from the truncated FFT in an OFDM system is less significant than in the usual single carrier systems, due to the existence of the CP.

Since $\tilde{\mathbf{s}}_i = \text{diag}\left(1, \dots, \exp(-j\frac{2\pi(M-1)iT_{\text{CP}}}{MT_{\text{S}}})\right)\tilde{\mathbf{s}}_1, i \in (2, 3, \dots, N_{\text{T}})$, (85) becomes

$$\begin{aligned}\tilde{\mathbf{X}}[n] &= \text{diag}(\tilde{\mathbf{s}}_1)\mathcal{V}(\bar{\boldsymbol{\tau}})\mathbf{A}[n] + \tilde{\mathbf{W}}[n], \\ \mathcal{V}(\bar{\boldsymbol{\tau}}) &= \left(\mathbf{V}(\boldsymbol{\tau}_1), \mathbf{V}(\boldsymbol{\tau}_2 + T_{\text{CP}}), \dots, \mathbf{V}(\boldsymbol{\tau}_{N_{\text{T}}} + (N_{\text{T}} - 1)T_{\text{CP}})\right), \\ \bar{\boldsymbol{\tau}} &= \left(\boldsymbol{\tau}_1, \boldsymbol{\tau}_2 + T_{\text{CP}}, \dots, \boldsymbol{\tau}_{N_{\text{T}}} + (N_{\text{T}} - 1)T_{\text{CP}}\right) \in \mathbb{C}^d.\end{aligned}\tag{88}$$

From (88), the problem of estimating the time delays for multiple transmit antennas in a multipath channel is isomorphic to that for a single transmit antenna in a multipath channel, and the time delay vector $\bar{\boldsymbol{\tau}}$ can be estimated by the IQML algorithm. The details including the complexity and convergence analysis can be found in [161, 162]. After obtaining the estimate $\hat{\boldsymbol{\tau}}$, the spatial signatures can be estimated by the least squares algorithm as follows

$$\hat{\mathbf{A}}[n] = \left(\mathbf{S}^{\text{H}}(\hat{\boldsymbol{\tau}})\mathbf{S}(\hat{\boldsymbol{\tau}})\right)^{-1}\mathbf{S}^{\text{H}}(\hat{\boldsymbol{\tau}})\mathbf{X}[n].\tag{89}$$

The covariance matrix of the spatial signature $\boldsymbol{\alpha}_{i,j}$ can be estimated by averaging the sample covariance matrices corresponding to $\boldsymbol{\alpha}_{i,j}$ as

$$\hat{\boldsymbol{\Sigma}}_{\boldsymbol{\alpha}_{i,j}} = \frac{1}{N_{\text{av}}}\sum_{n=1}^{N_{\text{av}}}\hat{\boldsymbol{\alpha}}_{i,j}[n]\hat{\boldsymbol{\alpha}}_{i,j}[n]^{\text{H}}.\tag{90}$$

3.2.3 Identifiability and the Cramér-Rao lower bound

The identifiability condition and the CRLB bound are similar to those in [161], where identifiability conditions for three different scenarios have been developed. They included a synchronous case, identical signals in the asynchronous case and distinct signals in the asynchronous case. By adopting the training signals from Section 3.2.1, the received signal can be considered as the superposition of several delayed versions of the identical training signal. Thus, the identifiability condition for the identical signal in the asynchronous case, i.e., Theorem 3.2 in [161], applies herein. As in [161], the signal is assumed to be unambiguous⁵. Because we also assume that the time delay of each cluster is within T_{CP} , and taking the artificial delay into account, the signal would need to be only locally unambiguous within $N_{\text{T}}T_{\text{CP}}$. The identifiability from [161] is described in the following theorem.

Theorem 1 *Suppose an N_{R} element array receives d identical waveforms with distinct delays $\boldsymbol{\tau}$. If the signal is unambiguous, the delay vector $\boldsymbol{\tau}$ and the spatial*

⁵The signal in the M -dimensional topological space is said to be unambiguous if every collection of M distinct vectors from the signal manifold is linearly independent.

signature matrix $\mathbf{A}[n]$ may be uniquely⁶ determined, provided that

$$d < \frac{M + m'}{2} \quad (91)$$

where $m' = \text{rank}(\mathbf{A}[n])$. If, instead

$$d < \frac{2m'}{2m' + 1}M \quad (92)$$

$\boldsymbol{\tau}$ and $\mathbf{A}[n]$ may be uniquely determined with probability one.

As in [161], Theorem 1 implies that $d < M$ clusters can be uniquely identified if $d < N_{\text{R}}$ and hence, $m' = d$. It is also demonstrated that when $m' = N_{\text{R}}$, the upper bound in (91) approaches $d < M/2$ for large M . If the identifiability condition of Theorem 1 is met, and signal and noise are uncorrelated, the maximum likelihood (ML) algorithms proposed in [161] can be developed to estimate $\boldsymbol{\tau}$ and $\mathbf{A}[n]$. Let $\tau_i, 1 \leq i \leq d$ be the i th element of the vector $\boldsymbol{\tau}$. $\frac{ds}{dt}(\cdot)$ defines the derivative of $s_1(t)$ with respect to t . \odot denotes the Hadamard product. The ML estimates are statistically efficient and achieve the CRLB, and the CRLB can be expressed as [161, 165]

$$\begin{aligned} \text{CRLB}(\hat{\boldsymbol{\tau}}) &= \frac{\sigma^2}{2} [\text{Re}(\mathbf{D}^{\text{H}}(\boldsymbol{\tau}) \mathbf{P}_{\mathbf{S}(\boldsymbol{\tau})}^{\perp} \mathbf{D}(\boldsymbol{\tau})) \odot (\mathbf{A}\mathbf{A}^{\text{H}})^{\text{T}}]^{-1}, \\ \mathbf{P}_{\mathbf{S}(\boldsymbol{\tau})}^{\perp} &= \mathbf{I}_M - \mathbf{S}(\boldsymbol{\tau})(\mathbf{S}^{\text{H}}(\boldsymbol{\tau})\mathbf{S}(\boldsymbol{\tau}))^{-1}\mathbf{S}^{\text{H}}(\boldsymbol{\tau}), \\ \mathbf{D}(\boldsymbol{\tau}) &= (\mathbf{s}'(\tau_1), \mathbf{s}'(\tau_2), \dots, \mathbf{s}'(\tau_d)) \in C^{M \times d}, \\ \mathbf{s}'(\tau_i) &= -\left(\frac{ds}{dt}(-\tau_i), \frac{ds}{dt}(T_{\text{S}} - \tau_i), \dots, \frac{ds}{dt}((M-1)T_{\text{S}} - \tau_i)\right)^{\text{T}}. \end{aligned} \quad (93)$$

The CRLB of the spatial signature can be extracted from [165]. However, it is very complicated to derive. The simple alternative of deriving the CRLB of spatial signature is assuming the time delays are known parameters, and consequently, the signal matrix $\mathbf{S}(\boldsymbol{\tau})$ is a known matrix. The CRLB of the spatial signature $\mathbf{A}[n]$ can be found in [86, Eqs. (15.56), (15.59)]. Furthermore, the LS based spatial signature estimator [161] is the optimum estimator which achieves the CRLB.

3.2.4 Numerical examples

A numerical example based on computer simulations is presented to illustrate the performance of the IQML algorithm for the time delay and the spatial signature estimation in the MIMO-OFDM system detailed in Chapter 4. Two transmit antennas and four receive antennas were employed, each channel from a transmit

⁶As mentioned in [161], when the complex amplitude of the training signal is unknown, the identifiability condition guarantees the uniqueness of the spatial signature within a scalar ambiguity. We assumed all the information about the training signal is known in this work, hence, Theorem 1 grants the uniqueness without any ambiguity.

Table 1. Channel parameters

Source	Cluster	Delay [I/Q symbols]	Mean AOA	Power
1	1	2.3	$\pi/4$	0.3220
	2	4.5	$\pi/3$	0.1184
	3	6.2	$\pi/4$	0.0436
	4	8.0	$\pi/5$	0.0160
2	1	2.0	$\pi/4$	0.3220
	2	4.2	$\pi/3$	0.1184
	3	5.0	$\pi/4$	0.0436
	4	7.0	$\pi/5$	0.0160

antenna to the receive antenna array contains four clusters of scatterers. The power delay profile and the mean AOA of each cluster of rays from two transmit antennas are listed in Table 1. The delay unit symbol in Table 1 refers to an I/Q symbol rather than an OFDM symbol. Specifically, one OFDM symbol contains K I/Q symbols. The powers of the clusters are normalized so that the sum of the powers of the rays is normalized to unity. The delays are arbitrarily chosen with the constraint that the support of the equivalent CIR is less than the length of the CP. The length of the training signal is two OFDM symbols, which is detailed in Chapter 4. In order to decrease the error from the mismatched model, oversampling rate at 4 samples/symbol is performed. As in [161], to reduce the computational load and to improve the numerical stability of the algorithm, the frequency data $\tilde{\mathbf{X}}[n]$ within a window are utilized so that only the data with significant amplitude are processed. The CRLB is calculated correspondingly by considering the data only inside the window.

Fig. 7⁷ shows the RMSE of the time delay estimation and the spatial signature estimation. The statistical efficiency of the IQML algorithm is demonstrated to be valid, and the training signal of two OFDM symbols is enough to make the algorithm close to the CRLB. In addition, the training signals usually are periodically retransmitted in practical systems. If the power delay profile of the channel varies slowly, the estimates of the time delays corresponding to several channel shots can be averaged out, resulting in further reduction in the delay estimation error.

3.3 Joint the time delay, angle of arrival and angle of departure estimation

Based on the correlated-transmit-receive MIMO model in Section 3.1.2, the spatial signature matrix $\mathbf{A}[n]$ defined in the preceding section can be parameterized

⁷The unit samples of the y-axis are only for the measure of the time delay estimation.

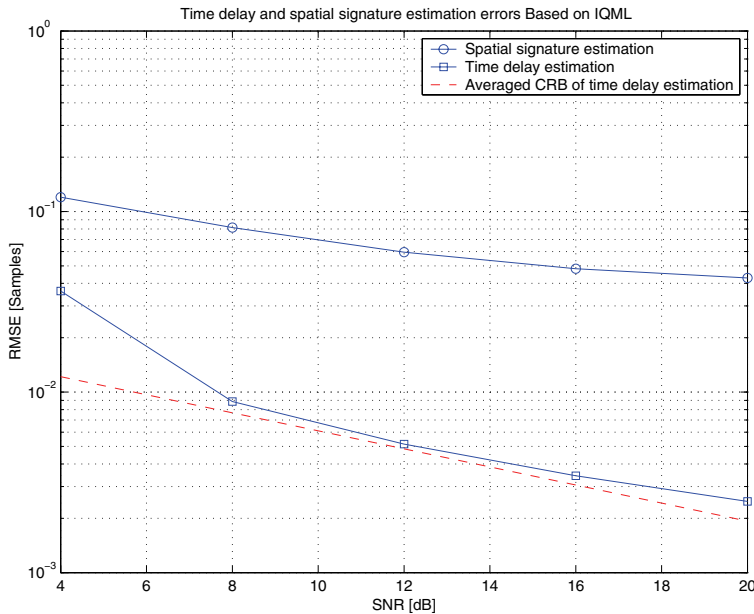


Fig. 7. RMSEs of the time delay and spatial signature estimation based on IQML, $N_T = 2$, $N_R = 4$.

in terms of AOAs and AODs. On top of this, this section applies the ideas of [163, 117] and shows that the spatial signature matrix in the correlated-transmit-receive MIMO model can be further decomposed into such a form that the 2-D unitary ESPRIT algorithm can be utilized to jointly estimate the AOAs and the AODs. As a result, by virtue of the training signal proposed in Section 3.2.1, the IQML algorithm followed by the 2-D unitary ESPRIT algorithm provides a reduced complexity method of jointly estimating the time delay, the AOAs and the AODs compared to the RELAX-like algorithm reviewed in Section 2.2.3. The identifiability and the CRLB of the algorithm are analyzed. The performance of the proposed algorithm is also studied using computer simulations.

3.3.1 Signal model

The training signals given in Section 3.2.1 are employed for the MIMO system with significant correlation at both ends of the link. Let $\boldsymbol{\tau} = (\tau_1, \tau_2, \dots, \tau_d)^T \in \mathbb{R}^d$ denote the delay vector whose entries stand for the time delays of the different clusters shown in Fig. 5. As in Section 3.2.1, the delayed training signal from the i th transmit antenna caused by the j th cluster is defined as $\mathbf{s}_i(\tau_j) =$

$\left(s_i(-\tau_j), s_i(T_s - \tau_j), \dots, s_i((M-1)T_s - \tau_j)\right)^T \in \mathbb{C}^M, 1 \leq i \leq N_T, 1 \leq j \leq d$. Matrix $\mathbf{S}_i(\boldsymbol{\tau}) = \left(\mathbf{s}_i(\tau_1), \mathbf{s}_i(\tau_2), \dots, \mathbf{s}_i(\tau_d)\right) \in \mathbb{C}^{M \times d}$ denotes all the delayed training signals through different clusters originating from the i th transmit antenna. As in (84), the received training signal $\mathbf{X}[n] \in \mathbb{C}^{M \times N_R}$ during the n th block by the receive antenna array is described as

$$\begin{aligned} \mathbf{X}[n] &= \mathbf{S}(\boldsymbol{\tau})\mathbf{A}[n] + \mathbf{W}[n], \\ \mathbf{S}(\boldsymbol{\tau}) &= \left(\mathbf{S}_1(\boldsymbol{\tau}), \mathbf{S}_2(\boldsymbol{\tau}), \dots, \mathbf{S}_{N_T}(\boldsymbol{\tau})\right) \in \mathbb{C}^{M \times N_T d}. \end{aligned} \quad (94)$$

Provided that the identifiability conditions of Theorem 1 in Section 3.2.3 are met in (94), the delay vector $\boldsymbol{\tau}$ and spatial signature matrix $\mathbf{A}[n]$ can be estimated by the IQML algorithm described in Section 3.2.2. It is of interest to note that the delay vector estimate can be further improved by averaging the time delay estimates associated with the same cluster. Consequently the estimate of the spatial signature matrix $\mathbf{A}[n]$ can be improved accordingly.

Let us assume that a uniform linear array is employed at both the transmit side and the receive side.⁸ The transmit and the receive antenna elements are spaced at a distance of Δ_T and Δ_R wavelengths, respectively. We define the following

⁸The elements of the ULA are assumed to be omnidirectional antenna elements, this is a general assumption for all the ULAs in this thesis.

expressions

$$\begin{aligned}
\theta_{i,j} &= \exp(j2\pi\Delta_{\text{R}}\sin\theta_{\text{R},i,j}), i = 1, 2, \dots, d, j = 1, 2, \dots, l_i, \\
\phi_{i,j} &= \exp(j2\pi\Delta_{\text{T}}\sin\theta_{\text{T},i,j}), i = 1, 2, \dots, d, j = 1, 2, \dots, l_i, \\
\boldsymbol{\gamma}_i[n] &= (\gamma_{i,1}[n], \dots, \gamma_{i,l_i}[n])^{\text{T}}, \\
\boldsymbol{\Delta}\boldsymbol{\gamma}_i[n] &= \text{diag}(\boldsymbol{\gamma}_i[n]), \\
\mathbf{A}_{\theta,i} &= \begin{pmatrix} 1 & \dots & 1 \\ \theta_{i,1} & \dots & \theta_{i,l_i} \\ \vdots & & \vdots \\ \theta_{i,1}^{N_{\text{R}}-1} & \dots & \theta_{i,l_i}^{N_{\text{R}}-1} \end{pmatrix} \in \mathbb{C}^{N_{\text{R}} \times l_i}, i = 1, \dots, d, \\
\mathbf{a}_{\theta,i,j} &= \left(1, \theta_{i,j}, \dots, \theta_{i,j}^{N_{\text{R}}-1}\right)^{\text{T}}, \\
\mathbf{A}_{\phi,i} &= \begin{pmatrix} 1 & \dots & 1 \\ \phi_{i,1} & \dots & \phi_{i,l_i} \\ \vdots & & \vdots \\ \phi_{i,1}^{N_{\text{T}}-1} & \dots & \phi_{i,l_i}^{N_{\text{T}}-1} \end{pmatrix} \in \mathbb{C}^{N_{\text{T}} \times l_i}, i = 1, \dots, d, \\
\mathbf{a}_{\phi,i,j} &= \left(1, \phi_{i,j}, \dots, \phi_{i,j}^{N_{\text{T}}-1}\right)^{\text{T}}, \\
\mathbf{A}_i[n] &= \mathbf{A}_{\phi,i}\boldsymbol{\Delta}\boldsymbol{\gamma}_i[n]\mathbf{A}_{\theta,i}^{\text{T}} \in \mathbb{C}^{N_{\text{T}} \times N_{\text{R}}}, i = 1, \dots, d \\
\mathcal{A}[n] &= \left(\mathcal{A}_1[n]^{\text{T}}, \dots, \mathcal{A}_d[n]^{\text{T}}\right)^{\text{T}} \in \mathbb{C}^{N_{\text{T}}d \times N_{\text{R}}}, \\
\mathcal{S}(\tau_i) &= \left(\mathbf{s}_1(\tau_i), \dots, \mathbf{s}_{N_{\text{T}}}(\tau_i)\right) \in \mathbb{C}^{M \times N_{\text{T}}}, i = 1, \dots, d \\
\mathcal{S}(\boldsymbol{\tau}) &= \left(\mathcal{S}(\tau_1), \dots, \mathcal{S}(\tau_d)\right) \in \mathbb{C}^{M \times N_{\text{T}}d}.
\end{aligned}$$

To extract the AOA and the AOD of each path from the spatial signature matrix $\mathbf{A}[n]$, we reformulate the signal model in (94) as

$$\begin{aligned}
\mathbf{X}[n] &= \sum_{i=1}^d \left(\mathbf{s}_1(\tau_i), \dots, \mathbf{s}_{N_{\text{T}}}(\tau_i)\right) \mathbf{A}_{\phi,i}\boldsymbol{\Delta}\boldsymbol{\gamma}_i[n]\mathbf{A}_{\theta,i}^{\text{T}} + \mathbf{W}[n], \\
&= \mathcal{S}(\boldsymbol{\tau})\mathcal{A}[n] + \mathbf{W}[n].
\end{aligned} \tag{95}$$

We denote $\mathbf{e}_{i,j} \in \mathbb{R}^j$, $i = 1, \dots, j$ as the j -dimensional unit vector with one at the i th entry and zeros for the others. After some mathematical manipulations, we find that

$$\begin{aligned}
\mathcal{S}(\boldsymbol{\tau}) &= \mathcal{S}(\boldsymbol{\tau})\boldsymbol{\Gamma}, \\
\mathcal{A}[n] &= \boldsymbol{\Gamma}^{\text{T}}\mathbf{A}[n], \\
\boldsymbol{\Gamma} &= \begin{pmatrix} \mathbf{I}_d \otimes \mathbf{e}_{1,N_{\text{T}}}^{\text{T}} \\ \vdots \\ \mathbf{I}_d \otimes \mathbf{e}_{N_{\text{T}},N_{\text{T}}}^{\text{T}} \end{pmatrix} \in \mathbb{R}^{N_{\text{T}}d \times N_{\text{T}}d}.
\end{aligned} \tag{96}$$

It is obvious from (96) that the estimate of $\mathcal{A}[n]$ can be calculated from the estimate of the spatial signature matrix $\mathbf{A}[n]$ obtained by the IQML algorithm considered in Section 3.2.2. Based on the transformed spatial signature matrix $\mathcal{A}[n]$, a joint AOA and AOD estimation algorithm is derived in the noise-free case in the subsequent section. The impact of the noise on the algorithm performance is analyzed and studied by the computer simulations, the results being reported in Section 3.3.4.

3.3.2 2-D unitary ESPRIT based joint angle of arrival and angle of departure estimation

The shift-invariance structure present in the decomposition $\mathcal{A}_i[n] = \mathbf{A}_{\phi,i} \Delta_{\gamma_i}[n] \mathbf{A}_{\theta,i}^T$ can be exploited to jointly estimate $(\theta_{i,j}, \phi_{i,j}), i = 1, \dots, d, j = 1, \dots, l_i$ as in [117] where the time delay and AOA are jointly estimated. We denote diagonal matrices $\boldsymbol{\theta}_i = \text{diag}(\theta_{i,1}, \dots, \theta_{i,l_i})$ and $\boldsymbol{\phi}_i = \text{diag}(\phi_{i,1}, \dots, \phi_{i,l_i})$. The main idea is outlined as follows. For some $m < N_R$, we define

$$\begin{aligned} \dot{\mathbf{A}}_{\theta,i} &= \begin{pmatrix} 1 & \cdots & 1 \\ \theta_{i,1} & \cdots & \theta_{i,l_i} \\ \vdots & & \vdots \\ \theta_{i,1}^{m-1} & \cdots & \theta_{i,l_i}^{m-1} \end{pmatrix}, \\ \ddot{\mathbf{A}}_{\theta,i} &= \begin{pmatrix} 1 & \cdots & 1 \\ \theta_{i,1} & \cdots & \theta_{i,l_i} \\ \vdots & & \vdots \\ \theta_{i,1}^{N_R-m} & \cdots & \theta_{i,l_i}^{N_R-m} \end{pmatrix}. \end{aligned} \quad (97)$$

We denote $\mathcal{A}_i^j[n], j = 1, \dots, m$ as the matrix constructed from the j th column to $(N_R - m + j)$ th column of $\mathcal{A}_i[n]$. As in [117], we construct a Hankel matrix $\mathcal{A}_{H,i}[n]$ by left shifting and stacking m copies of $\mathcal{A}_i[n]$, hence $\mathcal{A}_{H,i}[n]$ can be expressed as

$$\mathcal{A}_{H,i}[n] = \begin{pmatrix} \mathcal{A}_i^1[n] \\ \vdots \\ \mathcal{A}_i^m[n] \end{pmatrix} \in \mathbb{C}^{N_T m \times (N_R - m + 1)}, \quad (98)$$

and

$$\begin{aligned} \mathcal{A}_{H,i}[n] &= \mathcal{A}_{\phi,i} \Delta_{\gamma_i}[n] \ddot{\mathbf{A}}_{\theta,i}^T, \\ \mathcal{A}_{\phi,i} &= \begin{pmatrix} \mathbf{A}_{\phi,i} \\ \mathbf{A}_{\phi,i} \boldsymbol{\theta}_i \\ \vdots \\ \mathbf{A}_{\phi,i} \boldsymbol{\theta}_i^{m-1} \end{pmatrix}, \\ &= \dot{\mathbf{A}}_{\theta,i} \diamond \mathbf{A}_{\phi,i}, \end{aligned} \quad (99)$$

where \diamond denotes the column-wise Kronecker product. If we choose the parameter m such that $mN_T \geq l_i$ and $N_R - m + 1 \geq l_i$, and if all factors in (99) are full rank, then $\mathcal{A}_{H,i}[n]$ has rank l_i . By virtue of SVD, we can estimate $\mathcal{A}_{\phi,i}$ up to an $l_i \times l_i$ factor at the right. According to [117], determination of l_i is possible if there is a possible integer m such that $\mathcal{A}_{H,i}[n]$ becomes singular, which implies at least one of these inequalities is a strict inequality.

The shift-invariant structures present in $\mathcal{A}_{\phi,i}[n]$ can be employed to estimate $\phi_{i,j}$ and $\theta_{i,j}$ from $\mathcal{A}_{H,i}[n]$. As in [117], let us define the selection matrices

$$\begin{aligned}
\mathbf{J}_{1\theta} &= \begin{pmatrix} \mathbf{I}_{m-1} & \mathbf{0}_{m-1} \end{pmatrix}, \\
\mathbf{J}_{x\theta} &= \mathbf{J}_{1\theta} \otimes \mathbf{I}_{N_T}, \\
\mathbf{J}_{2\theta} &= \begin{pmatrix} \mathbf{0}_{m-1} & \mathbf{I}_{m-1} \end{pmatrix}, \\
\mathbf{J}_{y\theta} &= \mathbf{J}_{2\theta} \otimes \mathbf{I}_{N_T}, \\
\mathbf{J}_{1\phi} &= \begin{pmatrix} \mathbf{I}_{N_T-1} & \mathbf{0}_{N_T-1} \end{pmatrix}, \\
\mathbf{J}_{x\phi} &= \mathbf{I}_m \otimes \mathbf{J}_{1\phi}, \\
\mathbf{J}_{2\phi} &= \begin{pmatrix} \mathbf{0}_{N_T-1} & \mathbf{I}_{N_T-1} \end{pmatrix}, \\
\mathbf{J}_{y\phi} &= \mathbf{I}_m \otimes \mathbf{J}_{2\phi},
\end{aligned} \tag{100}$$

where $\mathbf{0}_K \in \mathbb{R}^K$ is K -dimensional zero vector. We apply the selection matrices in (100) to (98) as follows

$$\begin{cases} \mathbf{X}_{\phi,i}[n] = \mathbf{J}_{x\phi} \mathcal{A}_{H,i}[n], \\ \mathbf{Y}_{\phi,i}[n] = \mathbf{J}_{y\phi} \mathcal{A}_{H,i}[n], \end{cases}
\begin{cases} \mathbf{X}_{\theta,i}[n] = \mathbf{J}_{x\theta} \mathcal{A}_{H,i}[n], \\ \mathbf{Y}_{\theta,i}[n] = \mathbf{J}_{y\theta} \mathcal{A}_{H,i}[n]. \end{cases} \tag{101}$$

These matrices have the following matrix factor decompositions

$$\begin{cases} \mathbf{X}_{\phi,i}[n] = \mathcal{A}_{x\phi,i} \Delta_{\gamma_i}[n] \ddot{\mathbf{A}}_{\theta,i}^T, \\ \mathbf{Y}_{\phi,i}[n] = \mathcal{A}_{x\phi,i} \phi_i \Delta_{\gamma_i}[n] \ddot{\mathbf{A}}_{\theta,i}^T, \end{cases}
\begin{cases} \mathbf{X}_{\theta,i}[n] = \mathcal{A}_{x\theta,i} \Delta_{\gamma_i}[n] \ddot{\mathbf{A}}_{\theta,i}^T, \\ \mathbf{Y}_{\theta,i}[n] = \mathcal{A}_{x\theta,i} \theta_i \Delta_{\gamma_i}[n] \ddot{\mathbf{A}}_{\theta,i}^T, \end{cases} \tag{102}$$

where $\mathcal{A}_{x\phi,i} = \mathbf{J}_{x\phi} \mathcal{A}_{\phi,i}$ and $\mathcal{A}_{x\theta,i} = \mathbf{J}_{x\theta} \mathcal{A}_{\phi,i}$. If the decompositions in (102) are low rank factorization, we can apply the 2-D ESPRIT algorithm [163] to estimate θ_i and ϕ_i from which the AOs and AODs can be calculated straightforwardly. Due to the fact from (102) that

$$\begin{aligned}
\mathbf{Y}_{\phi,i} - \lambda \mathbf{X}_{\phi,i} &= \mathcal{A}_{x\phi,i} (\phi_i - \lambda \mathbf{I}_{l_i}) \Delta_{\gamma_i}[n] \ddot{\mathbf{A}}_{\theta,i}^T, \\
\mathbf{Y}_{\theta,i} - \lambda \mathbf{X}_{\theta,i} &= \mathcal{A}_{x\theta,i} (\theta_i - \lambda \mathbf{I}_{l_i}) \Delta_{\gamma_i}[n] \ddot{\mathbf{A}}_{\theta,i}^T,
\end{aligned} \tag{103}$$

$\boldsymbol{\theta}_i$ and $\boldsymbol{\phi}_i$ are obtained by the rank reducing numbers of the pencil $(\mathbf{Y}_{\theta,i}, \mathbf{X}_{\theta,i})$ and the $(\mathbf{Y}_{\phi,i}, \mathbf{X}_{\phi,i})$, respectively. This generalized eigenvalue decomposition problem can be solved by finding the nonzero eigenvalues of $\mathbf{X}_{\theta,i}^\dagger \mathbf{Y}_{\theta,i}$ and $\mathbf{X}_{\phi,i}^\dagger \mathbf{Y}_{\phi,i}$. Since $\mathbf{X}_{\theta,i}^\dagger \mathbf{Y}_{\theta,i}$ and $\mathbf{X}_{\phi,i}^\dagger \mathbf{Y}_{\phi,i}$ have the same eigenvectors caused by the factor $\ddot{\mathbf{A}}_{\theta,i}^\top$, the correct pairing of $\phi_{i,j}$ and $\theta_{i,j}$ is obtained by the joint diagonalization of the following matrices

$$\begin{aligned}\mathbf{X}_{\theta,i}^\dagger \mathbf{Y}_{\theta,i} &= \mathbf{T}^{-1} \boldsymbol{\theta}_i \mathbf{T}, \\ \mathbf{X}_{\phi,i}^\dagger \mathbf{Y}_{\phi,i} &= \mathbf{T}^{-1} \boldsymbol{\phi}_i \mathbf{T}.\end{aligned}\quad (104)$$

To improve the performance of the algorithm, some data extension techniques, e.g., spatial smoothing and forward-backward averaging [117], are applied to the matrix $\mathcal{A}_{H,i}[n]$. This is followed by the real processing, which transforms the complex matrix into a real matrix. Finally, the simultaneous diagonalization of two real matrices can be obtained from the SVD of the complex matrix with two real matrices as the real and imaginary part. We detail the whole procedure of joint AOA and AODs estimation in the following steps.

Step 1: Spatial smoothing and forward-backward averaging

Spatial smoothing [166] was originally proposed for solving the usual AOA problem when coherent signals are present. This technique has been integrated into the shift-invariance joint angle and delay estimation (SIJADE) algorithm in [117]. In the same fashion as [117], for integers $2 \leq m_1 \leq N_R$ and $1 \leq m_2 \leq N_T - 1$, let us define

$$\mathcal{A}_i^{(r,l)}[n] = \begin{pmatrix} \mathcal{A}_{i,r,l}[n] & \cdots & \mathcal{A}_{i,r,N_R-m_1+l}[n] \\ \vdots & & \vdots \\ \mathcal{A}_{i,N_T-m_2+r,l}[n] & \cdots & \mathcal{A}_{i,N_T-m_2+r,N_R-m_1+l}[n] \end{pmatrix}, 1 \leq r \leq m_2, 1 \leq l \leq m_1,$$

and redefine $\mathcal{A}_{H,i}[n]$ in (98) as

$$\mathcal{A}_{H,i}[n] = \begin{pmatrix} \mathcal{A}_i^{(1,1)}[n] & \cdots & \mathcal{A}_i^{(m_2,1)}[n] \\ \vdots & & \vdots \\ \mathcal{A}_i^{(1,m_1)}[n] & \cdots & \mathcal{A}_i^{(m_2,m_1)}[n] \end{pmatrix} \in \mathbb{C}^{m_1(N_T-m_2+1) \times m_2(N_R-m_1+1)}.\quad (105)$$

We define the matrix $\mathbf{\Pi}_N$ as the matrix with reverse order of the rows of \mathbf{I}_N . Let $(\cdot)^*$ denote the complex conjugate of the matrix (\cdot) . The extension of the matrix $\mathcal{A}_{H,i}[n]$ by forward-backward averaging is obtained as

$$\begin{aligned}\mathcal{A}_{e,H,i}[n] &= \left(\mathcal{A}_{H,i}[n], \mathbf{\Pi}_{m_1(N_T-m_2+1)} \mathcal{A}_{H,i}^*[n] \right) \in \mathbb{C}^{m_1(N_T-m_2+1) \times 2m_2(N_R-m_1+1)}, \\ &= \left(\mathcal{A}_{\phi,i} \Delta_{\gamma_i}[n] \ddot{\mathcal{A}}_{\theta,i}^\top, \mathbf{\Pi}_{m_1(N_T-m_2+1)} \mathcal{A}_{\phi,i}^* \Delta_{\gamma_i}^*[n] (\ddot{\mathcal{A}}_{\theta,i}^\top)^* \right),\end{aligned}\quad (106)$$

where $\ddot{\mathcal{A}}_{\theta,i}^\top = \left(\ddot{\mathbf{A}}_{\theta,i}^\top, \boldsymbol{\phi}_i \ddot{\mathbf{A}}_{\theta,i}^\top, \dots, \boldsymbol{\phi}_i^{m_2-1} \ddot{\mathbf{A}}_{\theta,i}^\top \right) \in \mathbb{C}^{l_i \times m_2(N_R-m_1+1)}$, and $\ddot{\mathbf{A}}_{\theta,i}$ is

shown in (97) with m_1 replacing m . It can be shown that

$$\begin{aligned}
\mathbf{\Pi}_{m_1(N_T-m_2+1)} \mathcal{A}_{\phi,i}^* &= \left(\mathbf{\Pi}_{m_1} (\dot{\mathbf{A}}_{\theta,i})^* \right) \diamond \left(\mathbf{\Pi}_{N_T-m_2+1} \mathbf{A}_{\phi,i}^* \right), \\
&= \left(\dot{\mathbf{A}}_{\theta,i} \boldsymbol{\theta}_i^{-(m_1-1)} \right) \diamond \left(\mathbf{A}_{\phi,i} \boldsymbol{\phi}_i^{-(N_T-m_2)} \right), \\
&= \left(\dot{\mathbf{A}}_{\theta,i} \diamond \mathbf{A}_{\phi,i} \right) \boldsymbol{\theta}_i^{-(m_1-1)} \boldsymbol{\phi}_i^{-(N_T-m_2)}, \\
&= \left(\mathcal{A}_{\phi,i} \right) \boldsymbol{\theta}_i^{-(m_1-1)} \boldsymbol{\phi}_i^{-(N_T-m_2)}, \tag{107}
\end{aligned}$$

where $\dot{\mathbf{A}}_{\theta,i}$ is denoted in (97) with m replaced by m_1 .

Substituting (107) into (106), (106) becomes

$$\begin{aligned}
\mathcal{A}_{e,H,i}[n] &= \mathcal{A}_{i,1} \mathcal{A}_{i,2}, \\
\mathcal{A}_{i,1} &= \mathcal{A}_{\phi,i} \boldsymbol{\theta}_i^{-(m_1-1)/2} \boldsymbol{\phi}_i^{-(N_T-m_2)/2}, \\
&= \left(\dot{\mathbf{A}}_{\theta,i} \boldsymbol{\theta}_i^{-(m_1-1)/2} \right) \diamond \left(\mathbf{A}_{\phi,i} \boldsymbol{\phi}_i^{-(N_T-m_2)/2} \right), \\
&\triangleq \bar{\mathbf{A}}_{\theta,i} \diamond \bar{\mathbf{A}}_{\phi,i}, \\
\mathcal{A}_{i,2} &= \left(\boldsymbol{\theta}_i^{(m_1-1)/2} \boldsymbol{\phi}_i^{(N_T-m_2)/2} \Delta_{\gamma_i}^T [n] \ddot{\mathcal{A}}_{\theta,i}^T \boldsymbol{\theta}_i^{-(m_1-1)/2} \boldsymbol{\phi}_i^{-(N_T-m_2)/2} \Delta_{\gamma_i}^* [n] (\ddot{\mathcal{A}}_{\theta,i}^T)^* \right),
\end{aligned}$$

it is interesting to note that $\bar{\mathbf{A}}_{\theta,i}$ and $\bar{\mathbf{A}}_{\phi,i}$ have the conjugate centrosymmetric property which is exploited by the unitary ESPRIT algorithm in the following procedure.

Step 2: Real processing and rank reduction

To use the 2-D ESPRIT to perform the joint diagonalization [163] for the joint AOA and AODs estimation, real processing is needed to transform the matrix $\mathcal{A}_{e,H,i}[n]$ into a real matrix so that the eigenvalues of the matrix are real. It is shown in the following that complex matrix $\mathcal{A}_{e,H,i}[n]$ can be made real by two transform matrices \mathbf{T}_L and \mathbf{T}_R which are left-multiplied and right-multiplied to $\mathcal{A}_{e,H,i}[n]$, respectively. In detail, \mathbf{T}_L and \mathbf{T}_R are expressed as

$$\begin{aligned}
\mathbf{T}_L &= \mathbf{Q}_{m_1}^H \otimes \mathbf{Q}_{N_T-m_2+1}^H, \\
\mathbf{T}_R &= \begin{pmatrix} \mathbf{I}_{m_2(N_R-m_1+1)} & j\mathbf{I}_{m_2(N_R-m_1+1)} \\ \mathbf{I}_{m_2(N_R-m_1+1)} & -j\mathbf{I}_{m_2(N_R-m_1+1)} \end{pmatrix}, \tag{108}
\end{aligned}$$

where $j^2 = -1$, the unitary matrices \mathbf{Q}_m and \mathbf{Q}_{N_T} are defined as

$$\mathbf{Q}_N = \begin{cases} \frac{1}{\sqrt{2}} \begin{pmatrix} \mathbf{I}_K & j\mathbf{I}_K \\ \mathbf{\Pi}_K & -j\mathbf{\Pi}_K \end{pmatrix}, & N = 2K, \\ \frac{1}{\sqrt{2}} \begin{pmatrix} \mathbf{I}_K & 0 & j\mathbf{I}_K \\ \mathbf{0}_K^T & \sqrt{2} & \mathbf{0}_K^T \\ \mathbf{\Pi}_K & 0 & -j\mathbf{\Pi}_K \end{pmatrix}, & N = 2K + 1. \end{cases} \tag{109}$$

Due to the conjugate centrosymmetric property of $\bar{\mathbf{A}}_{\theta,i}$ and $\bar{\mathbf{A}}_{\phi,i}$, we have the

following real matrices

$$\begin{aligned} D_{\theta,i} &= \mathbf{Q}_{m_1}^H \bar{\mathbf{A}}_{\theta,i}, \\ D_{\phi,i} &= \mathbf{Q}_{N_T-m_2+1}^H \bar{\mathbf{A}}_{\phi,i}. \end{aligned} \quad (110)$$

Consequently, $\mathbf{A}_{i,1}$ becomes a real matrix $\mathbf{A}_{i,1,R}$ by left-multiplication of \mathbf{T}_L as

$$\begin{aligned} \mathbf{A}_{i,1,R} &= \mathbf{T}_L \mathbf{A}_{i,1}, \\ &= D_{\theta,i} \diamond D_{\phi,i}. \end{aligned} \quad (111)$$

Similarly, $\mathbf{A}_{i,2}$ is converted to a real matrix $\mathbf{A}_{i,2,R}$ by right-multiplication of \mathbf{T}_R

$$\begin{aligned} \mathbf{A}_{i,2,R} &= \mathbf{A}_{i,2} \mathbf{T}_R, \\ &= 2 \left(\text{Re}(\theta_i^{(m_1-1)/2}) \phi_i^{(N_T-m_2)/2} \Delta_{\gamma_i}[n] \ddot{\mathbf{A}}_{\theta,i}^T, \right. \\ &\quad \left. - \text{Im}(\theta_i^{(m_1-1)/2}) \phi_i^{(N_T-m_2)/2} \Delta_{\gamma_i}[n] \ddot{\mathbf{A}}_{\theta,i}^T \right). \end{aligned} \quad (112)$$

As a result, the complex matrix $\mathbf{A}_{e,H,i}[n]$ can be transformed to a real matrix $\mathbf{A}_{e,R,i}[n]$ as follows

$$\begin{aligned} \mathbf{A}_{e,R,i}[n] &= \mathbf{T}_L \mathbf{A}_{e,H,i}[n] \mathbf{T}_R, \\ &= \mathbf{A}_{i,1,R} \mathbf{A}_{i,2,R}. \end{aligned} \quad (113)$$

In the next step, the l_i -dimensional subspace spanned by the $\mathbf{A}_{i,1,R}$ is exploited to extract the information about the AOA and the AODs. However, due to the noise, $\mathbf{A}_{e,R,i}[n]$ is full rank in practice. We apply the SVD to $\mathbf{A}_{e,R,i}[n]$, and utilize the l_i -dimensional dominant column spaces $\mathbf{U}_{i,R}$ as the approximation of the space spanned by $\mathbf{A}_{i,1,R}[n]$, i.e., $\mathbf{A}_{i,1,R}[n] = \mathbf{U}_{i,R} \mathbf{T}$ where $\mathbf{T} \in \mathbb{R}^{l_i \times l_i}$ is invertible.

Step 3: 2-D unitary ESPRIT

By virtue of the shift-invariant structures present in $\bar{\mathbf{A}}_{\theta,i}$ and $\bar{\mathbf{A}}_{\phi,i}$, the following expressions can be obtained

$$\begin{aligned} \mathbf{J}_{x\theta} \mathbf{T}_L^H \mathbf{T}_L \mathbf{A}_{i,1} \boldsymbol{\theta}_i &= \mathbf{J}_{y\theta} \mathbf{T}_L^H \mathbf{T}_L \mathbf{A}_{i,1}, \\ \mathbf{J}_{x\phi} \mathbf{T}_L^H \mathbf{T}_L \mathbf{A}_{i,1} \boldsymbol{\phi}_i &= \mathbf{J}_{y\phi} \mathbf{T}_L^H \mathbf{T}_L \mathbf{A}_{i,1}, \end{aligned} \quad (114)$$

where $\mathbf{J}_{x\theta}$, $\mathbf{J}_{y\theta}$, $\mathbf{J}_{x\phi}$ and $\mathbf{J}_{y\phi}$ can be obtained from (100) replacing m and N_T by m_1 and $N_T - m_2 + 1$, respectively. It follows from (111) that

$$\mathbf{J}_{x\theta} \mathbf{T}_L^H \mathbf{A}_{i,1,R} \boldsymbol{\theta}_i = \mathbf{J}_{y\theta} \mathbf{T}_L^H \mathbf{A}_{i,1,R}, \quad (115)$$

$$\mathbf{J}_{x\phi} \mathbf{T}_L^H \mathbf{A}_{i,1,R} \boldsymbol{\phi}_i = \mathbf{J}_{y\phi} \mathbf{T}_L^H \mathbf{A}_{i,1,R}. \quad (116)$$

We pre-multiply $\mathbf{Q}_{m_1-1}^H \otimes \mathbf{Q}_{N_T-m_2+1}^H$ and $\mathbf{Q}_{m_1}^H \otimes \mathbf{Q}_{N_T-m_2}^H$ to the both sides of (115) and (116), respectively. As a consequence, we obtain

$$\left(\mathbf{Q}_{m_1-1}^H \mathbf{J}_{1\theta} \mathbf{Q}_{m_1} \otimes \mathbf{I}_{N_T-m_2+1} \right) \mathbf{A}_{i,1,R} \boldsymbol{\theta}_i = \left(\mathbf{Q}_{m_1-1}^H \mathbf{J}_{2\theta} \mathbf{Q}_{m_1} \otimes \mathbf{I}_{N_T-m_2+1} \right) \mathbf{A}_{i,1,R}, \quad (117)$$

$$\left(\mathbf{I}_{m_1} \otimes \mathbf{Q}_{N_T-m_2}^H \mathbf{J}_{1\phi} \mathbf{Q}_{N_T-m_2+1} \right) \mathbf{A}_{i,1,R} \boldsymbol{\phi}_i = \left(\mathbf{I}_{m_1} \otimes \mathbf{Q}_{N_T-m_2}^H \mathbf{J}_{2\phi} \mathbf{Q}_{N_T-m_2+1} \right) \mathbf{A}_{i,1,R}. \quad (118)$$

It is interesting to note that

$$\begin{aligned} \left(\mathbf{Q}_{m_1-1}^H \mathbf{J}_{1\theta} \mathbf{Q}_{m_1} \otimes \mathbf{I}_{N_T-m_2+1} \right)^* &= \left(\mathbf{Q}_{m_1-1}^H \mathbf{J}_{2\theta} \mathbf{Q}_{m_1} \otimes \mathbf{I}_{N_T-m_2+1} \right), \\ \left(\mathbf{I}_{m_1} \otimes \mathbf{Q}_{N_T-m_2}^H \mathbf{J}_{1\phi} \mathbf{Q}_{N_T-m_2+1} \right)^* &= \left(\mathbf{I}_{m_1} \otimes \mathbf{Q}_{N_T-m_2}^H \mathbf{J}_{2\phi} \mathbf{Q}_{N_T-m_2+1} \right). \end{aligned}$$

We define

$$\begin{aligned} \mathbf{B}_\theta &= \left(\mathbf{Q}_{m_1-1}^H \mathbf{J}_{2\theta} \mathbf{Q}_{m_1} \otimes \mathbf{I}_{N_T-m_2+1} \right), \\ &= \mathbf{B}_{\theta,R} + j\mathbf{B}_{\theta,I}, \\ \mathbf{B}_\phi &= \left(\mathbf{I}_{m_1} \otimes \mathbf{Q}_{N_T-m_2}^H \mathbf{J}_{2\phi} \mathbf{Q}_{N_T-m_2+1} \right) \\ &= \mathbf{B}_{\phi,R} + j\mathbf{B}_{\phi,I}, \\ \tilde{\theta}_{i,j} &= \tan\left(\pi \Delta_R \sin(\theta_{R,i,j})\right), i = 1, \dots, d, j = 1, \dots, l_i, \\ \tilde{\phi}_{i,j} &= \tan\left(\pi \Delta_T \sin(\theta_{T,i,j})\right), i = 1, \dots, d, j = 1, \dots, l_i, \\ \tilde{\boldsymbol{\theta}}_i &= \text{diag}\left(\tilde{\theta}_{i,1}, \dots, \tilde{\theta}_{i,l_i}\right), \\ \tilde{\boldsymbol{\phi}}_i &= \text{diag}\left(\tilde{\phi}_{i,1}, \dots, \tilde{\phi}_{i,l_i}\right). \end{aligned} \tag{119}$$

We apply (119) to (117) and (118), and the following expressions can be obtained with some mathematical manipulation

$$\begin{aligned} \mathbf{B}_{\theta,R} \mathcal{A}_{i,1,R} \tilde{\boldsymbol{\theta}}_i &= \mathbf{B}_{\theta,I} \mathcal{A}_{i,1,R}, \\ \mathbf{B}_{\phi,R} \mathcal{A}_{i,1,R} \tilde{\boldsymbol{\phi}}_i &= \mathbf{B}_{\phi,I} \mathcal{A}_{i,1,R}. \end{aligned} \tag{120}$$

It follows that

$$\begin{aligned} \mathbf{T} \tilde{\boldsymbol{\theta}}_i \mathbf{T}^{-1} &= (\mathbf{B}_{\theta,R} \mathbf{U}_{i,R})^\dagger \mathbf{B}_{\theta,I} \mathbf{U}_{i,R}, \\ \mathbf{T} \tilde{\boldsymbol{\phi}}_i \mathbf{T}^{-1} &= (\mathbf{B}_{\phi,R} \mathbf{U}_{i,R})^\dagger \mathbf{B}_{\phi,I} \mathbf{U}_{i,R}. \end{aligned} \tag{121}$$

Due to the fact that two matrices on the right hand side of (121) have the same eigenvectors, i.e., the column vectors of \mathbf{T} , the AOAs and AODs are able to be jointly estimated by a complex eigenvalue decomposition as follows

$$\begin{aligned} \boldsymbol{\Lambda}_i &= \text{EIG}\left((\mathbf{B}_{\theta,R} \mathbf{U}_{i,R})^\dagger \mathbf{B}_{\theta,I} \mathbf{U}_{i,R} + j(\mathbf{B}_{\phi,R} \mathbf{U}_{i,R})^\dagger \mathbf{B}_{\phi,I} \mathbf{U}_{i,R}\right), \\ \tilde{\boldsymbol{\theta}}_i &= \text{Re}\left(\boldsymbol{\Lambda}_i\right), \\ \tilde{\boldsymbol{\phi}}_i &= \text{Im}\left(\boldsymbol{\Lambda}_i\right). \end{aligned} \tag{122}$$

It is observed from (121) that $\tilde{\theta}_{i,j}$ and $\tilde{\phi}_{i,j}$ corresponding to the same eigenvector, i.e., the column vector of \mathbf{T} are associated with the same propagation path.

3.3.3 Identifiability and the Cramér-Rao lower bound

As in [117], the necessary conditions for identifying θ_i and ϕ_i from (102) and (106) are

$$\begin{aligned} a) \quad & l_i \leq (m_1 - 1)(N_T - m_2 + 1), \\ b) \quad & l_i \leq m_1(N_T - m_2), \\ c) \quad & l_i \leq 2m_2(N_R - m_1 + 1). \end{aligned} \tag{123}$$

Because all l_i paths within the i th cluster have the approximately the same time delay τ_i , different paths will have different AOAs and AODs. Therefore, (123) also guarantees the submatrices $\mathcal{A}_{x\phi,i}$ and $\mathcal{A}_{x\theta,i}$ of $\mathcal{A}_{\phi,i}$ and $\mathcal{A}_{\theta,i}$ are of full rank l_i . As a consequence, (123) shows the necessary and sufficient conditions for identifiability of l_i rays. Subject to (123), the maximum number of rays within a cluster that can be identified for given N_T and N_R can be optimizing over m_1 and m_2 . When we assume continuous parameters m_1 and m_2 , analytical optimal solutions are possible.

As shown in the preceding section, the AOAs $\theta_{R,i} \in \mathbb{R}^{l_i}, i = 1, \dots, d$ and the AODs $\theta_{T,i} \in \mathbb{R}^{l_i}, i = 1, \dots, d$ can be estimated from the spatial signature estimate $\hat{\mathcal{A}}_i[n]$. Due to the estimation error, $\hat{\mathcal{A}}_i[n]$ can be expressed as

$$\hat{\mathcal{A}}_i[n] = \mathbf{A}_{\phi,i} \Delta_{\gamma,i}[n] \mathbf{A}_{\theta,i}^T + \mathbf{W}_i[n], \tag{124}$$

where $\mathbf{W}_i[n]$ is the estimation error matrix whose elements are assumed to be i.i.d complex Gaussian random variables with zero-mean and variance σ_s^2 . $\text{vec}(\cdot)$ stacks all the columns of the matrix into a single column vector. We define the following expressions

$$\begin{aligned} \hat{\mathbf{a}}_{\theta,\phi,i}[n] &= \text{vec}(\hat{\mathcal{A}}_i[n]), \\ \mathbf{A}_{\theta,\phi,i} &= \mathbf{A}_{\theta,i} \diamond \mathbf{A}_{\phi,i}, \\ \mathbf{w}_i[n] &= \text{vec}(\mathbf{W}_i[n]), \\ \hat{\mathbf{a}}_{\theta,\phi,i}[n] &= \mathbf{A}_{\theta,\phi,i} \gamma_i[n] + \mathbf{w}_i[n]. \end{aligned} \tag{125}$$

We assume the path gains $\gamma_i[n]$ are unknown deterministic parameters, as in [165, 117], the CRLB of the AOAs $\theta_{R,i} = (\theta_{R,i,1}, \dots, \theta_{R,i,l_i})^T$ and AODs $\theta_{T,i} =$

Table 2. Parameters of two-path cluster

Path	AOA [Degree]	AOD [Degree]	Path gain
1	15	-10	1
2	-15	20	0.8

$(\theta_{T,i,1}, \dots, \theta_{T,i,l_i})^T$ can be described as

$$\begin{aligned}
\text{CRLB}(\boldsymbol{\theta}_{R,i}, \boldsymbol{\theta}_{T,i}) &= \frac{\sigma_{\mathbb{S}}^2}{2} \text{Re} \left(\boldsymbol{\Lambda}_{\gamma,i}^H \mathbf{D}^H \mathbf{P}_A^\perp \mathbf{D} \boldsymbol{\Lambda}_{\gamma,i} \right)^{-1}, \\
\boldsymbol{\Lambda}_{\gamma,i} &= \mathbf{I}_2 \otimes \boldsymbol{\Delta}_{\gamma,i}, \\
\mathbf{P}_A^\perp &= \mathbf{I}_{N_T N_R} - \mathbf{A}_{\theta,\phi,i} (\mathbf{A}_{\theta,\phi,i}^H \mathbf{A}_{\theta,\phi,i})^{-1} \mathbf{A}_{\theta,\phi,i}^H, \\
\mathbf{D} &= \left(\mathbf{A}'_{\theta,i} \diamond \mathbf{A}_{\phi,i}, \mathbf{A}_{\theta,i} \diamond \mathbf{A}'_{\phi,i} \right), \\
\mathbf{A}'_{\theta,i} &= \left(\frac{d\mathbf{a}_{\theta_{i,1}}}{d\theta_{R,i,1}}(\theta_{R,i,1}), \dots, \frac{d\mathbf{a}_{\theta_{i,l_i}}}{d\theta_{R,i,l_i}}(\theta_{R,i,l_i}) \right), \\
\mathbf{A}'_{\phi,i} &= \left(\frac{d\mathbf{a}_{\phi_{i,1}}}{d\theta_{T,i,1}}(\theta_{T,i,1}), \dots, \frac{d\mathbf{a}_{\phi_{i,l_i}}}{d\theta_{T,i,l_i}}(\theta_{T,i,l_i}) \right). \tag{126}
\end{aligned}$$

3.3.4 Numerical examples

A numerical example based on computer simulations is presented to illustrate the performance of the 2-D unitary ESPRIT algorithm for joint AOAs and AODs estimation. Two propagation paths are assumed to be present within a specified cluster, the AOAs, AODs and the amplitudes of the path gain are listed in Table 2. Four transmit antennas and four receive antennas with one wavelength antenna spacing were employed, and $m = 3$ in (97) is chosen.

Fig. 8 shows the RMSE of the AOAs and AODs estimation. The statistical efficiency of the 2-D unitary ESPRIT algorithm is demonstrated to be valid. In particular the algorithm is close to the CRLB in the high SNR region. To improve the performance of the algorithm in the low SNR region, we need more spatial signature estimate observations. The training signals usually are periodically retransmitted in practical systems. The accuracy of the AOA and the AOD estimates can be improved by averaging out several estimates of the AOAs and the AODs obtained within the channel coherence time.

The algorithm presented in this section has the same computational procedure as the SIJADE proposed in [117], hence the performance of the algorithm has the same features as the SIJADE in [117]. Extensive numerical results about the resolution of the SIJADE, the impacts of the stacking factor m_1 and m_2 on the performance of SIJADE and comparisons to other algorithm such as 2-D IQML

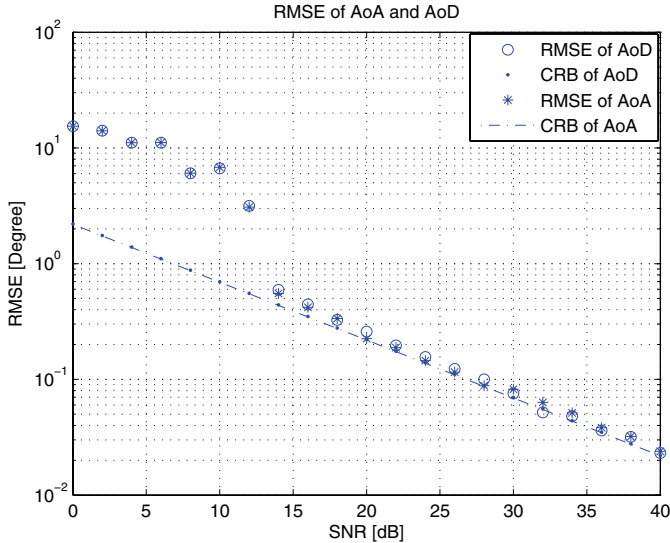


Fig. 8. RMSEs of the AOAs and AODs based on 2-D ESPRIT algorithm, $d_i = 2$.

have been detailed in [117]. These results are not repeated in this thesis.

As proposed later in Chapter 5, the AOAs and the AODs can be applied to the mobile positioning algorithm in the NLOS scenarios. We assume in Chapter 5 that the multiple FSs receiving the signal transmitted from the MS of interest have knowledge about the AOA and the AOD of the NLOS path. One way of obtaining the AOA and the AOD in the FSs is to employ the 2-D unitary ESPRIT algorithm presented in this section. To demonstrate the performance of the proposed positioning algorithm which utilizes the practical AOA and AOD estimates, the effects of the SNR and the true values of the AOAs and AODs on the RMSE of the AOA and AOD estimates are illustrated in Figs. 9 and 10. We assume that each FS utilizes the 2-D unitary ESPRIT algorithm to estimate the AOA and the AOD of the NLOS path, and the first NLOS path in the time domain employed for positioning is the unique path within the cluster consisting of approximately the same delays, i.e., the spatial signature matrix $\mathcal{A}_1[n]$ is rank one. The ULAs of four antennas with half wavelength antenna spacing are equipped at both the MS and FSs. Due to the symmetric property of the AOA and AOD estimates in the 2-D unitary ESPRIT algorithm, the RMSE performance of AOD estimates only are presented in Figs. 9 and 10. The results show that the CRLB and the RMSE of 2-D unitary ESPRIT algorithm increase when the true value of the AOD becomes larger. Also the RMSE of 2-D unitary ESPRIT algorithm approaches the CRLB when the SNR increases and/or the true value of the AOD decreases. It is implied that those NLOS paths with high SNR and small AOD/AOA values

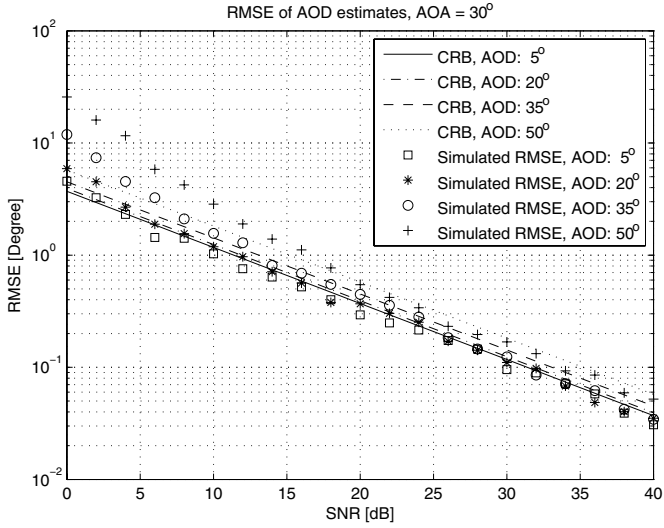


Fig. 9. RMSEs of the AOD estimates versus SNR, AOA: 30° .

should be given more weights in the positioning algorithm. The average CRLB and simulated RMSE of AOD estimates are also shown in Fig. 11. It shows that the RMSE is close to the CRLB when the SNR is higher than 10 dB. Consequently, the CRLB can be approximately exploited as the RMSE of the AOA and AOD estimates in Chapter 5 to demonstrate the performance of positioning algorithm with a real parameter estimator.

3.4 Conclusions

Two practical MIMO channel models, i.e., the correlated-receive independent-transmit MIMO channels and correlated-transmit-receive MIMO channels, were studied in this chapter. The former corresponds to a MIMO system where the structured antenna array is employed at the receiver side, whereas the transmit antennas are separated far away. The latter represents a MIMO system employing a structured antenna array at the both ends of the link. The correlated-receive independent-transmit MIMO channels are parameterized by the time delay and spatial signature matrix. In the case of the correlated-transmit-receive MIMO channels, the spatial signature matrix associated with a cluster consisting of all the paths of approximately the same delay can be further decomposed in terms of the AOA and the AOD of each path.

By virtue of the proposed training signals with cyclic shift structure, the IQML algorithm in [161] was utilized to estimate the time delays and spatial signature

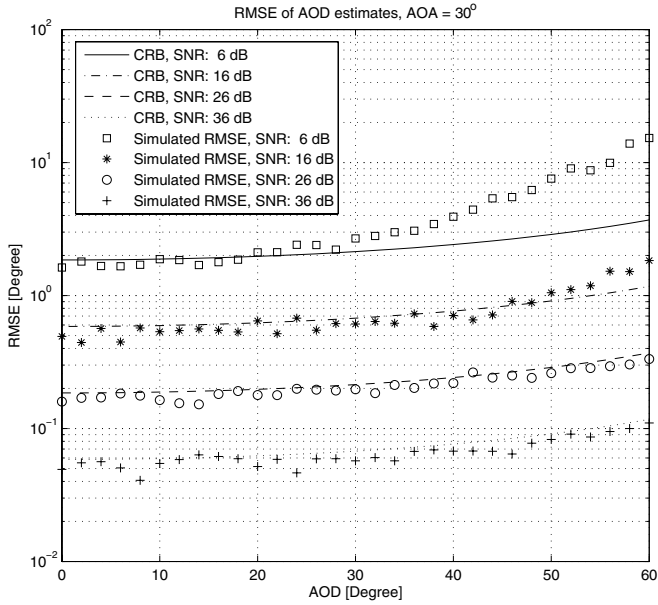


Fig. 10. RMSEs of the AOD estimates versus AOD, AOA: 30° .

matrix of the correlated-receive independent-transmit MIMO channels. The identifiability and CRLB of the algorithm were also presented. As a special case of the correlated-receive independent-transmit MIMO channels, the time delay and spatial signature matrix of the correlated-transmit-receive MIMO channels can be estimated by the IQML algorithm as well. Based on the spatial signature matrix estimate corresponding to a specific cluster, the 2-D unitary ESPRIT algorithm was given to jointly estimate the AOAs and the AODs of the paths within the cluster. As a result, the IQML algorithm followed by the 2-D unitary ESPRIT algorithm provide a novel method of jointly estimating the time delay, the AOA and the AOD of each path for the correlated-transmit-receive MIMO channels. The performance of the algorithms was studied using computer simulations. It was shown from the simulation results that the proposed algorithms are efficient estimators at a reasonable computational cost.

Although the 2-step algorithm, i.e., the combination of the IQML and the 2-D unitary ESPRIT shows good performance at a reasonable computational complexity, it still could perform worse than the optimal ML algorithm for jointly estimating the time delay and the AOAs and the AODs. The RELAX-like algorithms reviewed in Chapter 2 are supposed to be able to achieve the asymptotic performance of the ML algorithm, but they have the risk of a low convergence rate when the initial estimate is far from the optimal solution. Hence, the estimates obtained by the proposed algorithm could be used as a good initial estimates of a

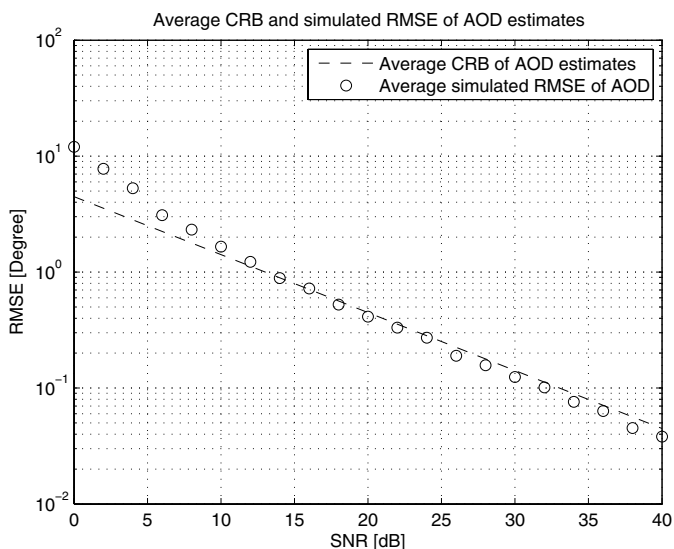


Fig. 11. Average RMSEs of the AOD estimates versus SNR.

RELAX-like algorithm if better results are desired.

It is interesting to note that the CRLB and the RMSE of the AOD and the AOA estimates depend not only on the SNR of the estimated spatial signature matrix but also the true values of the AOAs and the AODs. This implies that the positioning algorithms employing the AOA and AOD information can measure the reliability of the AOA and AOD estimates based on the region where the true values of the AOAs and the AODs are located.

It also should be pointed out that the AOA and the AOD estimates obtained by the proposed algorithm are referred to the normal line of the ULAs equipped at both the ends of the link so that the AOAs and the AODs defined in this chapter are relative angles with regard to unknown absolute directions, i.e., the orientations of the normal line of the ULAs. To obtain the absolute AOA and AOD referred to a fixed known direction; for example, the direction to north, as needed in the positioning algorithm proposed in Chapter 5, requires that the FS and the MS exchange the information about the orientation of their ULAs. This is not an easy task, and how to figure it out in practice needs further study.

4 Channel estimation for a MIMO–OFDM system with spatially correlated channels

The previous work on the MIMO–OFDM channel estimation has mainly concentrated on frequency- and time-domain filtering and has assumed that the channels between different transmit-receive antenna pairs are independent from each other. As discussed in Sections 2.1 and 3.1, the practical MIMO channels can be correlated significantly at the receiver only or at both the ends of the link. Therefore, the spatial correlation should be taken into account in the channel estimator optimization. This chapter focuses on the correlated-receive independent-transmit MIMO channels described in Section 3.1.1, and develops an optimal MMSE channel estimator taking advantage of the receive correlation in addition to the time- and frequency-domain correlation. Moreover, the idea in this chapter can be straightforwardly extended to the correlated-transmit-receive MIMO channels.

It is also of importance to study the impact of the channel properties and the channel estimator on the MIMO system performance. The performance of STBC over uncorrelated MIMO channels has been studied in [22, 24], and over an correlated MIMO channels in [167, 168, 169, 170, 171]. In all the aforementioned references, ideal channel state information (CSI) is assumed in the receiver. Considering channel estimation errors, the symbol error rate (SER) of STBC over uncorrelated MIMO channel has been given in [172]. However, to the author's knowledge, the effect of channel estimation errors on the bit error probability (BEP) of the STBC–OFDM system over correlated MIMO channels has not been analyzed in the open literature.

In this chapter, we wish to optimize the mean square error (MSE) performance of MIMO channel estimation in the presence of spatial correlation. The approach is motivated by the desire to discover the ultimate channel estimation structures and performance limits to be able to benchmark simpler suboptimal channel estimators, although this causes an unavoidable increase in the estimator computational complexity. To still maintain practical relevance, a two-step channel estimator solution is derived and analyzed. The first step consists of an IQML based algorithm used for estimating the time delay and the spatial signature as proposed in Section 3.2. Since the power delay profile and the distribution of the scatterers change slowly, the time delay and the spatial signature can be estimated only in the setup

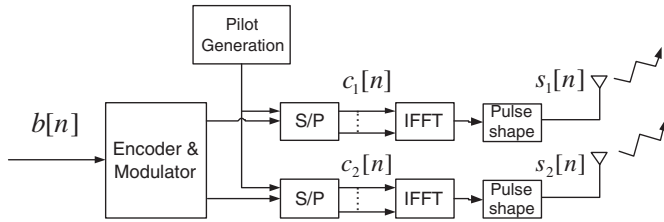
phase of the link. The second estimation step consists of a joint spatio-temporal (JST) filtering based MMSE channel estimator for a MIMO-OFDM system. It is based on the spatial correlation information acquired in the first estimation step. The frequency-domain correlation is also implicitly taken advantage of by filtering the finite length channel taps based on the estimated power delay profile. The performance of the proposed algorithms in terms of root mean square error (RMSE) is studied by analysis and computer simulations. Finally, the BEP of the STBC-OFDM with channel estimation errors is analyzed. We derive an exact expression for the BEP of the quadrature phase-shift keying (QPSK) modulated STBC-OFDM system over correlated MIMO channels. The closed-form BEP formula include the impacts, not only of fading and receiver noise, but also of the channel estimation errors and spatial correlation that occurred at the receiver side.

The chapter is organized as follows. Section 4.1 defines the frame structure of the considered MIMO-OFDM system and the channel statistics of the correlated-receive independent-transmit MIMO channels. The JST filtering based MMSE channel estimation algorithm is derived in Section 4.2. The BEP analysis of the STBC-OFDM system with channel estimation errors in the correlated-receive independent-transmit MIMO channels is presented in Section 4.3 and conclusions are drawn in Section 4.4.

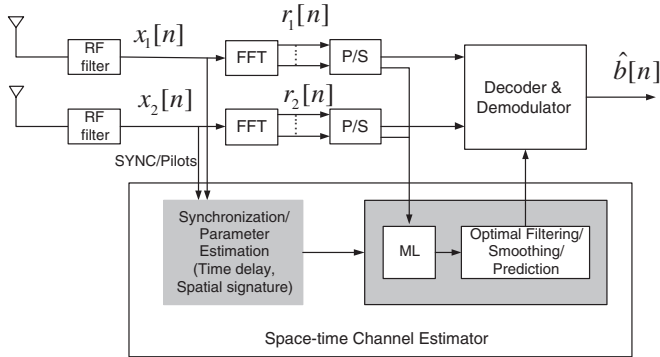
4.1 The correlated MIMO-OFDM system model

4.1.1 Frame structure

The block diagram of a MIMO-OFDM system with $N_T = N_R = 2$ is shown in Fig. 12. We consider an OFDM frame structure similar to that defined in HIPERLAN/2 standard [173]. It is illustrated in Fig. 13. The sample rate is 20 MHz, each OFDM symbol has $K = 64$ subcarriers, the OFDM symbol duration is $T_{\text{OFDM}} = 3.2 \mu\text{s}$, the burst duration is $T_B = T_{\text{OFDM}} + T_{\text{CP}} = 4 \mu\text{s}$, the number of the cyclic prefix (CP) samples is $L - 1 = 16$. It is shown in Fig. 13 that a leading SYNC pilot slot followed by N consecutive protocol data units (PDU) form one receive antenna processing window. In each PDU, there are 16 OFDM symbols, the 1st and the 9th symbol are pilot symbols termed as preamble and midamble, respectively. The leading SYNC pilot signal is meant for initial synchronization, and we use it to estimate the time delay and the spatial signature. The pilot symbols inside the PDU are used to estimate the channel impulse response. Thus, there are $16N$ blocks in one receive antenna processing window which are time-indexed by $n \in \mathcal{S} = \{1, 2, \dots, 16N\}$, the pilot block time-index set is denoted by $\mathcal{S}_P = \{1, 9, 16 + 1, 16 + 9, \dots, (N - 1)16 + 1, (N - 1)16 + 9\}$, and the data block time-index set is denoted by $\mathcal{S}_D = \mathcal{S} \setminus \mathcal{S}_P$. The cardinality of \mathcal{S}_P is denoted by N_P .



(a) Transmitter



(b) Receiver

Fig. 12. The MIMO-OFDM system.

4.1.2 Channel statistics

Based on the correlated-receive independent-transmit MIMO channel model described in Section 3.1.1, the statistics of the vector CIR at the receive antenna array are derived in this section. We denote the impulse responses of the transmit pulse shaping filter and receive pulse shaping filter as $g_T(t)$ and $g_R(t)$, respectively. The impulse response of the overall pulse shaping filter is $g(t)$ which is the convolution of $g_T(t)$ and $g_R(t)$. Let $[0, L_g T_s)$ be the support of $\sum_{i=1}^{N_T} \sum_{j=1}^{d_i} g(t - \tau_{i,j})$. The equivalent vector CIR $\mathbf{h}_i[n; t] \in \mathbb{C}^{N_R}$ during block n from the i th transmit antenna to the receive antenna array can be represented as

$$\mathbf{h}_i[n; t] = \sum_{j=1}^{d_i} g(t - \tau_{i,j}) \boldsymbol{\alpha}_{i,j}[n]. \quad (127)$$

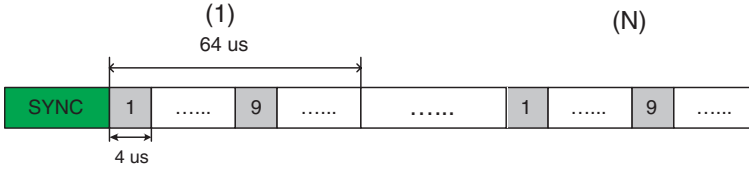


Fig. 13. OFDM frame structure, the pilot symbols are shadowed.

The discrete time representation of the vector CIR $\mathbf{h}_i[n; t]$ is

$$\mathbf{h}_i[n; l] = \sum_{j=1}^{d_i} g(lT_s - \tau_{i,j}) \boldsymbol{\alpha}_{i,j}[n] \in \mathbb{C}^{N_R}, 0 \leq l \leq L_g - 1. \quad (128)$$

Vector $\mathbf{h}_i[n; l] = (h_{i1}[n; l], h_{i2}[n; l], \dots, h_{iN_R}[n; l])^T \in \mathbb{C}^{N_R}$ denotes the l th vector tap of the vector CIR from the i th transmit antenna to the receive antenna array.

As with the assumptions in Section 3.1.1, the clusters are independent of each other, and the correlation matrix $\boldsymbol{\Sigma}_{\boldsymbol{\alpha}_{i,j}[n], \boldsymbol{\alpha}_{i',j'}[n']} \in \mathbb{C}^{N_R \times N_R}$ of the spatial signature vector can be described as

$$\boldsymbol{\Sigma}_{\boldsymbol{\alpha}_{i,j}[n], \boldsymbol{\alpha}_{i',j'}[n']} = \mathbb{E}(\boldsymbol{\alpha}_{i,j}[n] \boldsymbol{\alpha}_{i',j'}[n']^H) = \delta[i - i'] \delta[j - j'] \rho_{i,j}[n - n'] \boldsymbol{\Sigma}_{\boldsymbol{\alpha}_{i,j}}, \quad (129)$$

where $\delta[\cdot]$ is the Dirac's delta function, $\rho_{i,j}[n - n']$ stands for the temporal correlation between the spatial signatures at blocks n and n' , and $\boldsymbol{\Sigma}_{\boldsymbol{\alpha}_{i,j}} \in \mathbb{C}^{N_R \times N_R}$ denotes the spatial correlation of the spatial signature resulting from the j th cluster of rays corresponding to the i th transmit antenna. The temporal correlation $\rho_{i,j}[\cdot]$ depends on the Doppler spectrum. To simplify the problem, we assume that the Doppler spectrum is the same for different values of i and j , and distributes according to the Jakes's model. Therefore, the indices i and j can be left out from $\rho_{i,j}[\cdot]$ in the sequel.

We assume a uniform linear array at the receiver and the receive antenna spacing is Δ_R wavelengths. We further assume that the AOA of the individual ray from the j th cluster related to the i th transmit antenna at the receive antenna array is Gaussian distributed with the mean AOA $\bar{\theta}_{R,i,j}$ and angular spread $\sigma_{\theta_{R,i,j}}$. When the angular spread is small, the spatial correlation matrix $(\boldsymbol{\Sigma}_{\boldsymbol{\alpha}_{i,j}})_{p,q}$ can be approximated as [174]

$$\begin{aligned} (\boldsymbol{\Sigma}_{\boldsymbol{\alpha}_{i,j}})_{p,q} &= |\gamma_{i,j}|^2 \exp(-j2\pi|p - q|\Delta \cos(\bar{\theta}_{R,i,j})) \\ &\quad \exp(-\frac{1}{2}(2\pi|p - q|\Delta \sin(\bar{\theta}_{R,i,j})\sigma_{\theta_{R,i,j}})), \end{aligned} \quad (130)$$

where $|\gamma_{i,j}|^2$ is the total power of the rays in the j th cluster for the i th transmit antenna. Because the correlation between different vector taps is minor, we only consider the autocorrelation of the vector CIR $\mathbf{h}_i[n; l]$ from (128) and (129). The

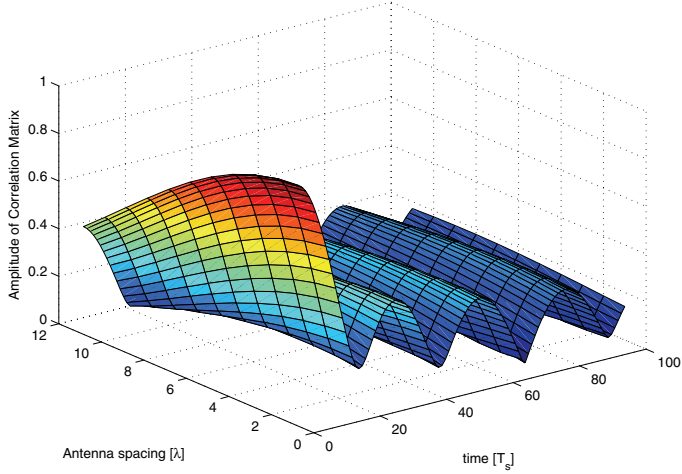
Correlation Matrix of Space-Time Channel, Normalized Doppler spread: 0.02, mean AOA: $\pi/4$, angular spread: 3° 

Fig. 14. Amplitude of the correlation of the vector valued CIR, mean AOA: $\pi/4$, angular spread: 3° , normalized Doppler spread: 0.02.

autocorrelation matrix $\Sigma_{\mathbf{h}_i[n;l], \mathbf{h}_i[n';l]} \in \mathbb{C}^{N_R \times N_R}$, $0 \leq l \leq L_g$ can be expressed as

$$\Sigma_{\mathbf{h}_i[n;l], \mathbf{h}_i[n';l]} = \underbrace{\rho[n - n']}_{\text{temporal correlation}} \underbrace{\sum_{j=1}^{d_i} g(lT_s - \tau_{i,j})^2 \Sigma_{\alpha_{i,j}}}_{\text{spatial correlation.}} \quad (131)$$

With the assumption that only one cluster exists between the i th transmit antenna and the receive antenna array, the mean AOA is $\pi/4$, the angular spread is 3° , and the normalized Doppler spread is 0.02, Fig. 14 shows the amplitude of the correlation of the vector valued CIR $\mathbf{h}_i[n, l]$ versus the antenna spacing and time.

4.2 Minimum mean square error channel estimation

By virtue of the leading SYNC signal with the structure described in Section 3.2.1, the IQML algorithm presented in Section 3.2.2 can be utilized to estimate $\hat{\boldsymbol{\tau}}$ and $\hat{\mathbf{A}}[n]$. Given the pulse shaping function $g(t)$ and estimates of $\hat{\boldsymbol{\tau}}$ and $\hat{\mathbf{A}}[n]$, the vector CIR estimate can be obtained straightforwardly as in (128). However, the main usage of the SYNC signal transmitted during the initial stage of the link is to obtain the estimates of the time delay and spatial correlation which are

assumed to change slowly.¹ Moreover, the spatial correlation of the vector CIR $\mathbf{h}_i[n, l]$ can be calculated as in (131). Based on the spatial correlation estimate and pilot symbols in the receive processing window, a JST filtering based MMSE CIR estimation algorithm is derived in this section. As a consequence, a two-step enhanced channel estimation algorithm, the IQML algorithm followed by the JST filtering based MMSE algorithm is formulated.

4.2.1 Signal model

To achieve a better accuracy of time delay estimation, the sampling rate $1/T_s$ is larger than the actual symbol rate, i.e., oversampling is applied. However, the channel estimation for the synchronized detection will be performed at the symbol rate. In an OFDM system, $T_{\text{syimb}} = T_{\text{OFDM}}/K$ denotes the sample duration at the symbol rate. We also assume that the duration of the CIR is less than the length of the CP. Thus, $L_g T_s \leq (L-1)T_{\text{syimb}}$. When the range of the CIR taps is $0 \leq l \leq L_g - 1$, the CIR is the discrete representation of the continuous CIR at the oversampling rate. On the other hand, if the range of the CIR taps is $0 \leq l \leq L - 1$, the CIR is sampled at the symbol rate. Therefore, at the symbol rate, the vector CIR of the i th transmitter at time n can be expressed in the matrix form as

$$\mathbf{H}_i[n] = \left(\mathbf{h}_i[n; 0], \mathbf{h}_i[n; 1], \dots, \mathbf{h}_i[n; L-1] \right)^T \in \mathbb{C}^{L \times N_R}. \quad (132)$$

Correspondingly, the channel frequency response (CFR) at time n can be expressed as

$$\tilde{\mathbf{H}}_i[n] = \mathbf{F}_K^L \mathbf{H}_i[n] \in \mathbb{C}^{K \times N_R}. \quad (133)$$

As with (131), the autocorrelation matrix $\Sigma_{\mathbf{h}_i[n;l], \mathbf{h}_i[n';l]} \in \mathbb{C}^{N_R \times N_R}$, $0 \leq l \leq L-1$ can be expressed as

$$\Sigma_{\mathbf{h}_i[n;l], \mathbf{h}_i[n';l]} = \rho[n-n'] \underbrace{\sum_{j=1}^{d_i} g(lT_{\text{syimb}} - \tau_{i,j})^2 \Sigma_{\boldsymbol{\alpha}_{i,j}}}_{= \Sigma_{\mathbf{h}_i[l]}}. \quad (134)$$

From (132) and (133), matrices $\mathbf{H}[n] = \left(\mathbf{H}_1^T[n], \dots, \mathbf{H}_{N_T}^T[n] \right)^T \in \mathbb{C}^{N_T L \times N_R}$ and $\tilde{\mathbf{H}}[n] = \left(\tilde{\mathbf{H}}_1^T[n], \tilde{\mathbf{H}}_2^T[n], \dots, \tilde{\mathbf{H}}_{N_T}^T[n] \right)^T \in \mathbb{C}^{N_T K \times N_R}$ denote the concatenations of CIR and CFR matrices from all the transmit antennas to the receive antenna array at time n , respectively. The transmitted OFDM symbol from the i th transmit antenna at time n is $\mathbf{c}_i[n] = \left(c_i[n, 1], c_i[n, 2], \dots, c_i[n, K] \right)^T \in \Xi^K$ where Ξ is the modulation symbol alphabet. Thus, at time n , the received signal

¹According to (130), spatial correlation depends on the total power, mean AOAs and angular spread of rays in the cluster of scatterers, they are assumed to change slowly.

block $\mathbf{R}[n] = \left(\mathbf{r}[n, 0], \mathbf{r}[n, 1], \dots, \mathbf{r}[n, K-1] \right)^\top \in \mathbb{C}^{K \times N_R}$, $\mathbf{r}[n, k] \in \mathbb{C}^{N_R}$ after FFT can be expressed as

$$\mathbf{R}[n] = \mathbf{C}[n] \tilde{\mathbf{H}}[n] + \mathbf{W}[n], \quad (135)$$

where

$$\begin{aligned} \mathbf{C}[n] &= \left(\mathbf{C}_1[n] \quad \mathbf{C}_2[n] \quad \dots \quad \mathbf{C}_{N_T}[n] \right) \in \Xi^{K \times N_T K}, \\ \mathbf{C}_i[n] &= \text{diag}(\mathbf{c}_i[n]) \in \Xi^{K \times K}, i = 1, 2, \dots, N_T, \end{aligned}$$

$\mathbf{W}[n] = \left(\mathbf{w}[n, 0], \mathbf{w}[n, 1], \dots, \mathbf{w}[n, K-1] \right)^\top \in \mathbb{C}^{K \times N_R}$ is the noise matrix at time n . Noise is assumed to be white in both the time and space domains so that the noise covariance matrix is $\boldsymbol{\Sigma}_{\mathbf{w}} = \text{E}(\text{vec}(\mathbf{w})\text{vec}(\mathbf{w})^H) = \sigma_{\mathbf{w}}^2 \mathbf{I}_{KN_R}$.

Replacing the CFR $\tilde{\mathbf{H}}[n]$ with the CIR $\mathbf{H}[n]$ in (135) and combining the partial FFT matrix \mathbf{F}_K^L into the data matrix $\mathbf{C}[n]$, (135) can be described in terms of the CIR as

$$\mathbf{R}[n] = \mathbf{C}[n] \mathbf{H}[n] + \mathbf{W}[n], \quad (136)$$

where

$$\mathbf{C}[n] = \left(\mathbf{C}_1[n] \mathbf{F}_K^L \quad \dots \quad \mathbf{C}_{N_T}[n] \mathbf{F}_K^L \right) \in \mathbb{C}^{K \times N_T L}.$$

Since the matrix $\mathbf{C}[n]$, $n \in \mathcal{S}_p$, in (136) contains the pilot symbols independent of the block index $n \in \mathcal{S}_p$, it is denoted as \mathbf{C}^2 , and (136) can be represented as

$$\mathbf{R}[n] = \mathbf{C} \mathbf{H}[n] + \mathbf{W}[n], n \in \mathcal{S}_p. \quad (137)$$

4.2.2 Minimum mean square error channel estimation

The proposed MMSE channel estimator contains two steps, i.e, the ML based unbiased estimation and JST filtering. The block diagram of the proposed space-time MMSE channel estimation algorithm is illustrated in Fig. 15, and JST filtering window is depicted in Fig. 16.

From (137), the ML estimate of CIR $\mathbf{H}[n]$ at time $n \in \mathcal{S}_p$ becomes

$$\hat{\mathbf{H}}_{\text{ML}}[n] = (\mathbf{C}^H \boldsymbol{\Sigma}_{\mathbf{w}}^{-1} \mathbf{C})^{-1} \mathbf{C}^H \boldsymbol{\Sigma}_{\mathbf{w}}^{-1} \mathbf{R}[n], n \in \mathcal{S}_p. \quad (138)$$

We assume that the different transmit antennas are uncorrelated, and different taps of the CIR are uncorrelated as well. Thus, each tap of the CIR can be estimated separately from the other ones. We define the ML channel estimate vector for the l th tap of the channel from the i th transmit antenna to the receive antenna array as

²The pilot symbols constructing the matrix \mathbf{C} are designed according to the optimal training sequence method proposed in [134] which leads to the minimum estimation variance. Subsequently the more general optimal training sequence design for the MIMO-OFDM system has been addressed in [142].

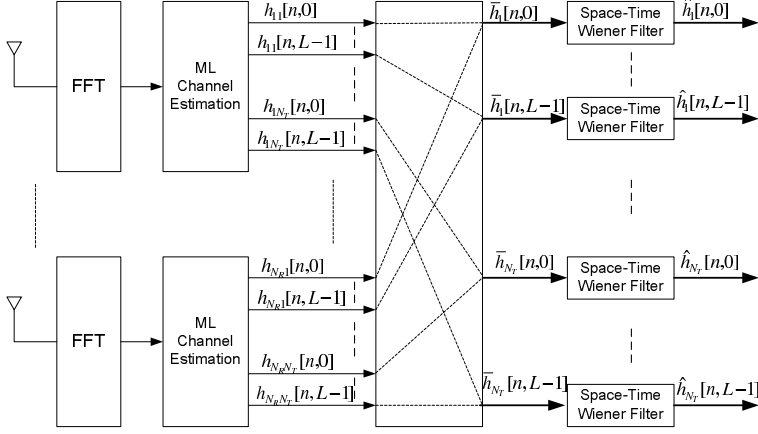


Fig. 15. Space-Time MMSE channel estimator.

$$\hat{\mathbf{h}}_{\text{ML}i}[l] = \left(\hat{\mathbf{h}}_{\text{ML}i}^{\text{T}}[n_1, l], \hat{\mathbf{h}}_{\text{ML}i}^{\text{T}}[n_2, l], \dots, \hat{\mathbf{h}}_{\text{ML}i}^{\text{T}}[n_{N_{\text{P}}}, l] \right)^{\text{T}} \in \mathbb{C}^{N_{\text{R}}N_{\text{P}}}, n_1, n_2, \dots, n_{N_{\text{P}}} \in \mathcal{S}_{\text{P}}, l \in \{0, 1, \dots, L-1\}.$$

It is shown in [120, Eq.(12-73)], [86] that the l th tap of the MMSE CIR estimate $\hat{\mathbf{h}}_{\text{MMSE}i}[n, l]$ related to the i th transmit antenna at time $n \in \mathcal{S}$ can be expressed as

$$\hat{\mathbf{h}}_{\text{MMSE}i}[n, l] = \mathcal{W}_i^{\text{H}}[n, l] \hat{\mathbf{h}}_{\text{ML}i}[l], \quad (139)$$

where

$$\mathcal{W}_i[n, l] = \Sigma_{\hat{\mathbf{h}}_{\text{ML}i}[l]}^{-1} \Sigma_{\mathbf{h}_i[n, l], \hat{\mathbf{h}}_{\text{ML}i}[l]}^{\text{H}}. \quad (140)$$

The crosscovariance matrix $\Sigma_{\mathbf{h}_i[n, l], \hat{\mathbf{h}}_{\text{ML}j}[l]} \in \mathbb{C}^{N_{\text{R}} \times N_{\text{P}}N_{\text{R}}}$ and the autocovariance matrix $\Sigma_{\hat{\mathbf{h}}_{\text{ML}i}[l]} \in \mathbb{C}^{N_{\text{P}}N_{\text{R}} \times N_{\text{P}}N_{\text{R}}}$ of the observed vector can be described as

$$\Sigma_{\mathbf{h}_i[n, l], \hat{\mathbf{h}}_{\text{ML}i}[l]} = \left(\rho[n - n_1], \rho[n - n_2], \dots, \rho[n - n_{N_{\text{P}}}] \right) \otimes \Sigma_{\mathbf{h}_i}[l], \quad (141)$$

$$\Sigma_{\hat{\mathbf{h}}_{\text{ML}i}[l]} = \mathcal{T} \otimes \Sigma_{\mathbf{h}_i}[l] + \Sigma_{\mathbf{w}}, \quad (142)$$

where

$$\mathcal{T} = \begin{pmatrix} \rho[0] & \rho[n_1 - n_2] & \dots & \rho[n_1 - n_{N_{\text{P}}}] \\ \rho[n_2 - n_1] & \rho[0] & \dots & \rho[n_2 - n_{N_{\text{P}}}] \\ \vdots & \vdots & \ddots & \vdots \\ \rho[n_{N_{\text{P}}} - n_1] & \rho[n_{N_{\text{P}}} - n_2] & \dots & \rho[0] \end{pmatrix},$$

$$\Sigma_{\mathbf{w}} = \sigma_{\text{N}}^2 (\mathbf{C}^{\text{H}}\mathbf{C})_{iN_{\text{T}}+l, iN_{\text{T}}+l}^{-1} \mathbf{I}_{N_{\text{R}}N_{\text{P}}},$$

and $\Sigma_{\mathbf{h}_i}[l]$ can be found in (134).

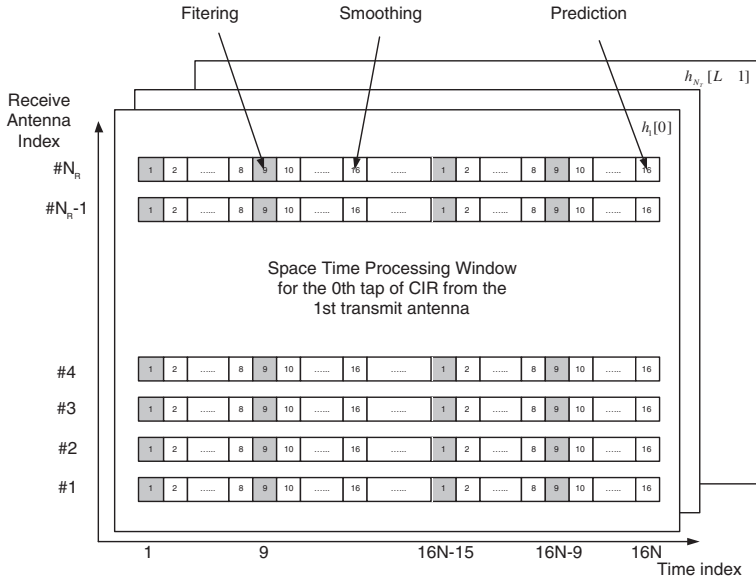


Fig. 16. Joint spatial-temporal filtering window.

By looking at the structure of matrix $\Sigma_{\hat{\mathbf{h}}_{\text{ML}j}}$ in (142), it is found to be a block-Toeplitz matrix. There are several fast and numerically accurate algorithms for the inverse of the Toeplitz and block-Toeplitz matrices, e.g., the Levinson algorithm [175] and the generalized Schur algorithm [176]. The complexities of these algorithms are of $\mathcal{O}((N_R N_P)^2)$ or even smaller. Compared to the conventional temporal filtering MMSE channel estimator [134], the increase in the complexity of the JST MMSE algorithm is due to two reasons: the IQML algorithm for spatial signature estimation and the larger JST filtering window.

4.2.3 Mean square error analysis and examples

At time n , the estimation error vector is defined as $\mathbf{e}_{\mathbf{h}_i}[n, l] = \mathbf{h}_i[n, l] - \hat{\mathbf{h}}_{\text{MMSE}i}[n, l]$. From [120, Eq.(12-73)], the error covariance matrix $\Sigma_{\mathbf{e}_{\mathbf{h}_i}}[n, l]$ of $\hat{\mathbf{h}}_{\text{MMSE}i}[n, l]$ can be described as

$$\Sigma_{\mathbf{e}_{\mathbf{h}_i}}[n, l] = \Sigma_{\mathbf{h}_i[l]} - \Sigma_{\mathbf{h}_i[n, l], \hat{\mathbf{h}}_{\text{ML}i}[l]} \Sigma_{\hat{\mathbf{h}}_{\text{ML}i}[l]}^{-1} \Sigma_{\mathbf{h}_i[n, l], \hat{\mathbf{h}}_{\text{ML}i}[l]}^{\text{H}}, n \in \mathcal{S}. \quad (143)$$

Due to the edge effect [120], within the processing window, the MSE of the parameter estimates for the blocks located close to the middle of the processing window is less than the MSE for blocks located near the two ends. To evaluate the MSE of the channel tap estimate for the whole processing window, we denote the average

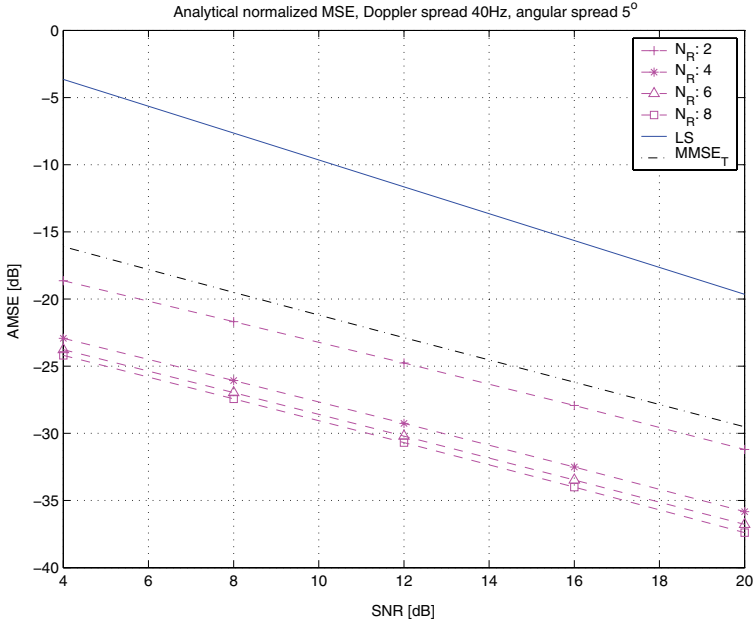


Fig. 17. Analytical NMSE (AMSE) for different numbers of receive antennas, Doppler spread 40 Hz, angular spread 5° , $N_T = 2$ 4PDUs/processing window. LS: the estimator based on the LS algorithm, $MMSE_T$: the estimator based on the temporal filtering MMSE algorithm.

estimation error variance for each channel tap by $\sigma_{\hat{e}_h}^2$ as follows

$$\sigma_{\hat{e}_h}^2 = \sum_{n \in \mathcal{S}} \sum_{i=1}^{N_T} \sum_{l=0}^{L-1} \text{tr}(\mathbf{\Sigma}_{\mathbf{e}_{h_i}}[n, l]) / (16NN_TN_RL). \quad (144)$$

By substituting (143) into (144), the average estimation error variance for each channel tap can be computed, and the analytical NMSE (AMSE) can be obtained as $AMSE = N_R L \sigma_{\hat{e}_h}^2 / \sum_{l=0}^{L-1} \text{tr}(\mathbf{\Sigma}_{\mathbf{h}_i}[l])$.

In order to elaborate the performance gain by taking advantage of the spatial correlation, we studied the impacts of the spatial correlation on the analytical NMSE of the channel estimation. The number of transmit antennas is 2, the receive antenna spacing is $\lambda/2$, the Doppler spread is 40Hz, and 4 PDUs are in one processing window. The power delay profile and mean AOAs related to each cluster are shown in Table 1.³

Fig. 17 shows the analytical NMSEs of the channel estimator based on the LS algorithm, the temporal filtering based MMSE algorithm [134], and the JST

³When the angular spread of each cluster is 5° , and the number of receive antennas is 4, the mean amplitude of the off-diagonal entries of the spatial correlation matrix is 0.89.

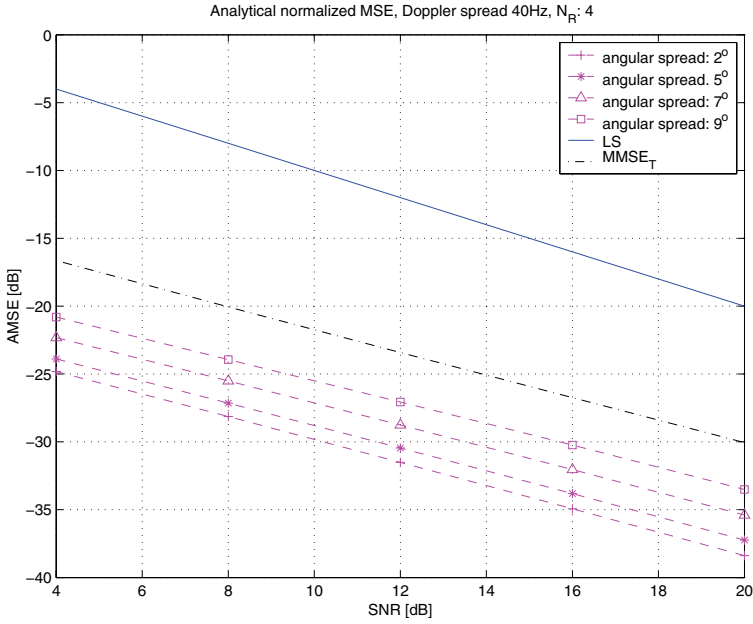


Fig. 18. Analytical NMSE (AMSE) for different angular spreads, Doppler spread 40 Hz, $N_R = 4$, $N_T = 2$, 4PDU's/processing window. LS: the estimator based on the LS algorithm, $MMSE_T$: the estimator based on the temporal filtering MMSE algorithm.

filtering based MMSE algorithm with different numbers of receive antennas. It can be seen that NMSE is significantly reduced compared to the conventional temporal filtering MMSE algorithm by increasing the number of receive antennas if the spatial correlation exists. The number of receive antennas herein refers to the number of receive antennas considered in the spatio-temporal processing window. It is interesting to note from Fig. 17 that there is a more significant performance gain when the number of receive antennas is increased from 1 to 4 than from 4 to 8. This is understandable since the spatial correlation does not increase significantly when the number of receive antennas is increased from 4 to 8.

Fig. 18 shows the analytical NMSEs of MMSE channel estimation algorithms with four receive antennas and different angular spreads associated with each cluster of rays. It shows that the performance gain of the JST filtering MMSE channel estimation over the temporal filtering MMSE channel estimation [134] will be reduced when the angular spread is increased. This is because the spatial correlation is reduced when the angular spread is increased.

Fig. 19 shows the simulation results when the IQML based time delay and spatial signature estimation algorithm were employed, spatial correlation was estimated from the spatial signature estimation and used for the MMSE channel

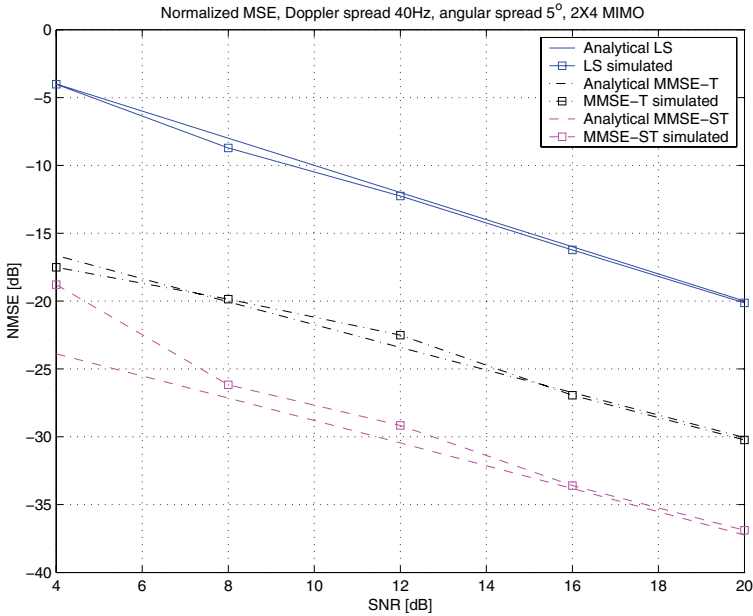


Fig. 19. NMSE, Doppler spread 40 Hz, $N_R = 4$, $N_T = 2$, 4PDUs/processing window, 6 samples/symbol for IQML. LS: the estimator based on the LS algorithm, MMSE-T: the estimator based on the temporal filtering MMSE algorithm, MMSE-ST: the JST MMSE channel estimator.

estimator. During the simulation, we compared the estimated CIR with the ideal CIR, then we obtained the estimation error, and we normalized it by the ideal CIR. By averaging this normalized estimation error, we found the simulated NMSE. It shows that the JST filtering MMSE channel estimation outperforms significantly the temporal filtering [134]. When the signal to noise ratio (SNR) increases, the simulated NMSE of spatial-temporal filtering MMSE channel estimator approaches the analytical NMSE, since the accuracy of the spatial correlation estimation will be improved along with the increased SNR as shown in Fig. 7.

4.3 Bit error probability of STBC-OFDM with channel estimation errors

Channel estimation errors lead to a performance loss in terms of the BEP of the system. Taking the channel estimation errors into account, the closed form expression of the BEP of the QPSK modulated STBC-OFDM system over the correlated-receive independent-transmit MIMO channels is derived in this section.

4.3.1 The signal model

The STBC–OFDM system considered herein is identical to that in [138]. The information bits are firstly modulated by a QPSK modulator. Each STBC code word is transmitted from N_T transmit antennas and across several consecutive OFDM symbol durations at a particular OFDM subcarrier. The STBC code words at different OFDM subcarriers are independently encoded. We also assume that the channel is constant during one STBC code word transmission.

For the sake of simplicity, we consider the case of $N_T = 2$, i.e., the Alamouti codes [23]. We denote $\tilde{\mathbf{h}}_j[k] = \left(\tilde{h}_{1,j}[k], \tilde{h}_{2,j}[k] \right)^T$, where $\tilde{h}_{i,j}[k], i \in \{1, 2\}, j \in \{1, 2, \dots, N_R\}, k \in \{1, 2, \dots, K\}$ stands for the CFR at the k th subcarrier over the channel between the i th transmit antenna and the j th receive antenna. Let $\mathbf{B}[k] = \begin{pmatrix} b_1[k] & b_2[k] \\ b_2^*[k] & -b_1^*[k] \end{pmatrix}$ be the STBC code word transmitted at the k th subcarrier, all the symbols in the same row of $\mathbf{B}[k]$ are transmitted simultaneously from the different transmit antennas. At the k th subcarrier of the j th receive antenna, two consecutive received symbols $\mathbf{r}_j[k] = \left(r_{j,1}[k], r_{j,2}[k] \right)^T$ corresponding to one STBC code word can be depicted as

$$\mathbf{r}_j[k] = \sqrt{\frac{\gamma}{N_T}} \mathbf{B}[k] \tilde{\mathbf{h}}_j[k] + \mathbf{w}_j[k], \quad (145)$$

where γ is the SNR of the received signal. Due to the independence of two transmit antennas, the CFR vector $\tilde{\mathbf{h}}_j[k]$ is a circularly symmetric complex Gaussian random vector, i.e., $\tilde{\mathbf{h}}_j[k] \sim \mathcal{CN}(0, \mathbf{I}_2)$. The unit variance of $\tilde{h}_{i,j}[k]$ follows from the normalization of the power delay profile, i.e., $\sum_{l=0}^{L-1} \mathbb{E}(|h_{i,j}[l]|^2) = 1$. (See Appendix A1.206).

The CFR estimate vector $\hat{\tilde{\mathbf{h}}}_j[k]$ based on the MMSE channel estimator can be approximately described as

$$\hat{\tilde{\mathbf{h}}}_j[k] = \tilde{\mathbf{h}}_j[k] + \boldsymbol{\xi}_j[k], \quad (146)$$

where $\boldsymbol{\xi}_j[k] \sim \mathcal{CN}(0, \mathbf{I}_2 \sigma_{\boldsymbol{\xi}}^2)$ is independent of $\mathbf{w}_j[k]$, and $\sigma_{\boldsymbol{\xi}}^2$ is the MSE of the CFR estimate. Due to the structure of Alamouti code, (145) can be reformulated as

$$\mathbf{r}_j[k] = \sqrt{\frac{\gamma}{N_T}} \tilde{\mathbf{H}}_j[k] \mathbf{b}[k] + \mathbf{w}_j[k], \quad (147)$$

where $\mathbf{r}_j[k] = \left(r_{j,1}[k], r_{j,2}[k] \right)^T$, $\tilde{\mathbf{H}}_j[k] = \begin{pmatrix} h_{1,j}[k] & h_{2,j}[k] \\ -h_{2,j}^*[k] & h_{1,j}^*[k] \end{pmatrix}$, and $\mathbf{b}[k] = \left(b_1[k], b_2[k] \right)^T$.

4.3.2 Bit error probability analysis

Based on (146) and (147), a simple calculation gives the conditional probability density function (PDF)

$$p\left(\mathbf{r}_j[k]|\hat{\mathbf{h}}_j[k], \mathbf{b}[k]\right) = \mathcal{CN}\left(\frac{1}{1+\sigma_{\xi}^2}\sqrt{\frac{\gamma}{N_T}}\hat{\mathbf{H}}_j[k]\mathbf{b}[k], \frac{1+\sigma_{\xi}^2+\gamma\sigma_{\xi}^2}{1+\sigma_{\xi}^2}\mathbf{I}_2\right). \quad (148)$$

The maximum ratio combiner (MRC) is employed in the receiver. Its output is

$$\mathbf{q}'[k] = \sum_{j=1}^{N_R} \hat{\mathbf{H}}_j^H[k] \mathbf{r}_j[k], \quad (149)$$

the conditional PDF $p\left(\mathbf{q}'[k]|\hat{\mathbf{H}}_j[k], \mathbf{b}[k], j = 1, 2, \dots, N_R\right)$ follows from (148) to be

$$\mathcal{CN}\left(\frac{1}{1+\sigma_{\xi}^2}\sqrt{\frac{\gamma}{N_T}}\left(\sum_{j=1}^{N_R} \hat{\mathbf{h}}_j[k]^H \hat{\mathbf{h}}_j[k]\right)\mathbf{b}[k], \frac{1+\sigma_{\xi}^2+\gamma\sigma_{\xi}^2}{1+\sigma_{\xi}^2}\left(\sum_{j=1}^{N_R} \hat{\mathbf{h}}_j[k]^H \hat{\mathbf{h}}_j[k]\right)\mathbf{I}_2\right). \quad (150)$$

We define the decision statistic vector $\mathbf{q}[k]$ as

$$\mathbf{q}[k] = \left(\frac{1+\sigma_{\xi}^2+\gamma\sigma_{\xi}^2}{1+\sigma_{\xi}^2}\left(\sum_{j=1}^{N_R} \hat{\mathbf{h}}_j[k]^H \hat{\mathbf{h}}_j[k]\right)\right)^{-1/2} \mathbf{q}'[k]. \quad (151)$$

We define the vector $\hat{\mathbf{h}}_k = \left(\hat{h}_{1,1}[k], \dots, \hat{h}_{1,N_R}[k], \hat{h}_{2,1}[k], \dots, \hat{h}_{2,N_R}[k]\right)^T \in \mathbb{C}^{2N_R}$ and $\beta = \left((1+\sigma_{\xi}^2+\gamma\sigma_{\xi}^2)(1+\sigma_{\xi}^2)\right)^{-1}$. The conditional PDF of the decision statistic vector $\mathbf{q}[k]$ ⁴ becomes

$$\mathcal{CN}\left(\sqrt{\frac{\gamma\beta\hat{\mathbf{h}}_k^H \hat{\mathbf{h}}_k}{N_T}}\mathbf{b}[k], \mathbf{I}_2\right). \quad (152)$$

The transmitted bits are to be demodulated by the following rules

$$\text{Re}(q_i[k]) \begin{cases} \text{Re}(b_i[k])=1 \\ \geq \\ \text{Re}(b_i[k])=-1 \end{cases} 0, \quad (153)$$

$$\text{Im}(q_i[k]) \begin{cases} \text{Im}(b_i[k])=1 \\ \geq \\ \text{Im}(b_i[k])=-1 \end{cases} 0. \quad (154)$$

The conditional BEP of the transmitted data at the k th subcarrier based on the instantaneous channel estimates can be expressed as $P_k = Q\left(\sqrt{\frac{\gamma\beta}{2N_T}}\|\hat{\mathbf{h}}_k\|\right)$.

⁴The decision statistic vector $\mathbf{q}[k]$ is a biased estimate of the transmitted bits, consequently, it cannot be straightforwardly applied to the multilevel modulation case.

Table 3. Channel parameters

Source	Cluster	Delay [Symbols]	Mean DOA	Power
1	1	2.3	$\pi/4$	0.6439
	2	4.5	$\pi/3$	0.2369
	3	6.2	$\pi/4$	0.0871
	4	8.0	$\pi/5$	0.0321
2	1	2.0	$\pi/3$	0.6439
	2	4.2	$\pi/4$	0.2369
	3	5.0	$\pi/3$	0.0871
	4	7.0	$\pi/6$	0.0321

If the eigenvalues $\lambda_1, \lambda_2, \dots, \lambda_{2N_R}$ of the covariance matrix $\Sigma_{\mathbf{h}_k}^z$ are distinct⁵, the average $\bar{P}_k = \mathbb{E} \left(Q \left(\sqrt{\frac{\gamma\beta}{2N_T}} \|\hat{\mathbf{h}}_k\| \right) \right)$ at the k th subcarrier is now [177, p. 102, (3-64)]

$$\bar{P}_k = \sum_{i=1}^{2N_R} \frac{\zeta_i}{2} \left(1 - \frac{1}{\sqrt{1 + \frac{4N_T}{\gamma\beta\lambda_i}}} \right), \quad (155)$$

where

$$\zeta_i = \prod_{i=1, i \neq j}^{2N_R} \frac{\lambda_i}{\lambda_i - \lambda_j}.$$

The covariance matrix $\Sigma_{\mathbf{h}[k]}^z$ becomes (See the proof in the Appendix)

$$\Sigma_{\mathbf{h}[k]}^z = \sum_{l=0}^{L-1} \begin{pmatrix} \Sigma_{\mathbf{h}_1[l]} & \mathbf{0} \\ \mathbf{0} & \Sigma_{\mathbf{h}_2[l]} \end{pmatrix} + \sigma_{\xi}^2 \mathbf{I}_{2N_R}. \quad (156)$$

It is observed from (156) that the covariance matrices $\Sigma_{\mathbf{h}[k]}^z, k \in 0, 1, \dots, K-1$ are identical. Hence the average BEP P_b over all the subcarriers of the STBC-OFDM system can be also described as (155).

4.3.3 Numerical examples

Fig. 20 shows plots of the BEP, according to (155) for $\gamma = 4, 8, 12, 16$ dB, as a function of σ_{ξ}^2 . The channel parameters are listed in Table 3, the angular spread

⁵Because we assume that the transmit antennas are independent, hence the channel covariance matrices corresponding to the different transmit antennas are different, this leads to the distinct eigenvalues with probability one.

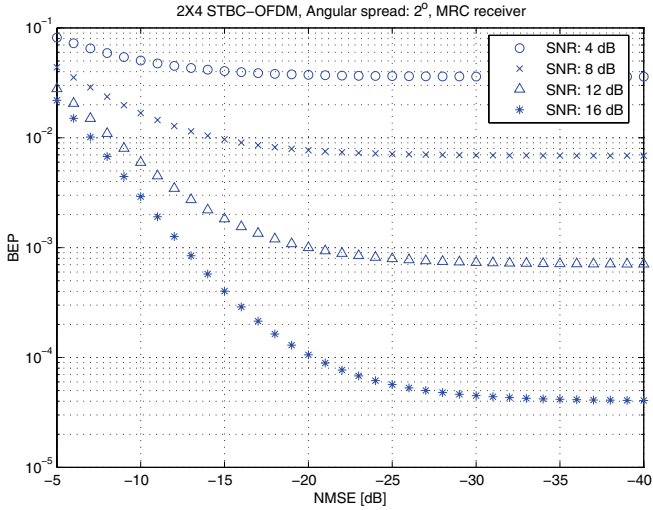


Fig. 20. Impact of the channel estimation error on the BEP of 2×4 STBC-OFDM over correlated MIMO channels.

of each cluster is assumed to be 2° , so that (130) is valid for calculating the spatial correlation. For any fixed SNR point, the BEP performance exhibits an error floor. This occurs when the MSE of the channel estimate is reduced to a certain point so that the system performance is dominated by the noise rather than channel estimation errors. It can also be observed that when the system operates at a high SNR, e.g., 16 dB, accurate channel estimates are required, otherwise the system performance would deteriorate significantly due to coarse channel estimates.

As in [172], we allow the SNRs corresponding to the pilot symbol and the data, i.e., γ_P and γ_D to be different. Fig. 21 shows the BEP of QPSK modulated 2×4 STBC-OFDM system with different channel estimators. It can be seen that with $\gamma_D - \gamma_P = 6, 12$ dB, the JST MMSE channel estimator outperforms about by 0.5 and 2 dB, respectively, the temporal filtering MMSE channel estimator at $\text{BEP} = 10^{-4}$.

4.4 Conclusions

Joint space-time filtering based MMSE channel estimation for the MIMO-OFDM system over the correlated-receive independent-transmit MIMO channels has been studied in this chapter. Based on the time delay and spatial signature estimation investigated in Chapter 3, the spatial correlation matrix of the vector valued CIR has been derived in Section 4.1.2. By taking the spatial correlation into account,

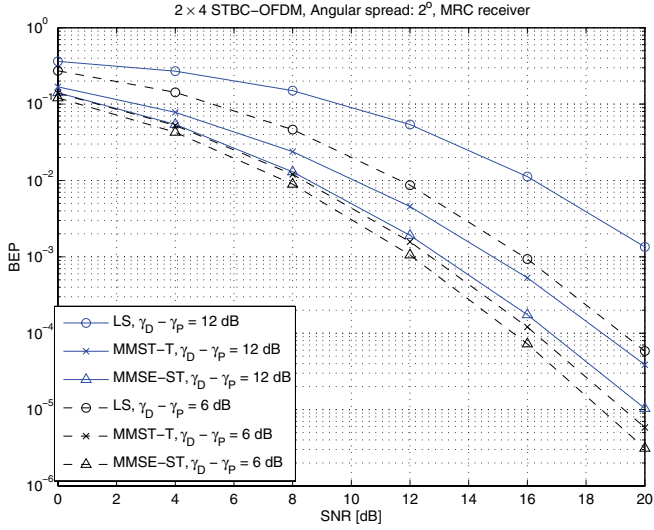


Fig. 21. The BER of 2×4 STBC-OFDM over correlated MIMO channels, 1PDUs/processing window. LS: the estimator based on the LS algorithm, MMSE-T: the estimator based on the temporal filtering MMSE algorithm, MMSE-ST: the JST MMSE channel estimator.

the JST MMSE channel estimation was derived. It was shown both analytically and through computer simulations to outperform the more conventional temporal MMSE channel estimator [134] in terms of estimate MSE when the signals in the receive antenna array elements were allowed to be significantly correlated. To illustrate the effect of channel estimation errors on the BER, a closed form expression of the BER for the QPSK modulated STBC-OFDM system over correlated MIMO channels was derived. It was shown that the JST MMSE channel estimator can achieve significant reductions in the required pilot symbol power levels.

The price for the improved performance offered by the JST MMSE channel estimator is the considerably higher implementation complexity which results from the complex spatial correlation estimation and more complicated JST Wiener filtering. The choice between two algorithms should depend on the performance-cost tradeoff and the setup of the system. It is shown from the analysis of the BER that the system performance is limited by both the operating SNR and the channel estimation errors. If the system is operating at a relatively low SNR, the SNR dominates the system performance. In this case, the better channel estimator can not furnish the better BER performance due to the high noise value. Therefore, the conventional MMSE channel estimator [134] and its simplified version [136] can provide good enough performance.

5 Positioning for non-line of sight propagation

As reviewed in Section 2.4.2, most of the research on positioning in the NLOS scenarios focuses on the NLOS error mitigation techniques, i.e., how to detect the errors and remove their impacts. However, according to the author's knowledge, positioning techniques which *benefit* from the NLOS propagation paths have not been well studied in the open literature. In a rich scattering environment, most of the propagation paths between the MS and FSs are NLOS, occasionally the first path between the MS and the home FS can be assumed as LOS. In this chapter, we present a novel positioning algorithm which takes advantage of the single-bounce NLOS paths by assuming prior knowledge about parameters of each NLOS path. Similar to the correlated-transmit-receive MIMO channel model in 3.1.2, each path is characterized by a triple $(\theta_T, \theta_R, \mathfrak{d})$ where θ_T and θ_R stands for the AOD and AOA, respectively, and \mathfrak{d} defines the distance of the propagation path which can be calculated from the time delay of the path. Assuming the parameter knowledge about the single-bounce NLOS paths, the geometry based methods for mobile positioning in NLOS scenarios were provided in [159, 160]. In [159], the Doppler shift for each NLOS path is assumed. The special location relation between scatterers and MS is required in [160], i.e., scatterers and the MS have to be located in a straight line. Therefore, the assumptions in [159, 160] are more difficult to achieve than the proposed method in this thesis. In addition, the analysis of the estimation error is not presented in [159, 160].

Prior information about the AOA, the AOD and the distance of each NLOS path at the FS can be obtained using the algorithms proposed in Section 3.3 or reviewed in Section 2.2.3 when both the FS and the MS are equipped with multiple antennas. In addition, two methods below also enable FS to acquire the information about the AODs of the NLOS paths.

(a) For the time-division-duplex (TDD) system, the channels for the forward link and the reverse link are symmetric. For the frequency-division-duplex (FDD) system, while the gains/phases of the propagating paths between transmitter and receiver would be different at different directions or carriers, one typically expects the AOAs, AODs and delays to be the same. Therefore, if the MS is able to estimate the AOAs of forward channels which correspond to the AODs of reverse channels, the MS can feedback the AOA information to the FS. The AOA estima-

tion at the MS can be achieved by exploiting either antenna array or the Doppler estimate with a known velocity [61].

(b) When the MS is equipped with a directional antenna, the signal transmission of the reverse link is designed in such a manner that the received signal at the specified time slot implies a predefined AOD. This method is feasible also for signals without a carrier, e.g., the pulse position modulated UWB system.

Based on these parameters and the geometrical relationship of the possible MS location implied from each NLOS path, a novel positioning algorithm is proposed and its performance is analyzed. It is interesting to note that the proposed algorithm is also able to take LOS paths into account as a special case shown in the Appendix. To summarize, the main contributions of this chapter are three-fold:

1) *Possible region and position of the MS:* Based on the measurement $(\theta_T, \theta_R, \vartheta)$ of an NLOS path, we derive the possible region of the MS. It turns out to be a line segment. With the aid of two NLOS paths, the position estimate of the MS is derived as the intersection of two lines. We assume that all the measurements are corrupted by Gaussian noise, the RMSE of the each coordinate of the position estimate is analyzed.

2) *Least squares algorithm considering multiple NLOS paths:* Aiming at the minimum equation-error norm [66], the LS algorithm is proposed for estimating the position of the MS in the presence of multiple NLOS paths. Additionally, LOS paths are incorporated into the general LS algorithm. The RMSE of the coordinate estimate is also analyzed and compared to simulation results.

3) *Maximum likelihood algorithm and the Cramér-Rao lower bound for joint MS and scatterers position estimation:* Based on the knowledge of the parameters of multiple NLOS paths, we derive the ML algorithm for jointly the MS's and scatterers' position estimation. The performance of the algorithm in terms of RMSE is studied by analysis and computer simulations.

The chapter is organized as follows. Section 5.1 includes the system model. Section 5.2 derives the possible region of the MS with the knowledge about the NLOS path, and the geometric approach is addressed to estimate the position of the MS. The LS algorithm employing multiple NLOS paths is discussed in Section 5.3. The ML algorithm and CRLB for the joint MS and scatterers position estimation are derived in Section 5.4. Numerical results are presented in Section 5.5 and conclusions are drawn in Section 5.6.

5.1 System model

Fig. 22 shows the system model where we concentrate on positioning a single mobile. Let N_f denote the number of FSs which perceive the transmitted signal from the MS. As shown in Fig. 22, no LOS paths exist between the MS and any connected FS¹. Each propagation path is parameterized by a triple $(\theta_T, \theta_R, \vartheta)$, i.e., the AOD θ_T , the AOA θ_R and the distance ϑ of the propagation path from the MS to the corresponding FS. We assume each FS has knowledge of the number

¹As shown in the Appendix, LOS can be included as a special case.

Table 4. Setup of the positioning algorithm

Who?	What are dealt with?
the home FS	all the propagation paths from the MS to the home FS
IPC	all the propagation paths from the MS to all the FSs controlled by the IPC
IPC	all the strongest paths from the MS to each FS controlled by the IPC

of paths corresponding to the MS, and the parameters associated with each path. Depending on the requirement of the positioning accuracy and the positioning algorithm to be performed, the proposed algorithm can be employed in either the FS or the information processing center (IPC) which controls several FSs, such as the radio network controller (RNC) in a cellular network. If the positioning algorithm is performed in the home FS, only the propagation paths corresponding to that particular FS can be utilized. On the other hand, if the positioning of the MS is performed in the information processing center or RNC, the proposed algorithm would take advantage of the information about either all the propagation paths or only the strongest path related to each connected FS. In summary, the proposed algorithm can be employed in three setups which are described in Table 4.

For simplicity, we will focus on the third setup in Table 4 where the positioning algorithm is run in the IPC taking only the strongest paths corresponding to each controlled FS into account. However, it is straightforward to apply the proposed idea to the other two scenarios mentioned in Table 4.

5.2 Geometric approach with two fixed stations

5.2.1 Algorithm derivation

To set up the stage for the proposed algorithm, we need to discover the possible region of the MS when the FS has information on the AOD θ_T , AOA θ_R and distance d of the strongest path. However, it needs to have knowledge about the position of the scatterer (x_s, y_s) . As shown in Fig. 23, (x_f, y_f) defines the position of the FS, and r stands for the distance between the FS and the scatterer. Therefore, the possible coordinates of the scatterer are

$$\begin{aligned} x_s &= x_f + r\sin\theta_R, r \in (0, \mathfrak{d}), \\ y_s &= y_f + r\cos\theta_R, r \in (0, \mathfrak{d}), \end{aligned} \tag{157}$$

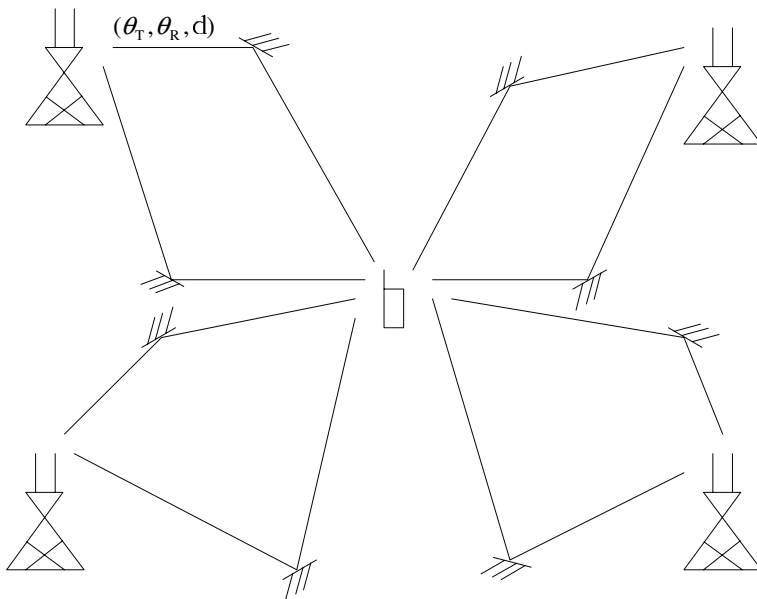


Fig. 22. System model in the NLOS scenario.

and the coordinates of the MS are expressed as follows

$$\begin{aligned} x &= x_s - (\mathfrak{d} - r)\sin\theta_T, r \in (0, \mathfrak{d}), \\ y &= y_s - (\mathfrak{d} - r)\cos\theta_T, r \in (0, \mathfrak{d}). \end{aligned} \quad (158)$$

It follows by substituting (157) into (158) that the possible position of the MS can be described as the following straight-line equation² of the slope-intercept form

$$y = k(\theta_T, \theta_R)x + b(\theta_T, \theta_R, \mathfrak{d}), \quad (159)$$

where

$$k(\theta_T, \theta_R) = \frac{\cos\theta_T + \cos\theta_R}{\sin\theta_T + \sin\theta_R}, \quad (160)$$

$$b(\theta_T, \theta_R, \mathfrak{d}) = -k(\theta_T, \theta_R)(x_f - \mathfrak{d}\sin\theta_T) + y_f - \mathfrak{d}\cos\theta_T. \quad (161)$$

This implies that if we have knowledge about two propagation paths originating from the MS, the position of the MS can be estimated as the intersection of two lines which are derived from (159). For example, assume that the strongest paths from the MS to two FSs located at the coordinates (x_{f1}, y_{f1}) and (x_{f2}, y_{f2}) are parameterized by $\boldsymbol{\vartheta}_1 = (\theta_{T1}, \theta_{R1}, \mathfrak{d}_1)^T$ and $\boldsymbol{\vartheta}_2 = (\theta_{T2}, \theta_{R2}, \mathfrak{d}_2)^T$, respectively. Let

²Precisely speaking, the possible region of the MS should be a line segment instead of a line of infinite length, however the line expression simplifies the derivation of the proposed algorithm without the loss of accuracy of the positioning algorithm.

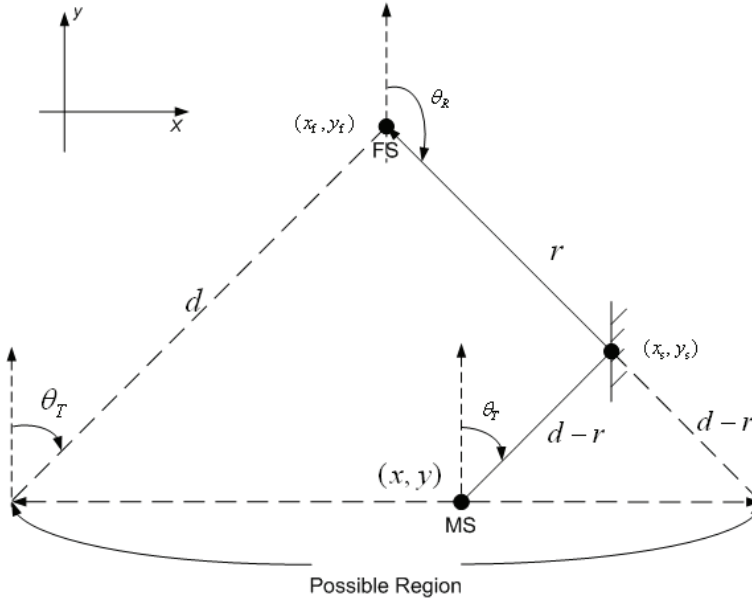


Fig. 23. Possible region of the MS.

$\boldsymbol{\vartheta}_G = (\boldsymbol{\vartheta}_1^T, \boldsymbol{\vartheta}_2^T)^T$ be the parameter vector of both paths. The coordinates (x, y) of the MS can be determined as the intersection of the following two linear equations:

$$\begin{aligned} y &= k_1x + b_1, \\ y &= k_2x + b_2, \end{aligned} \quad (162)$$

where $k_i = k(\theta_{Ti}, \theta_{Ri})$, $b_i = b(\theta_{Ti}, \theta_{Ri}, d_i)$, $i = 1, 2$. It follows that the coordinates of the MS become if $k_1 \neq k_2$

$$x(\boldsymbol{\vartheta}_G) = \frac{b_2 - b_1}{k_1 - k_2}, \quad (163)$$

$$y(\boldsymbol{\vartheta}_G) = \frac{k_1b_2 - k_2b_1}{k_1 - k_2}. \quad (164)$$

For the simplicity of the exposition, we define $\hat{x}_G = x(\boldsymbol{\vartheta}_G)$ and $\hat{y}_G = y(\boldsymbol{\vartheta}_G)$ as the coordinate estimates in the presence of parameter $\boldsymbol{\vartheta}_G$ estimation errors.

5.2.2 Root mean square error analysis

Let $\theta_{Ti}^o, \theta_{Ri}^o, d_i^o, i = 1, 2$ denote the actual AODs, AOA and distances of the propagation paths of interest. We assume that the estimated parameters θ_{Ti}, θ_{Ri}

and \mathfrak{d}_i $i = 1, 2$ are independently Gaussian distributed random variables[165]³, i.e., $\theta_{\text{T}i} \sim \mathcal{N}(\theta_{\text{T}i}^o, \sigma_{\theta_{\text{T}i}}^2)$, $\theta_{\text{R}i} \sim \mathcal{N}(\theta_{\text{R}i}^o, \sigma_{\theta_{\text{R}i}}^2)$ and $\mathfrak{d}_i \sim \mathcal{N}(\mathfrak{d}_i^o, \sigma_{\mathfrak{d}_i}^2)$. We define $\boldsymbol{\vartheta}_i^o = (\theta_{\text{T}i}^o, \theta_{\text{R}i}^o, \mathfrak{d}_i^o)^{\text{T}}$, $i = 1, 2$ as the parameter vector of actual values. Let $\boldsymbol{\vartheta}_{\text{G}}^o = (\boldsymbol{\vartheta}_1^{o\text{T}}, \boldsymbol{\vartheta}_2^{o\text{T}})^{\text{T}}$ denote the actual parameter vector of two paths. When the variances of the estimated parameters are small, according to the Taylor expansion, the estimated coordinates of the MS can be approximated as follows

$$x(\boldsymbol{\vartheta}_{\text{G}}) \approx x(\boldsymbol{\vartheta}_{\text{G}}^o) + \nabla x(\boldsymbol{\vartheta}_{\text{G}}^o)(\boldsymbol{\vartheta}_{\text{G}} - \boldsymbol{\vartheta}_{\text{G}}^o), \quad (165)$$

$$y(\boldsymbol{\vartheta}_{\text{G}}) \approx y(\boldsymbol{\vartheta}_{\text{G}}^o) + \nabla y(\boldsymbol{\vartheta}_{\text{G}}^o)(\boldsymbol{\vartheta}_{\text{G}} - \boldsymbol{\vartheta}_{\text{G}}^o), \quad (166)$$

where

$$\begin{aligned} \nabla x(\boldsymbol{\vartheta}_{\text{G}}) &= \frac{\partial x(\boldsymbol{\vartheta}_{\text{G}})}{\partial \boldsymbol{\vartheta}_{\text{G}}^{\text{T}}} \in \mathbb{R}^{1 \times 6}, \\ \nabla y(\boldsymbol{\vartheta}_{\text{G}}) &= \frac{\partial y(\boldsymbol{\vartheta}_{\text{G}})}{\partial \boldsymbol{\vartheta}_{\text{G}}^{\text{T}}} \in \mathbb{R}^{1 \times 6}. \end{aligned} \quad (167)$$

Let $(x^o, y^o) = (x(\boldsymbol{\vartheta}_{\text{G}}^o), y(\boldsymbol{\vartheta}_{\text{G}}^o))$ denote the true coordinates of the MS. We denote $k_1^o = k(\theta_{\text{T}1}^o, \theta_{\text{R}1}^o)$ and $k_2^o = k(\theta_{\text{T}2}^o, \theta_{\text{R}2}^o)$ as slopes corresponding to accurate linear equations. Let $b_1^o = b(\theta_{\text{T}1}^o, \theta_{\text{R}1}^o, \mathfrak{d}_1^o)$ and $b_2^o = b(\theta_{\text{T}2}^o, \theta_{\text{R}2}^o, \mathfrak{d}_2^o)$ denote the x -intercepts of accurate linear equations. The above gradient vectors $\nabla x(\boldsymbol{\vartheta}_{\text{G}}^o)$ and $\nabla y(\boldsymbol{\vartheta}_{\text{G}}^o)$ can be achieved from the following partial derivatives

$$\frac{\partial x(\boldsymbol{\vartheta}_{\text{G}}^o)}{\partial \theta_{\text{T}1}} = \frac{\frac{\partial b(\boldsymbol{\vartheta}_1^o)}{\partial \theta_{\text{T}}} (k_2^o - k_1^o) + (b_1^o - b_2^o) \frac{\partial k(\boldsymbol{\vartheta}_1^o)}{\partial \theta_{\text{T}}}}{(k_1^o - k_2^o)^2}, \quad (168)$$

$$\frac{\partial x(\boldsymbol{\vartheta}_{\text{G}}^o)}{\partial \theta_{\text{T}2}} = \frac{\frac{\partial b(\boldsymbol{\vartheta}_2^o)}{\partial \theta_{\text{T}}} (k_1^o - k_2^o) + (b_2^o - b_1^o) \frac{\partial k(\boldsymbol{\vartheta}_2^o)}{\partial \theta_{\text{T}}}}{(k_1^o - k_2^o)^2}, \quad (169)$$

$$\frac{\partial x(\boldsymbol{\vartheta}_{\text{G}}^o)}{\partial \theta_{\text{R}1}} = \frac{\frac{\partial b(\boldsymbol{\vartheta}_1^o)}{\partial \theta_{\text{R}}} (k_2^o - k_1^o) + (b_1^o - b_2^o) \frac{\partial k(\boldsymbol{\vartheta}_1^o)}{\partial \theta_{\text{R}}}}{(k_1^o - k_2^o)^2}, \quad (170)$$

$$\frac{\partial x(\boldsymbol{\vartheta}_{\text{G}}^o)}{\partial \theta_{\text{R}2}} = \frac{\frac{\partial b(\boldsymbol{\vartheta}_2^o)}{\partial \theta_{\text{R}}} (k_1^o - k_2^o) + (b_2^o - b_1^o) \frac{\partial k(\boldsymbol{\vartheta}_2^o)}{\partial \theta_{\text{R}}}}{(k_1^o - k_2^o)^2}, \quad (171)$$

$$\frac{\partial x(\boldsymbol{\vartheta}_{\text{G}}^o)}{\partial \mathfrak{d}_1} = \frac{\frac{\partial b(\boldsymbol{\vartheta}_1^o)}{\partial \mathfrak{d}}}{k_2^o - k_1^o}, \quad (172)$$

$$\frac{\partial x(\boldsymbol{\vartheta}_{\text{G}}^o)}{\partial \mathfrak{d}_2} = \frac{\frac{\partial b(\boldsymbol{\vartheta}_2^o)}{\partial \mathfrak{d}}}{k_1^o - k_2^o}, \quad (173)$$

³The MUSIC estimator was shown to be Gaussian distributed for sufficiently large measurements.

and

$$\frac{\partial y(\boldsymbol{\vartheta}_G^o)}{\partial \theta_{T1}} = \frac{\left(\frac{\partial k(\boldsymbol{\vartheta}_1^o)}{\partial \theta_T} b_2^o - k_2^o \frac{\partial b(\boldsymbol{\vartheta}_1^o)}{\partial \theta_T} \right) (k_1^o - k_2^o) + (k_2^o b_1^o - k_1^o b_2^o) \frac{\partial k(\boldsymbol{\vartheta}_1^o)}{\partial \theta_T}}{(k_1^o - k_2^o)^2}, \quad (174)$$

$$\frac{\partial y(\boldsymbol{\vartheta}_G^o)}{\partial \theta_{T2}} = \frac{\left(\frac{\partial b(\boldsymbol{\vartheta}_2^o)}{\partial \theta_T} k_1^o - b_1^o \frac{\partial k(\boldsymbol{\vartheta}_2^o)}{\partial \theta_T} \right) (k_1^o - k_2^o) + (k_1^o b_2^o - k_2^o b_1^o) \frac{\partial k(\boldsymbol{\vartheta}_2^o)}{\partial \theta_T}}{(k_1^o - k_2^o)^2}, \quad (175)$$

$$\frac{\partial y(\boldsymbol{\vartheta}_G^o)}{\partial \theta_{R1}} = \frac{\left(\frac{\partial k(\boldsymbol{\vartheta}_1^o)}{\partial \theta_R} b_2^o - k_2^o \frac{\partial b(\boldsymbol{\vartheta}_1^o)}{\partial \theta_R} \right) (k_1^o - k_2^o) + (k_2^o b_1^o - k_1^o b_2^o) \frac{\partial k(\boldsymbol{\vartheta}_1^o)}{\partial \theta_R}}{(k_1^o - k_2^o)^2}, \quad (176)$$

$$\frac{\partial y(\boldsymbol{\vartheta}_G^o)}{\partial \theta_{R2}} = \frac{\left(\frac{\partial b(\boldsymbol{\vartheta}_2^o)}{\partial \theta_R} k_1^o - b_1^o \frac{\partial k(\boldsymbol{\vartheta}_2^o)}{\partial \theta_R} \right) (k_1^o - k_2^o) + (k_1^o b_2^o - k_2^o b_1^o) \frac{\partial k(\boldsymbol{\vartheta}_2^o)}{\partial \theta_R}}{(k_1^o - k_2^o)^2}, \quad (177)$$

$$\frac{\partial y(\boldsymbol{\vartheta}_G^o)}{\partial \mathfrak{d}_1} = \frac{k_2^o \frac{\partial b(\boldsymbol{\vartheta}_1^o)}{\partial \mathfrak{d}}}{k_2^o - k_1^o}, \quad (178)$$

$$\frac{\partial y(\boldsymbol{\vartheta}_G^o)}{\partial \mathfrak{d}_2} = \frac{k_1^o \frac{\partial b(\boldsymbol{\vartheta}_2^o)}{\partial \mathfrak{d}}}{k_1^o - k_2^o}, \quad (179)$$

where

$$\begin{aligned} \frac{\partial k}{\partial \theta_T} &= \frac{-1 - \cos(\theta_T - \theta_R)}{(\sin \theta_T + \sin \theta_R)^2}, \\ \frac{\partial k}{\partial \theta_R} &= \frac{\partial k}{\partial \theta_T}, \\ \frac{\partial b}{\partial \theta_T} &= \frac{\partial k}{\partial \theta_T} (\mathfrak{d} \sin \theta_T - x_f) + k \mathfrak{d} \cos \theta_T + \mathfrak{d} \sin \theta_T, \\ \frac{\partial b}{\partial \theta_R} &= \frac{\partial k}{\partial \theta_R} (\mathfrak{d} \sin \theta_T - x_f), \\ \frac{\partial b}{\partial \mathfrak{d}} &= k \sin \theta_T - \cos \theta_T. \end{aligned} \quad (180)$$

Therefore, when the variances of the estimated parameters $\boldsymbol{\vartheta}_G$ are small, the variance of the estimation error of the coordinates (\hat{x}_G, \hat{y}_G) can be described as

$$\begin{aligned} \mathbf{E}(\hat{x}_G - x^o)^2 &\approx \nabla x(\boldsymbol{\vartheta}_G^o) \text{diag}(\sigma_{\theta_{T1}}^2, \sigma_{\theta_{R1}}^2, \sigma_{\mathfrak{d}_1}^2, \sigma_{\theta_{T2}}^2, \sigma_{\theta_{R2}}^2, \sigma_{\mathfrak{d}_2}^2) \nabla x^T(\boldsymbol{\vartheta}_G^o), \\ \mathbf{E}(\hat{y}_G - y^o)^2 &\approx \nabla y(\boldsymbol{\vartheta}_G^o) \text{diag}(\sigma_{\theta_{T1}}^2, \sigma_{\theta_{R1}}^2, \sigma_{\mathfrak{d}_1}^2, \sigma_{\theta_{T2}}^2, \sigma_{\theta_{R2}}^2, \sigma_{\mathfrak{d}_2}^2) \nabla y^T(\boldsymbol{\vartheta}_G^o). \end{aligned} \quad (181)$$

We denote the RMSE $\sigma_G = \sqrt{(\mathbf{E}(\hat{x}_G - x^o)^2 + \mathbf{E}(\hat{y}_G - y^o)^2) / 2}$ as the average RMSE of each estimated coordinate of the MS.

5.3 Least squares algorithm with multiple fixed stations

5.3.1 Algorithm derivation

The geometrical approach in Section 5.2 can be generalized to the case where N_f FSs located at $(x_{f,i}, y_{f,i}), i \in \{1, 2, \dots, N_f\}$ can receive the signal from the MS. Let $\boldsymbol{\vartheta} = \left(\boldsymbol{\vartheta}_1^T, \dots, \boldsymbol{\vartheta}_{N_f}^T\right)^T$ and $\boldsymbol{\vartheta}^o = \left(\boldsymbol{\vartheta}_1^{oT}, \dots, \boldsymbol{\vartheta}_{N_f}^{oT}\right)^T$ denote the parameter vector estimates and the parameter vector of actual values, respectively. In general, the RMSE of the estimated position can be improved by exploiting all the observations of different FSs. Let b_i and k_i denote the x -intercept and the slope of the linear equation associated with the strongest path received by the i th FS, respectively. Let b_i^o and k_i^o be the actual counterparts of b_i and k_i , respectively. To achieve the minimum equation-error norm, the LS coordinate estimate $(\hat{x}_{\text{LS}}, \hat{y}_{\text{LS}})$ of the MS can be obtained as

$$(\hat{x}_{\text{LS}}, \hat{y}_{\text{LS}}) = \arg \min_{(x,y)} \sum_{i=1}^{N_f} (k_i x + b_i - y)^2. \quad (182)$$

It follows straightforwardly that

$$\begin{aligned} \hat{x}_{\text{LS}}(\boldsymbol{\vartheta}) &= \frac{\sum_{i=1}^{N_f} b_i \sum_{i=1}^{N_f} k_i - N_f \sum_{i=1}^{N_f} b_i k_i}{N_f \sum_{i=1}^{N_f} k_i^2 - \left(\sum_{i=1}^{N_f} k_i\right)^2}, \\ \hat{y}_{\text{LS}}(\boldsymbol{\vartheta}) &= \frac{\sum_{i=1}^{N_f} b_i + \hat{x}_{\text{LS}} \sum_{i=1}^{N_f} k_i}{N_f}, \\ &= \frac{\sum_{i=1}^{N_f} b_i \sum_{i=1}^{N_f} k_i^2 - \sum_{i=1}^{N_f} k_i \sum_{i=1}^{N_f} b_i k_i}{N_f \sum_{i=1}^{N_f} k_i^2 - \left(\sum_{i=1}^{N_f} k_i\right)^2}. \end{aligned} \quad (183)$$

It is interesting to note that $(\hat{x}_{\text{LS}}, \hat{y}_{\text{LS}})$ equals $(\hat{x}_{\text{G}}, \hat{y}_{\text{G}})$ if $N_f = 2$. The possible region of the MS conducted from an NLOS path in the preceding discussion can be expressed by a linear equation which has a finite slope. There are two cases in which the slope k does not exist, one is the LOS case where the possible region shrinks to a point instead of a line segment, the other is the case in which the possible region is a line parallel to the y -axis. A more detailed discussion about the LS algorithm dealing with two special cases is presented in the Appendix 2.

5.3.2 Root mean square error analysis

As in Section 5.2.2, all estimated parameters are assumed to be independently Gaussian distributed random variables. When the variances of the estimated parameters $\boldsymbol{\vartheta}$ are small, we define $\boldsymbol{\sigma}_i^2 = (\sigma_{\theta_{T_i}}^2, \sigma_{\theta_{R_i}}^2, \sigma_{\delta_i}^2)^T, i = 1, 2, \dots, N_f$, the

estimated coordinates (183) of the MS are described as follows

$$\begin{aligned}\hat{x}_{\text{LS}}(\boldsymbol{\vartheta}) &\approx \hat{x}_{\text{LS}}(\boldsymbol{\vartheta}^\circ) + \nabla \hat{x}_{\text{LS}}(\boldsymbol{\vartheta}^\circ)(\boldsymbol{\vartheta} - \boldsymbol{\vartheta}^\circ), \\ \hat{y}_{\text{LS}}(\boldsymbol{\vartheta}) &\approx \hat{y}_{\text{LS}}(\boldsymbol{\vartheta}^\circ) + \nabla \hat{y}_{\text{LS}}(\boldsymbol{\vartheta}^\circ)(\boldsymbol{\vartheta} - \boldsymbol{\vartheta}^\circ),\end{aligned}\quad (184)$$

where

$$\begin{aligned}\nabla \hat{x}_{\text{LS}}(\boldsymbol{\vartheta}^\circ) &= \frac{\partial \hat{x}_{\text{LS}}(\boldsymbol{\vartheta}^\circ)}{\partial \boldsymbol{\vartheta}^\text{T}} \in \mathbb{R}^{1 \times 3N_f}, \\ \nabla \hat{y}_{\text{LS}}(\boldsymbol{\vartheta}^\circ) &= \frac{\partial \hat{y}_{\text{LS}}(\boldsymbol{\vartheta}^\circ)}{\partial \boldsymbol{\vartheta}^\text{T}} \in \mathbb{R}^{1 \times 3N_f}.\end{aligned}\quad (185)$$

The gradient vector $\nabla \hat{x}_{\text{LS}}(\boldsymbol{\vartheta}^\circ)$ in (184) is calculated as

$$\begin{aligned}\frac{\partial \hat{x}_{\text{LS}}(\boldsymbol{\vartheta}^\circ)}{\partial \theta_{\text{T}i}} &= \frac{\partial \hat{x}_{\text{LS}}(\boldsymbol{\vartheta}^\circ)}{\partial k_i} \frac{\partial k(\boldsymbol{\vartheta}_i^\circ)}{\partial \theta_{\text{T}}} + \frac{\partial \hat{x}_{\text{LS}}(\boldsymbol{\vartheta}^\circ)}{\partial b_i} \frac{\partial b(\boldsymbol{\vartheta}_i^\circ)}{\partial \theta_{\text{T}}}, i = 1, 2, \dots, N_f, \\ \frac{\partial \hat{x}_{\text{LS}}(\boldsymbol{\vartheta}^\circ)}{\partial \theta_{\text{R}i}} &= \frac{\partial \hat{x}_{\text{LS}}(\boldsymbol{\vartheta}^\circ)}{\partial k_i} \frac{\partial k(\boldsymbol{\vartheta}_i^\circ)}{\partial \theta_{\text{R}}} + \frac{\partial \hat{x}_{\text{LS}}(\boldsymbol{\vartheta}^\circ)}{\partial b_i} \frac{\partial b(\boldsymbol{\vartheta}_i^\circ)}{\partial \theta_{\text{R}}}, i = 1, 2, \dots, N_f, \\ \frac{\partial \hat{x}_{\text{LS}}(\boldsymbol{\vartheta}^\circ)}{\partial \mathfrak{d}_i} &= \frac{\partial \hat{x}_{\text{LS}}(\boldsymbol{\vartheta}^\circ)}{\partial b_i} \frac{\partial b(\boldsymbol{\vartheta}_i^\circ)}{\partial \mathfrak{d}}, i = 1, 2, \dots, N_f,\end{aligned}\quad (186)$$

where $\frac{\partial k}{\partial \theta_{\text{T}}}$, $\frac{\partial k}{\partial \theta_{\text{R}}}$, $\frac{\partial b}{\partial \theta_{\text{T}}}$, $\frac{\partial b}{\partial \theta_{\text{R}}}$ and $\frac{\partial b}{\partial \mathfrak{d}}$ are obtained from (180). Let $P = \sum_{i=1}^{N_f} k_i^\circ$, $Q = \sum_{i=1}^{N_f} (k_i^\circ)^2$, $W = \sum_{i=1}^{N_f} b_i^\circ k_i^\circ$ and $Z = \sum_{i=1}^{N_f} b_i^\circ$. Then, $\frac{\partial \hat{x}_{\text{LS}}(\boldsymbol{\vartheta}^\circ)}{\partial k_i}$ and $\frac{\partial \hat{x}_{\text{LS}}(\boldsymbol{\vartheta}^\circ)}{\partial b_i}$, $i = 1, 2, \dots, N_f$ are expressed as

$$\begin{aligned}\frac{\partial \hat{x}_{\text{LS}}(\boldsymbol{\vartheta}^\circ)}{\partial k_i} &= \frac{N_f b_i^\circ (P^2 - N_f Q) + Z (N_f Q + P^2) - 2N_f (k_i^\circ P Z + W (P - N_f k_i^\circ))}{(N_f Q - P^2)^2}, \\ \frac{\partial \hat{x}_{\text{LS}}(\boldsymbol{\vartheta}^\circ)}{\partial b_i} &= \frac{P - N_f k_i^\circ}{N_f Q - P^2}.\end{aligned}\quad (187)$$

As in (186), the gradient vector $\nabla \hat{y}_{\text{LS}}(\boldsymbol{\vartheta}^\circ)$ in (184) becomes

$$\begin{aligned}\frac{\partial \hat{y}_{\text{LS}}(\boldsymbol{\vartheta}^\circ)}{\partial \theta_{\text{T}i}} &= \frac{\partial \hat{y}_{\text{LS}}(\boldsymbol{\vartheta}^\circ)}{\partial k_i} \frac{\partial k(\boldsymbol{\vartheta}_i^\circ)}{\partial \theta_{\text{T}}} + \frac{\partial \hat{y}_{\text{LS}}(\boldsymbol{\vartheta}^\circ)}{\partial b_i} \frac{\partial b(\boldsymbol{\vartheta}_i^\circ)}{\partial \theta_{\text{T}}}, i = 1, 2, \dots, N_f, \\ \frac{\partial \hat{y}_{\text{LS}}(\boldsymbol{\vartheta}^\circ)}{\partial \theta_{\text{R}i}} &= \frac{\partial \hat{y}_{\text{LS}}(\boldsymbol{\vartheta}^\circ)}{\partial k_i} \frac{\partial k(\boldsymbol{\vartheta}_i^\circ)}{\partial \theta_{\text{R}}} + \frac{\partial \hat{y}_{\text{LS}}(\boldsymbol{\vartheta}^\circ)}{\partial b_i} \frac{\partial b(\boldsymbol{\vartheta}_i^\circ)}{\partial \theta_{\text{R}}}, i = 1, 2, \dots, N_f, \\ \frac{\partial \hat{y}_{\text{LS}}(\boldsymbol{\vartheta}^\circ)}{\partial \mathfrak{d}_i} &= \frac{\partial \hat{y}_{\text{LS}}(\boldsymbol{\vartheta}^\circ)}{\partial b_i} \frac{\partial b(\boldsymbol{\vartheta}_i^\circ)}{\partial \mathfrak{d}}, i = 1, 2, \dots, N_f,\end{aligned}\quad (188)$$

where $\frac{\partial \hat{y}_{\text{LS}}(\boldsymbol{\vartheta}^\circ)}{\partial k_i}$ and $\frac{\partial \hat{y}_{\text{LS}}(\boldsymbol{\vartheta}^\circ)}{\partial b_i}$, $i = 1, 2, \dots, N_f$ are expressed as

$$\begin{aligned}\frac{\partial \hat{y}_{\text{LS}}(\boldsymbol{\vartheta}^\circ)}{\partial k_i} &= \frac{\hat{x}_{\text{LS}}(\boldsymbol{\vartheta}^\circ) + P \frac{\partial \hat{x}_{\text{LS}}(\boldsymbol{\vartheta}^\circ)}{\partial k_i}}{N_f}, \\ \frac{\partial \hat{y}_{\text{LS}}(\boldsymbol{\vartheta}^\circ)}{\partial b_i} &= \frac{1 + P \frac{\partial \hat{x}_{\text{LS}}(\boldsymbol{\vartheta}^\circ)}{\partial b_i}}{N_f}.\end{aligned}\quad (189)$$

Therefore, the variance of the estimation error of the coordinates $(\hat{x}_{\text{LS}}, \hat{y}_{\text{LS}})$ is

$$\begin{aligned} \mathbb{E}(\hat{x}_{\text{LS}} - x^o)^2 &\approx \nabla \hat{x}_{\text{LS}}(\boldsymbol{\vartheta}^o) \text{diag}(\boldsymbol{\sigma}_1^2, \dots, \boldsymbol{\sigma}_{N_f}^2) \nabla \hat{x}_{\text{LS}}^T(\boldsymbol{\vartheta}^o), \\ \mathbb{E}(\hat{y}_{\text{LS}} - y^o)^2 &\approx \nabla \hat{y}_{\text{LS}}(\boldsymbol{\vartheta}^o) \text{diag}(\boldsymbol{\sigma}_1^2, \dots, \boldsymbol{\sigma}_{N_f}^2) \nabla \hat{y}_{\text{LS}}^T(\boldsymbol{\vartheta}^o). \end{aligned} \quad (190)$$

As in Section 5.2.2, we denote the RMSE $\sigma_{\text{LS}} = \sqrt{\mathbb{E}(\hat{x}_{\text{LS}} - x^o)^2 + \mathbb{E}(\hat{y}_{\text{LS}} - y^o)^2} / 2$ as the average RMSE of each estimated coordinate of the MS.

5.4 Maximum likelihood position estimation and the Cramér-Rao lower bound

5.4.1 Joint mobile station and scatterers' position estimation

Section 5.3 addressed using multiple FSs to improve the positioning accuracy of the MS. Indeed, all the observed parameters $\boldsymbol{\vartheta}$ provide information about not only the position of the MS but also the positions of the associated scatterers. We define $(x_{si}^o, y_{si}^o), i = 1, 2, \dots, N_f$ as the accurate coordinates of the scatterers. According to Fig. 23, the real parameter $\boldsymbol{\vartheta}_i^o$ depends on the coordinates (x_{si}^o, y_{si}^o) and (x^o, y^o) as follows

$$\begin{aligned} \theta_{\text{Ti}}^o &= \begin{cases} \arctan \frac{x_{si}^o - x^o}{y_{si}^o - y^o} & x_{si}^o \geq x^o, y_{si}^o \geq y^o \\ \pi + \arctan \frac{x_{si}^o - x^o}{y_{si}^o - y^o} & x_{si}^o \geq x^o, y_{si}^o < y^o \\ \pi + \arctan \frac{x_{si}^o - x^o}{y_{si}^o - y^o} & x_{si}^o < x^o, y_{si}^o < y^o \\ 2\pi + \arctan \frac{x_{si}^o - x^o}{y_{si}^o - y^o} & x_{si}^o < x^o, y_{si}^o \geq y^o \end{cases} \\ \theta_{\text{Ri}}^o &= \begin{cases} \arctan \frac{x_{si}^o - x_{fi}^o}{y_{si}^o - y_{fi}^o} & x_{si}^o \geq x_{fi}^o, y_{si}^o \geq y_{fi}^o \\ \pi + \arctan \frac{x_{si}^o - x_{fi}^o}{y_{si}^o - y_{fi}^o} & x_{si}^o \geq x_{fi}^o, y_{si}^o < y_{fi}^o \\ \pi + \arctan \frac{x_{si}^o - x_{fi}^o}{y_{si}^o - y_{fi}^o} & x_{si}^o < x_{fi}^o, y_{si}^o < y_{fi}^o \\ 2\pi + \arctan \frac{x_{si}^o - x_{fi}^o}{y_{si}^o - y_{fi}^o} & x_{si}^o < x_{fi}^o, y_{si}^o \geq y_{fi}^o \end{cases} \\ \vartheta_i^o &= \sqrt{(x_{si}^o - x^o)^2 + (y_{si}^o - y^o)^2} + \sqrt{(x_{si}^o - x_{fi}^o)^2 + (y_{si}^o - y_{fi}^o)^2} \quad (191) \end{aligned}$$

As in Section 5.2.2, all the estimated parameters are assumed to be independently Gaussian distributed random variables. We define

$$p(\boldsymbol{\vartheta}; x^o, y^o, (x_{si}^o, y_{si}^o)_{i=1,2,\dots,N_f})$$

as the parameterized joint PDF of all the observed parameters. Due to the assumption that all the observed parameters are independently Gaussian distributed random variables, the likelihood function

$$\mathcal{L}(\boldsymbol{\vartheta}; x^o, y^o, (x_{si}^o, y_{si}^o)_{i=1,2,\dots,N_f}) = \ln p(\boldsymbol{\vartheta}; x^o, y^o, (x_{si}^o, y_{si}^o)_{i=1,2,\dots,N_f})$$

can be expressed as

$$\begin{aligned} & \mathcal{L}(\boldsymbol{\vartheta}; x^o, y^o, (x_{s_i}^o, y_{s_i}^o)_{i=1,2,\dots,N_f}) \\ &= \sum_{i=1}^{N_f} \left(\ln \frac{1}{(2\pi)^{3/2} \sigma_{\theta_{T_i}} \sigma_{\theta_{R_i}} \sigma_{\mathfrak{d}_i}} \right) \\ & \quad - \sum_{i=1}^{N_f} \left(\frac{1}{2} \left(\frac{(\theta_{T_i} - \theta_{T_i}^o)^2}{\sigma_{\theta_{T_i}}^2} + \frac{(\theta_{R_i} - \theta_{R_i}^o)^2}{\sigma_{\theta_{R_i}}^2} + \frac{(\mathfrak{d}_i - \mathfrak{d}_i^o)^2}{\sigma_{\mathfrak{d}_i}^2} \right) \right). \end{aligned} \quad (192)$$

By ignoring the constant term in (192), we define the objective function as

$$\begin{aligned} & \mathcal{O}(\boldsymbol{\vartheta}; x^o, y^o, (x_{s_i}^o, y_{s_i}^o)_{i=1,2,\dots,N_f}) \\ &= \frac{1}{2} \sum_{i=1}^{N_f} \left(\frac{(\theta_{T_i} - \theta_{T_i}^o)^2}{\sigma_{\theta_{T_i}}^2} + \frac{(\theta_{R_i} - \theta_{R_i}^o)^2}{\sigma_{\theta_{R_i}}^2} + \frac{(\mathfrak{d}_i - \mathfrak{d}_i^o)^2}{\sigma_{\mathfrak{d}_i}^2} \right). \end{aligned} \quad (193)$$

The ML based joint MS and scatterers' position estimator becomes

$$\begin{aligned} & (\hat{x}_{\text{ML}}, \hat{y}_{\text{ML}}, (\hat{x}_{\text{MLS}_i}, \hat{y}_{\text{MLS}_i})_{i=1,2,\dots,N_f}) \\ &= \arg \min_{x^o, y^o, (x_{s_i}^o, y_{s_i}^o)_{i=1,2,\dots,N_f}} \mathcal{O}(\boldsymbol{\vartheta}; x^o, y^o, (x_{s_i}^o, y_{s_i}^o)_{i=1,2,\dots,N_f}). \end{aligned} \quad (194)$$

The above minimization problem is a non-linear programming problem which can be solved by various iterative procedures [115, Chap. 3], e.g., the steepest descent or conjugate gradient methods. All the iterative methods require an initial searching point. A good starting point leads to the global minimum, whereas a badly selected one may result in convergence to a local minimum. For example, the LS algorithm in Section 5.3 provides a reasonable initialization for the ML algorithm⁴.

5.4.2 The Cramér-Rao lower bound

Let us define $\boldsymbol{\varphi} = (x^o, y^o)^\text{T}$, $\mathbf{x}_s^o = (x_{s_1}^o, x_{s_2}^o, \dots, x_{s_{N_f}}^o)^\text{T}$, $\mathbf{y}_s^o = (y_{s_1}^o, y_{s_2}^o, \dots, y_{s_{N_f}}^o)^\text{T}$, $\boldsymbol{\psi} = (\mathbf{x}_s^{o\text{T}}, \mathbf{y}_s^{o\text{T}})^\text{T}$ and $\boldsymbol{\rho} = (\boldsymbol{\varphi}^\text{T}, \boldsymbol{\psi}^\text{T})^\text{T}$. The Fisher information matrix (FIM) $\mathbf{I}(\boldsymbol{\rho}) \in \mathbb{R}^{(2N_f+2) \times (2N_f+2)}$ can be expressed as

$$\mathbf{I}(\boldsymbol{\rho}) = \mathbb{E} \left(\frac{\partial \mathcal{L}(\boldsymbol{\vartheta}; \boldsymbol{\rho})}{\partial \boldsymbol{\rho}} \frac{\partial \mathcal{L}(\boldsymbol{\vartheta}; \boldsymbol{\rho})}{\partial \boldsymbol{\rho}^\text{T}} \right). \quad (195)$$

Therefore, the RMSE $\sigma_{\text{ML}} = \sqrt{(\mathbb{E}(\hat{x} - x^o)^2 + \mathbb{E}(\hat{y} - y^o)^2) / 2}$ of any unbiased positioning estimator has the lower bound

$$\sigma_{\text{ML}} \geq \text{CRLB} = \sqrt{\frac{(\mathbf{I}^{-1}(\boldsymbol{\rho}))_{11} + (\mathbf{I}^{-1}(\boldsymbol{\rho}))_{22}}{2}}. \quad (196)$$

⁴Even though the LS estimator only produces the position of the MS, the positions of scatterers can also be straightforwardly calculated from (157) and (158).

We partition the FIM $\mathbf{I}(\boldsymbol{\rho})$ as follows

$$\mathbf{I}(\boldsymbol{\rho}) = \begin{pmatrix} \mathbf{I}_{11} & \mathbf{I}_{12} \\ \mathbf{I}_{12}^T & \mathbf{I}_{22} \end{pmatrix}, \quad (197)$$

where

$$\begin{aligned} \mathbf{I}_{11} &= \mathbb{E} \left(\frac{\partial \mathcal{L}(\boldsymbol{\vartheta}; \boldsymbol{\rho})}{\partial \boldsymbol{\varphi}} \frac{\partial \mathcal{L}(\boldsymbol{\vartheta}; \boldsymbol{\rho})}{\partial \boldsymbol{\varphi}^T} \right) \in \mathbb{R}^{2 \times 2}, \\ \mathbf{I}_{12} &= \mathbb{E} \left(\frac{\partial \mathcal{L}(\boldsymbol{\vartheta}; \boldsymbol{\rho})}{\partial \boldsymbol{\varphi}} \frac{\partial \mathcal{L}(\boldsymbol{\vartheta}; \boldsymbol{\rho})}{\partial \boldsymbol{\psi}^T} \right) \in \mathbb{R}^{2 \times 2N_f}, \\ \mathbf{I}_{22} &= \mathbb{E} \left(\frac{\partial \mathcal{L}(\boldsymbol{\vartheta}; \boldsymbol{\rho})}{\partial \boldsymbol{\psi}} \frac{\partial \mathcal{L}(\boldsymbol{\vartheta}; \boldsymbol{\rho})}{\partial \boldsymbol{\psi}^T} \right) \in \mathbb{R}^{2N_f \times 2N_f}. \end{aligned} \quad (198)$$

To calculate the $\mathbf{I}(\boldsymbol{\rho})$, we need the following expressions

$$\begin{aligned} \frac{\partial \theta_{T_i}^o}{\partial x^o} &= -\frac{\partial \theta_{T_i}^o}{\partial x_{si}^o} \\ &= \frac{y^o - y_{si}^o}{(x_{si}^o - x^o)^2 + (y_{si}^o - y^o)^2}, \\ \frac{\partial \theta_{T_i}^o}{\partial y^o} &= -\frac{\partial \theta_{T_i}^o}{\partial y_{si}^o} \\ &= \frac{x_{si}^o - x^o}{(x_{si}^o - x^o)^2 + (y_{si}^o - y^o)^2}, \end{aligned} \quad (199)$$

$$\begin{aligned} \frac{\partial \theta_{R_i}^o}{\partial x^o} &= \frac{\partial \theta_{R_i}^o}{\partial y^o} \\ &= 0, \\ \frac{\partial \theta_{R_i}^o}{\partial x_{si}^o} &= \frac{y_{si}^o - y_{fi}}{(x_{si}^o - x_{fi})^2 + (y_{si}^o - y_{fi})^2}, \\ \frac{\partial \theta_{R_i}^o}{\partial y_{si}^o} &= \frac{x_{fi} - x_{si}^o}{(x_{si}^o - x_{fi})^2 + (y_{si}^o - y_{fi})^2}, \end{aligned} \quad (200)$$

and

$$\begin{aligned} \frac{\partial \vartheta_i^o}{\partial x^o} &= \frac{x^o - x_{si}^o}{\sqrt{(x_{si}^o - x^o)^2 + (y_{si}^o - y^o)^2}}, \\ \frac{\partial \vartheta_i^o}{\partial y^o} &= \frac{y^o - y_{si}^o}{\sqrt{(x_{si}^o - x^o)^2 + (y_{si}^o - y^o)^2}}, \\ \frac{\partial \vartheta_i^o}{\partial x_{si}^o} &= \frac{x_{si}^o - x^o}{\sqrt{(x_{si}^o - x^o)^2 + (y_{si}^o - y^o)^2}} + \frac{x_{si}^o - x_{fi}}{\sqrt{(x_{si}^o - x_{fi})^2 + (y_{si}^o - y_{fi})^2}}, \\ \frac{\partial \vartheta_i^o}{\partial y_{si}^o} &= \frac{y_{si}^o - y^o}{\sqrt{(x_{si}^o - x^o)^2 + (y_{si}^o - y^o)^2}} + \frac{y_{si}^o - y_{fi}}{\sqrt{(x_{si}^o - x_{fi})^2 + (y_{si}^o - y_{fi})^2}}. \end{aligned} \quad (201)$$

For the simplicity of the exposition, we define $\mathcal{L}(\boldsymbol{\vartheta}) \doteq \mathcal{L}(\boldsymbol{\vartheta}; \boldsymbol{\rho})$. The partial derivatives of $\mathcal{L}(\boldsymbol{\vartheta}; \boldsymbol{\rho})$ with respect to $x^o, y^o, \mathbf{x}_s^o, \mathbf{y}_s^o$ become

$$\begin{aligned}
\frac{\partial \mathcal{L}(\boldsymbol{\vartheta})}{\partial x^o} &= \sum_{i=1}^{N_f} \left(\frac{(\theta_{T_i} - \theta_{T_i}^o)}{\sigma_{\theta_{T_i}}^2} \frac{\partial \theta_{T_i}^o}{\partial x^o} + \frac{(\mathfrak{d}_i - \mathfrak{d}_i^o)}{\sigma_{\mathfrak{d}_i}^2} \frac{\partial \mathfrak{d}_i^o}{\partial x^o} \right), \\
\frac{\partial \mathcal{L}(\boldsymbol{\vartheta})}{\partial y^o} &= \sum_{i=1}^{N_f} \left(\frac{(\theta_{T_i} - \theta_{T_i}^o)}{\sigma_{\theta_{T_i}}^2} \frac{\partial \theta_{T_i}^o}{\partial y^o} + \frac{(\mathfrak{d}_i - \mathfrak{d}_i^o)}{\sigma_{\mathfrak{d}_i}^2} \frac{\partial \mathfrak{d}_i^o}{\partial y^o} \right), \\
\frac{\partial \mathcal{L}(\boldsymbol{\vartheta})}{\partial x_{si}^o} &= \frac{(\theta_{T_i} - \theta_{T_i}^o)}{\sigma_{\theta_{T_i}}^2} \frac{\partial \theta_{T_i}^o}{\partial x_{si}^o} + \frac{(\theta_{R_i} - \theta_{R_i}^o)}{\sigma_{\theta_{R_i}}^2} \frac{\partial \theta_{R_i}^o}{\partial x_{si}^o} + \frac{(\mathfrak{d}_i - \mathfrak{d}_i^o)}{\sigma_{\mathfrak{d}_i}^2} \frac{\partial \mathfrak{d}_i^o}{\partial x_{si}^o}, i = 1, 2, \dots, N_f, \\
\frac{\partial \mathcal{L}(\boldsymbol{\vartheta})}{\partial y_{si}^o} &= \frac{(\theta_{T_i} - \theta_{T_i}^o)}{\sigma_{\theta_{T_i}}^2} \frac{\partial \theta_{T_i}^o}{\partial y_{si}^o} + \frac{(\theta_{R_i} - \theta_{R_i}^o)}{\sigma_{\theta_{R_i}}^2} \frac{\partial \theta_{R_i}^o}{\partial y_{si}^o} + \frac{(\mathfrak{d}_i - \mathfrak{d}_i^o)}{\sigma_{\mathfrak{d}_i}^2} \frac{\partial \mathfrak{d}_i^o}{\partial y_{si}^o}, i = 1, 2, \dots, N_f.
\end{aligned} \tag{202}$$

Due to the above expressions, and the assumption that all the observed parameters $\boldsymbol{\vartheta}$ are independently distributed Gaussian random variables, we can obtain the following second order moments

$$\begin{aligned}
\mathbb{E} \left(\frac{\partial \mathcal{L}(\boldsymbol{\vartheta})}{\partial x^o} \right)^2 &= \sum_{i=1}^{N_f} \left(\frac{1}{\sigma_{\theta_{T_i}}^2} \left(\frac{\partial \theta_{T_i}^o}{\partial x^o} \right)^2 + \frac{1}{\sigma_{\mathfrak{d}_i}^2} \left(\frac{\partial \mathfrak{d}_i^o}{\partial x^o} \right)^2 \right), \\
\mathbb{E} \left(\frac{\partial \mathcal{L}(\boldsymbol{\vartheta})}{\partial y^o} \right)^2 &= \sum_{i=1}^{N_f} \left(\frac{1}{\sigma_{\theta_{T_i}}^2} \left(\frac{\partial \theta_{T_i}^o}{\partial y^o} \right)^2 + \frac{1}{\sigma_{\mathfrak{d}_i}^2} \left(\frac{\partial \mathfrak{d}_i^o}{\partial y^o} \right)^2 \right), \\
\mathbb{E} \left(\frac{\partial \mathcal{L}(\boldsymbol{\vartheta})}{\partial x^o} \frac{\partial \mathcal{L}(\boldsymbol{\vartheta})}{\partial y^o} \right) &= \sum_{i=1}^{N_f} \left(\frac{1}{\sigma_{\theta_{T_i}}^2} \left(\frac{\partial \theta_{T_i}^o}{\partial x^o} \right) \left(\frac{\partial \theta_{T_i}^o}{\partial y^o} \right) + \frac{1}{\sigma_{\mathfrak{d}_i}^2} \left(\frac{\partial \mathfrak{d}_i^o}{\partial x^o} \right) \left(\frac{\partial \mathfrak{d}_i^o}{\partial y^o} \right) \right),
\end{aligned} \tag{203}$$

$$\begin{aligned}
\mathbb{E}\left(\frac{\partial \mathcal{L}(\boldsymbol{\vartheta})}{\partial x^o} \frac{\partial \mathcal{L}(\boldsymbol{\vartheta})}{\partial x_{si}^o}\right) &= \frac{1}{\sigma_{\theta_{T_i}}^2} \left(\frac{\partial \theta_{T_i}^o}{\partial x^o}\right) \left(\frac{\partial \theta_{T_i}^o}{\partial x_{si}^o}\right) \\
&\quad + \frac{1}{\sigma_{\vartheta_i}^2} \left(\frac{\partial \vartheta_i^o}{\partial x^o}\right) \left(\frac{\partial \vartheta_i^o}{\partial x_{si}^o}\right), i = 1, 2, \dots, N_f, \\
\mathbb{E}\left(\frac{\partial \mathcal{L}(\boldsymbol{\vartheta})}{\partial y^o} \frac{\partial \mathcal{L}(\boldsymbol{\vartheta})}{\partial x_{si}^o}\right) &= \frac{1}{\sigma_{\theta_{T_i}}^2} \left(\frac{\partial \theta_{T_i}^o}{\partial y^o}\right) \left(\frac{\partial \theta_{T_i}^o}{\partial x_{si}^o}\right) \\
&\quad + \frac{1}{\sigma_{\vartheta_i}^2} \left(\frac{\partial \vartheta_i^o}{\partial y^o}\right) \left(\frac{\partial \vartheta_i^o}{\partial x_{si}^o}\right), i = 1, 2, \dots, N_f, \\
\mathbb{E}\left(\frac{\partial \mathcal{L}(\boldsymbol{\vartheta})}{\partial x^o} \frac{\partial \mathcal{L}(\boldsymbol{\vartheta})}{\partial y_{si}^o}\right) &= \frac{1}{\sigma_{\theta_{T_i}}^2} \left(\frac{\partial \theta_{T_i}^o}{\partial x^o}\right) \left(\frac{\partial \theta_{T_i}^o}{\partial y_{si}^o}\right) \\
&\quad + \frac{1}{\sigma_{\vartheta_i}^2} \left(\frac{\partial \vartheta_i^o}{\partial x^o}\right) \left(\frac{\partial \vartheta_i^o}{\partial y_{si}^o}\right), i = 1, 2, \dots, N_f, \\
\mathbb{E}\left(\frac{\partial \mathcal{L}(\boldsymbol{\vartheta})}{\partial y^o} \frac{\partial \mathcal{L}(\boldsymbol{\vartheta})}{\partial y_{si}^o}\right) &= \frac{1}{\sigma_{\theta_{T_i}}^2} \left(\frac{\partial \theta_{T_i}^o}{\partial y^o}\right) \left(\frac{\partial \theta_{T_i}^o}{\partial y_{si}^o}\right) \\
&\quad + \frac{1}{\sigma_{\vartheta_i}^2} \left(\frac{\partial \vartheta_i^o}{\partial y^o}\right) \left(\frac{\partial \vartheta_i^o}{\partial y_{si}^o}\right), i = 1, 2, \dots, N_f,
\end{aligned} \tag{204}$$

and

$$\begin{aligned}
\mathbb{E}\left(\frac{\partial \mathcal{L}(\boldsymbol{\vartheta})}{\partial x_{si}^o} \frac{\partial \mathcal{L}(\boldsymbol{\vartheta})}{\partial x_{sj}^o}\right) &= \begin{cases} 0 & i \neq j, \\ \frac{1}{\sigma_{\theta_{T_i}}^2} \left(\frac{\partial \theta_{T_i}^o}{\partial x_{si}^o}\right)^2 + \frac{1}{\sigma_{\theta_{R_i}}^2} \left(\frac{\partial \theta_{R_i}^o}{\partial x_{si}^o}\right)^2 + \frac{1}{\sigma_{\vartheta_i}^2} \left(\frac{\partial \vartheta_i^o}{\partial x_{si}^o}\right)^2 & i = j, \end{cases} \\
\mathbb{E}\left(\frac{\partial \mathcal{L}(\boldsymbol{\vartheta})}{\partial y_{si}^o} \frac{\partial \mathcal{L}(\boldsymbol{\vartheta})}{\partial y_{sj}^o}\right) &= \begin{cases} 0 & i \neq j, \\ \frac{1}{\sigma_{\theta_{T_i}}^2} \left(\frac{\partial \theta_{T_i}^o}{\partial y_{si}^o}\right)^2 + \frac{1}{\sigma_{\theta_{R_i}}^2} \left(\frac{\partial \theta_{R_i}^o}{\partial y_{si}^o}\right)^2 + \frac{1}{\sigma_{\vartheta_i}^2} \left(\frac{\partial \vartheta_i^o}{\partial y_{si}^o}\right)^2 & i = j, \end{cases} \\
\mathbb{E}\left(\frac{\partial \mathcal{L}(\boldsymbol{\vartheta})}{\partial x_{si}^o} \frac{\partial \mathcal{L}(\boldsymbol{\vartheta})}{\partial y_{sj}^o}\right) &= \begin{cases} 0 & i \neq j, \\ \frac{1}{\sigma_{\theta_{T_i}}^2} \left(\frac{\partial \theta_{T_i}^o}{\partial x_{si}^o}\right) \left(\frac{\partial \theta_{T_i}^o}{\partial y_{sj}^o}\right) + \frac{1}{\sigma_{\theta_{R_i}}^2} \left(\frac{\partial \theta_{R_i}^o}{\partial x_{si}^o}\right) \left(\frac{\partial \theta_{T_i}^o}{\partial y_{sj}^o}\right) \\ + \frac{1}{\sigma_{\vartheta_i}^2} \left(\frac{\partial \vartheta_i^o}{\partial x_{si}^o}\right) \left(\frac{\partial \vartheta_i^o}{\partial y_{sj}^o}\right) & i = j. \end{cases}
\end{aligned} \tag{205}$$

The FIM $\mathbf{I}(\boldsymbol{\rho})$ can be derived by substituting (199), (202) and (203)–(205) into (198) and (197).

5.5 Numerical examples

This section presents analytical and simulation results to illustrate the performance of the proposed LS algorithm and the ML algorithm. Fig. 24 shows the distribution of the MS and FSs along with the NLOS propagation paths. The positions of the MS, FSs and scatterers are given in Table 5. We assume the parameters associated

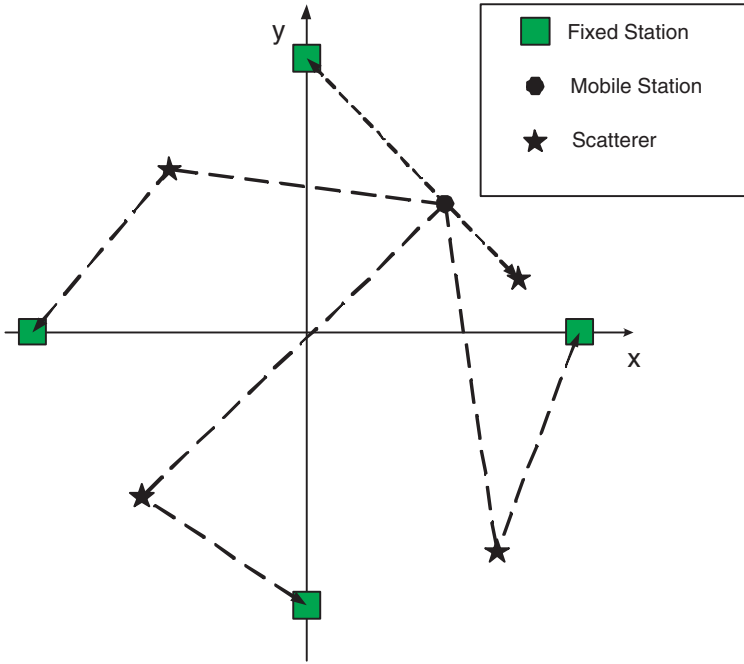


Fig. 24. The NLOS propagation path from the MS to the FSs.

to different propagation paths have the same normalized estimation error variance, i.e., $\sigma_{\theta_{T_i}}^2 = \sigma_{\theta_T}^2, \sigma_{\theta_{R_i}}^2 = \sigma_{\theta_R}^2, \sigma_{d_i}^2 = \sigma_d^2$, for all $i = 1, 2, 3, 4$.

5.5.1 Least squares algorithm

We examine the effects of the standard deviations of estimated parameters, i.e., $\sigma_{\theta_T}, \sigma_{\theta_R}$ and σ_d , on the RMSE of the LS based positioning algorithm. We also examine the impact of the number of FSs, i.e., the number of employed NLOS paths, on its performance. As shown in Fig. 24, there is an NLOS propagation path between the MS and each of the four FSs. When we only employ two out of the four NLOS paths, there are $\binom{4}{2}$ combinations of two NLOS paths. Different combinations may lead to different RMSE performances, e.g., the performance yielded by the FS pair (1, 2) could be different from that of the FS pair (3, 4). To obtain the average performance of employing the same number of NLOS paths, all RMSE performances under different FS combinations are averaged out.

1) *Effects of standard deviations of parameter estimates:* Figs. 25(a) and 25(b) show the analytical RMSE of the LS based positioning algorithm by virtue of all

four NLOS paths versus $(\sigma_{\theta_T}, \sigma_{\theta_R})$ when the standard deviation of the distance σ_d is 5m and 10m, respectively. It is found that the RMSE performance is more sensitive to σ_{θ_T} than σ_{θ_R} in the environment shown in Fig. 24. Fig. 26 shows the analytical RMSE performance with respect to $(\sigma_d, \sigma_{\theta_R})$ when $\sigma_{\theta_T} = \sigma_{\theta_R}$.

2) *Effects of the number of FSs:* Figs. 27–29 show the analytical and simulated RMSE performance of the LS positioning algorithm when 2, 3 or 4 NLOS paths are exploited. Fig. 27 shows how the number of FSs and σ_{θ_T} affect the RMSE performance given σ_{θ_R} and σ_d . Figs. 28 and 29 show the effect of the number of FSs employed along with σ_{θ_R} and σ_d , respectively. They show that the more NLOS paths used, the higher accuracy the LS algorithm achieves. All the simulations are performed with 1000 independent runs. The fact that the simulation results are close to the corresponding analytical ones confirms that the approximate analytical RMSE expressions derived in Section 5.3.2 are accurate when the standard deviations of the parameter estimates are reasonably small.

5.5.2 The maximum likelihood algorithm and the Cramér-Rao lower bound

Figs. 30–32 show the RMSE performance of the ML based algorithm and the corresponding CRLBs against σ_{θ_T} , σ_{θ_R} and σ_d , respectively. To highlight the performance gain of the ML algorithm over the LS algorithm, we also plot the performance of the LS algorithm in the figures. The MATLAB function *fmincon.m* is employed to find the ML solution of (194). All the simulations of the ML algorithm employ the solution yielded by the LS algorithm as the initial searching point. It shows that the ML algorithm does improve the performance significantly at the cost of increased computational complexity. It is also found that the LS algorithm is capable of providing a good starting point for the ML algorithm. It is interesting to note that the performance of the ML algorithm is close to the CRLB.

To demonstrate the performance of the proposed positioning algorithm utilizing the practical parameter estimates, e.g., the AOA and the AOD estimates developed in Section 3.3, Fig. 33 shows the CRLB and the RMSE of the ML based position estimates. In Fig. 33, the average standard deviations of the AOA and the AOD estimate errors shown in Fig. 11 are used to calculate the CRLB of position estimates at different SNR points. Accordingly, the simulation of the ML algorithm is based on the parameter estimates with the average standard deviations at different SNR points. The results demonstrate that the RMSE of the ML algorithm aided by the practical AOA and AOD estimates is rather close to the CRLB, provided that the FS has information about the orientation of the MS so that the absolute AOA and AOD can be obtained.

Table 5. Coordinates[Meter] of the MS, FSs and scatterers

MS	FS / Scatterer	FS / Scatterer	FS / Scatterer	FS / Scatterer
(25,25)	(0,50)/(40,10)	(-50,0)/(-25,30)	(0,-50)/(-30,-30)	(50,0)/(35,-40)

5.6 Conclusions

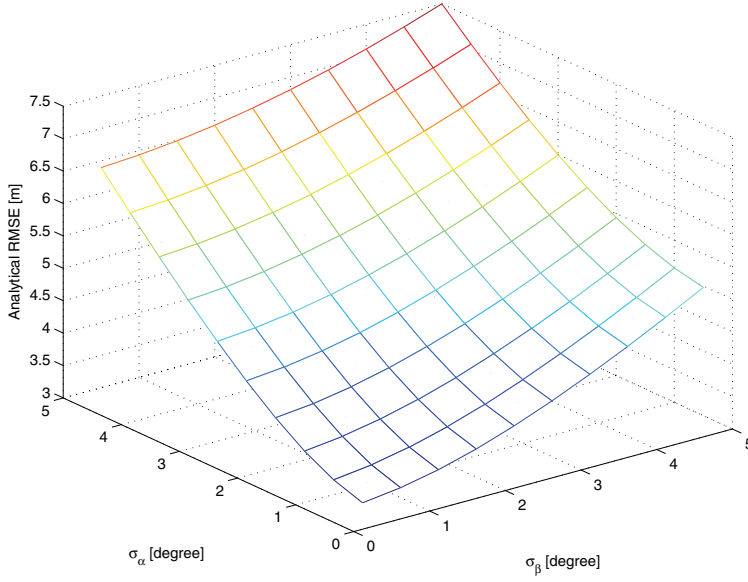
In this chapter, we considered the position estimation of the MS in the NLOS scenario. With knowledge about the AOA, the AOD and the distance associated with each NLOS path, a geometric approach to calculating the intersection of two line segments which were derived as possible regions for the MS was presented. To achieve the minimal equation-error norm, the LS algorithm was proposed for exploiting multiple NLOS paths to improve the positioning accuracy. The ML algorithm was further developed to improve the performance of the LS algorithm, and it was able to estimate the positions of both the MS and scatterers. The CRLB was also derived to benchmark the performance of the positioning algorithms. It was shown both analytically and through computer simulations that the proposed algorithms are able to estimate the MS position only by employing the NLOS paths, and the ML algorithm can achieve the optimal RMSE performance, i.e., the CRLB.

Several interesting related open research problems still remain. All the error analysis of the position estimates assume that the parameter estimates are independent random variables. In practice, these parameters are estimated from the same measurements, e.g., the received training signals. As a result, the parameter estimates can be correlated in practice. The error analysis of the position estimates considering the parameter estimate correlation needs to be further studied. Furthermore, when a two-dimensional position model is considered, vertical differences in the positions of the FSs, the MS and scatterers would introduce additional errors in the calculations. Another interesting problem is how to choose the NLOS paths in the presence of multiple NLOS paths. It is noted in Section 5.5, different combinations of NLOS paths lead to different performances. It was observed in Section 3.3 that the estimation error variances of the AOA and the AOD estimates depend on both the SNR of the received signal and the true values of the AOAs and the AODs. Consequently, the selection of the NLOS paths can be based on the accuracy of the parameter estimates associated with each path. This would enable more detailed performance-complexity trade-off in real positioning systems.

As mentioned at the beginning of the chapter, the task of obtaining knowledge about the NLOS path, i.e., the AOA and the AOD at the FS is rather challenging in practice, in particular, it is extremely hard to obtain angle information in impulse radio based systems. Assuming ULAs with omni-directional antenna elements, there is ambiguity about the side of the antenna array involved. Therefore, directional antenna array could be a better option in the proposed positioning system to resolve the ambiguity caused by the omni-directional antenna element. Also, the proposed algorithms require that the FS and the MS refer to the same

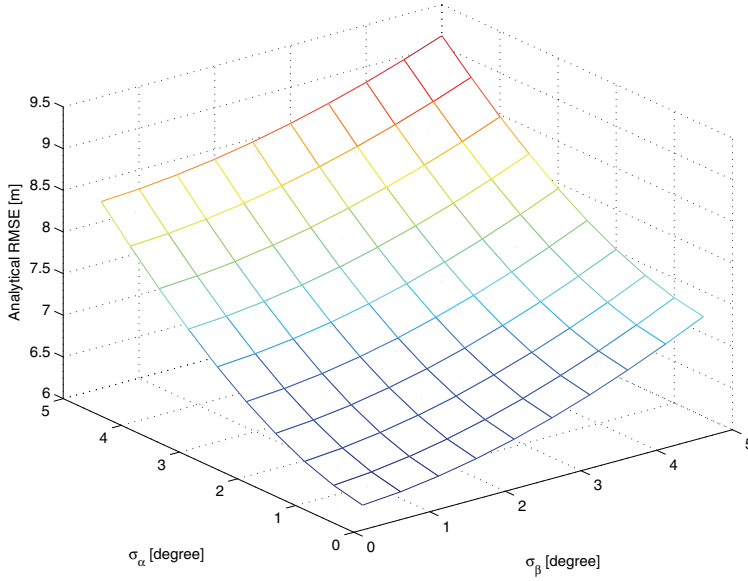
orientation. Obtaining the orientation of the MS at the FS side is obviously a challenging task, and definitely requires further study. Even though this problem were to be solved, the complexity of the whole positioning system would be relatively high, e.g, the AOD estimation needs an antenna array to be equipped at the MS side. Moreover, the problem of antenna calibration at both link ends must be taken into account. This makes it even more difficult to acquire accurate AOA and AOD values due to the frequency offsets caused by the different oscillators in the MSs and the FSs. All of this restrict the practicability of the proposed positioning algorithms. Their commercial use therefore requires further research and development.

Analytical RMSE versus standard deviations of AOA β estimate and AOD α estimate, $\sigma_d = 5$, 4 FSs



(a) $\sigma_d = 5\text{m}$

Analytical RMSE versus standard deviations of AOA β estimate and AOD α estimate, $\sigma_d = 10$, 4 FSs



(b) $\sigma_d = 10\text{m}$

Fig. 25. Analytical RMSE versus standard deviations of the AOA θ_R estimate and AOD θ_T estimate, 4 FSs.

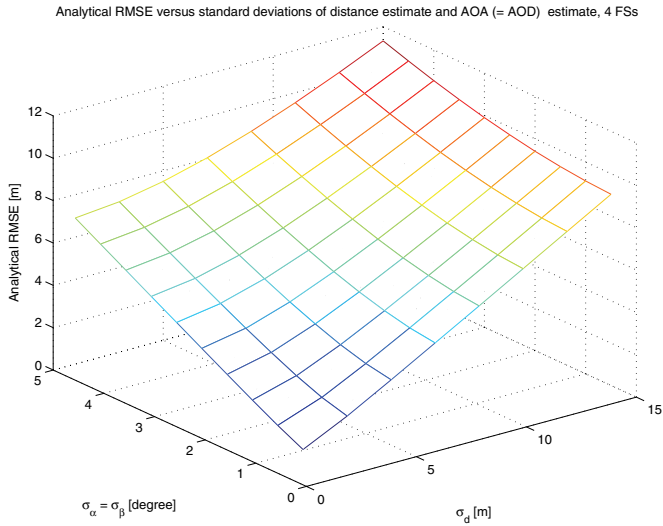


Fig. 26. Analytical RMSE versus standard deviations of the distance estimate and AOA (= AOD) estimate, 4 FSs.

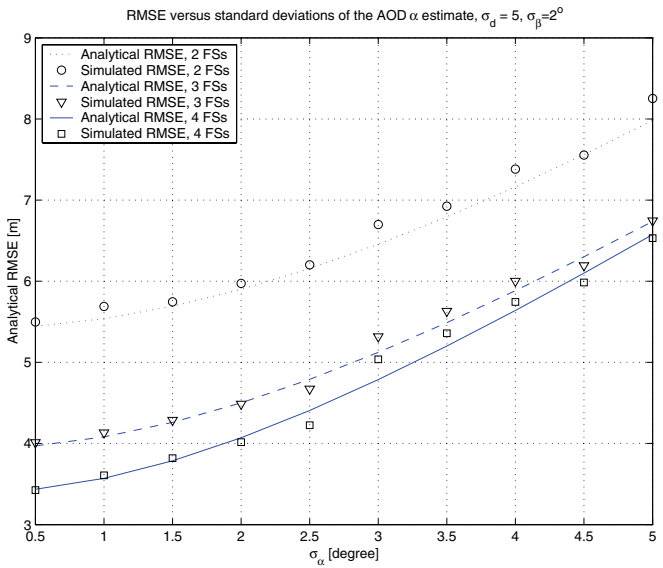


Fig. 27. RMSE versus standard deviations of the AOD θ_T estimate, $\sigma_d = 5\text{m}$, $\sigma_{\theta_R} = 2^\circ$.

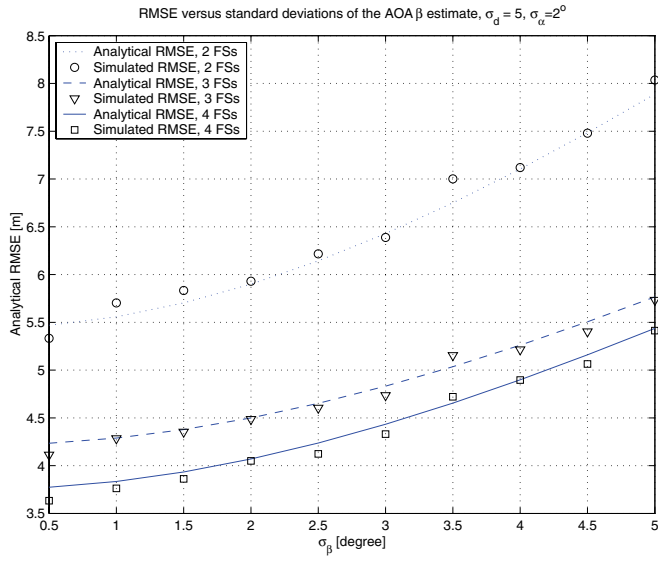


Fig. 28. RMSE versus standard deviations of the AOA θ_R estimate, $\sigma_d = 5\text{m}$, $\sigma_{\theta_T} = 2^\circ$.

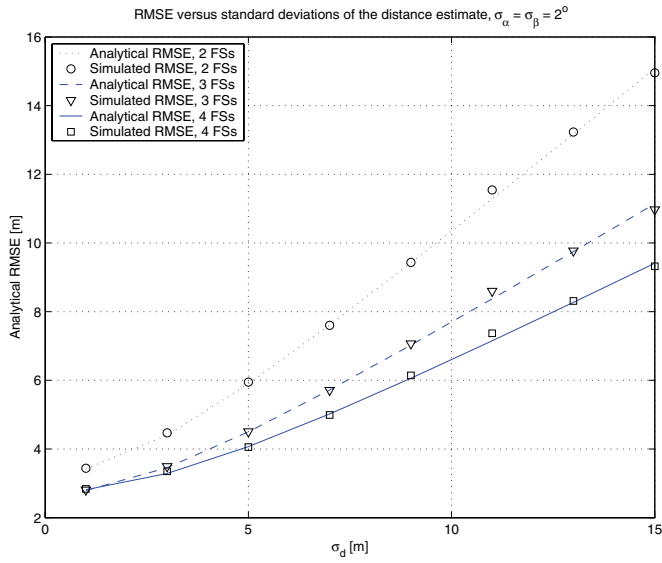


Fig. 29. RMSE versus standard deviations of the distance estimate, $\sigma_{\theta_T} = 2^\circ$.

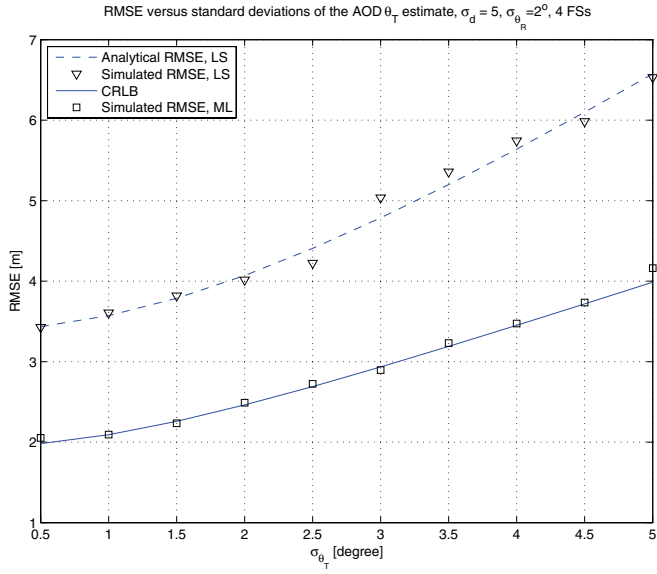


Fig. 30. RMSE of the ML algorithm and the CRLB, $\sigma_d = 5\text{m}$, $\sigma_{\theta_R} = 2^\circ$.

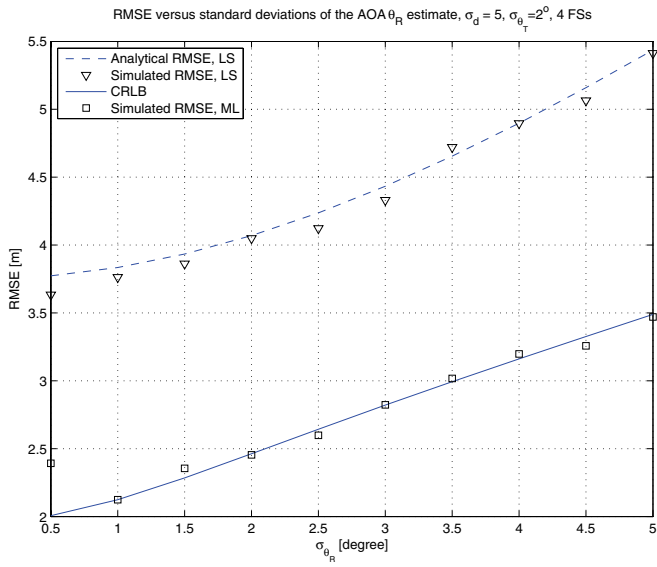


Fig. 31. RMSE of the ML algorithm and the CRLB, $\sigma_d = 5\text{m}$, $\sigma_{\theta_T} = 2^\circ$.

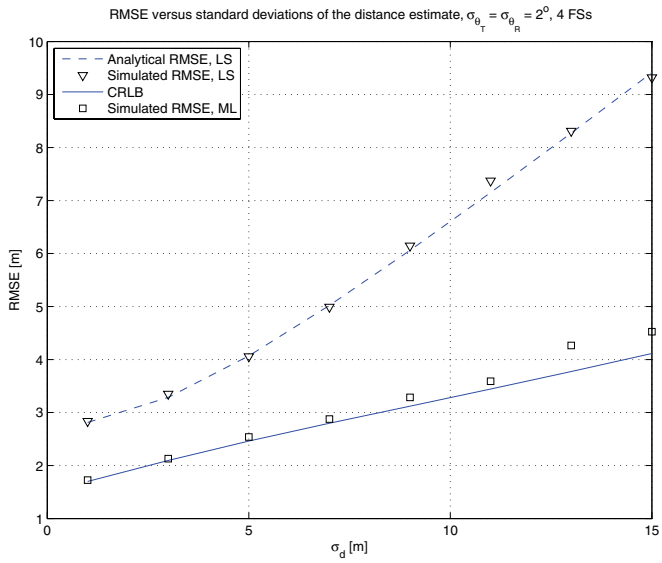


Fig. 32. RMSE of the ML algorithm and the CRLB, $\sigma_{\theta_T} = \sigma_{\theta_R} = 2^\circ$.

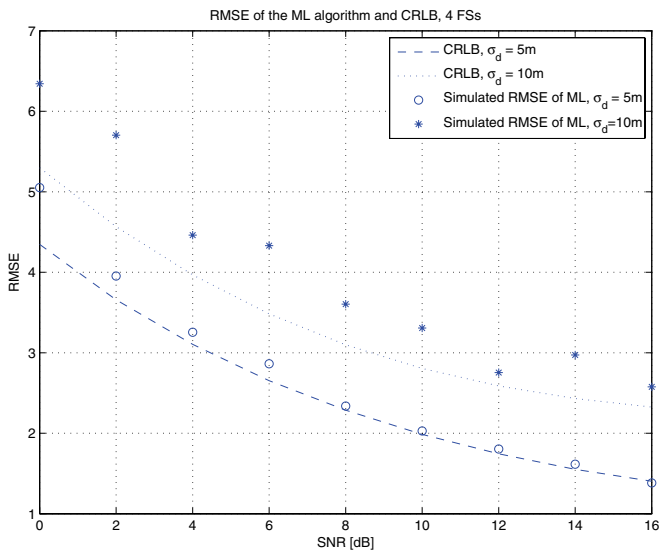


Fig. 33. RMSE of the ML algorithm and the CRLB, 4 FSs.

6 Conclusions

6.1 Summary and discussion

Wideband MIMO parameter estimation and its applications to MIMO-OFDM channel estimation and mobile positioning were considered. The literature on MIMO parameter and channel estimation and on mobile positioning was reviewed in Chapter 2. The problems to be studied in more detail were identified, based on the review.

Two practical MIMO channel models, i.e., the correlated-transmit-receive channel and the correlated-receive independent-transmit channel, and the associated space-time parameter estimation algorithms were considered in Chapter 3. Thanks to the specified structure of the proposed training signals for multiple transmit antennas, the IQML algorithm [161, 162] was applied to estimate the time delay and spatial signature for the correlated-receive independent-transmit MIMO channels. For the correlated-transmit-receive MIMO channels, the spatial signature matrix corresponding to a time delay can be further decomposed in such a way that the AOA and AOD can be estimated simultaneously by the 2-D unitary ESPRIT algorithm. Therefore, the combination of the IQML algorithm and the 2-D unitary ESPRIT algorithm provides a novel solution to jointly estimate the time delay, the AOA and the AOD for the correlated-transmit-receive MIMO channels. The identifiability and the CRLBs regarding the time delay, AOA and AOD estimation were also analyzed. It was demonstrated with the numerical examples that the proposed algorithms can obtain good performance at a reasonable cost.

Considering the correlated-receive independent-transmit MIMO channels developed in Chapter 3, a channel coefficient estimation for the MIMO-OFDM system was the topic of Chapter 4. The whole idea in Chapter 4 can be straightforwardly extended to the case of correlated-transmit-receive MIMO channels. Based on the parameters of the correlated-receive independent-transmit MIMO channels, the channel statistics in terms of the correlation matrix were developed. By virtue of the derived channel statistics, a JST filtering based MMSE channel estimator was proposed, which takes full advantage of the channel property. The MSE of the proposed channel estimator was analyzed, and its performance was also demonstrated in the computer simulations. It was shown that the proposed JST MMSE

channel estimator outperforms the more conventional temporal MMSE channel estimator [134] in terms of the estimate MSE when the signals in the receive antenna array elements were allowed to be significantly correlated. To study the effect of the channel estimator on the system performance, the closed-form BEP of the STBC-OFDM system with correlation at the receiver was developed by taking the channel estimation errors and channel statistics, i.e., correlation at the receiver, into account.

In addition to the application in channel coefficient estimation shown in Chapter 4, the channel parameters also play an important role in the field of mobile positioning which has been discussed in Chapter 2. An important open problem in mobile positioning area, i.e., the mobile positioning in the NLOS scenarios, was considered in Chapter 5. With knowledge of the time delay, the AOA and the AOD associated with each NLOS propagation path, a novel geometric approach was proposed to calculate the MS's position by only exploiting two NLOS paths. In contrast to the conventional NLOS mitigation techniques in the open literature, the proposed algorithm can benefit from the NLOS paths rather than cancelling them. In addition to finding of the geometric approach, the LS and the ML algorithms were developed to utilize multiple NLOS paths to improve the positioning accuracy. An interesting result also demonstrated that the ML algorithm is able to estimate the scatterers' positions as well as those of the MSs. The CRLB related to the positioning estimation in the NLOS scenarios was derived. It was shown both analytically and through computer simulations that the proposed algorithms are able to estimate the MS position only by employing the NLOS paths, and the ML algorithm is an efficient estimator, which can achieve the optimal RMSE performance, i.e., the CRLB.

The results of the thesis show that accurate channel parameter estimates are not only useful for characterizing the underlying propagation channel, but also able to improve the channel coefficient estimation needed by the post-processing, such as the equalization and the demodulation etc. Moreover, they are applicable to the MS positioning in the NLOS scenarios. It is suggested therefore that the practical future receiver, at least at a base station or a fixed station, should have channel parameter estimation capability so that it can be used to enhance channel estimation and also enable positioning in NLOS conditions. In fact, the potential usages of the channel parameters are not limited to the scope addressed in the thesis. For instance, advanced radio resource management [51, 52, 53] and link adaptation schemes taking advantage of the mobility and the position information of the MSs, such as bandwidth reservation and interference avoidance etc., also require the receiver to be able to achieve the necessary parameter estimates.

6.2 Future research directions

There are several interesting open problems in MIMO channel estimation and mobile positioning requiring further study. Some of them are briefly pointed out here.

An interesting approach to the time delay, the AOA and the AOD estimation algorithm has been presented in Chapter 3. As reviewed in Chapter 2, some similar approaches have been proposed in [118, 119]. A comparative study of these algorithms in more detail would be worth performing. For instance, the performance-complexity trade-off between different algorithms should be analyzed. As a consequence, the optimal selection between different approaches can be made for a certain scenario and application. Furthermore, all these algorithms are relatively complex; fast and simplified algorithms related to them would be an interesting topic for the practical usages.

Chapter 4 considered the MMSE channel estimation for the MIMO-OFDM system. The proposed JST structure improves the channel estimation accuracy at the cost of increased computational complexity. It would be interesting to study in more detail the realized gains with different MIMO transmission schemes, like spatial multiplexing and various space-time coding methods. The performance with forward error control coding should also be analyzed in more detail. This would enable a more detailed performance-complexity trade-off in real communication systems. Furthermore, an interesting further research topic would be the application of spatial signature estimates in radio link adaptation or radio resource management.

A mobile positioning algorithm which is able to utilize the NLOS paths was studied in Chapter 5. As mentioned previously, the algorithm requires the assumption that the FS has knowledge about the orientation of the MS. Practical implementation of such an assumption remains open and would be an interesting topic to study in the future. The alternative to solving this problem is to utilize the relative AOD information, for example, the angle-difference of departure (ADOD) instead of the absolute AOD. The idea is to exploit two NLOS paths to obtain the possible region of the MS. Six unknown coordinates in the 2-D coordinate system are involved in the scenarios of two NLOS paths, i.e., the coordinates of the MS and two unknown scatterers. Five relationships can be formed from measurements of two NLOS paths, i.e., two AOAs, two time delays and one ADOD. As a result, the possible region calculated from two NLOS paths would be a 1-D geometric object. A similar idea to that of Chapter 5 can be applied in such a case. The geometric approach, LS and ML algorithms can be employed to find the MS's position when three or more NLOS paths exist. Some preliminary research has been carried out. However, more details of such an idea need to be further studied, in particular, the error performance seems to be a crucial issue.

References

1. Gesbert D, Shafi M, Shiu D, Smith PJ & Naguib A (2003) From theory to practice: An overview of MIMO space-time coded wireless systems. *IEEE Journal on Selected Areas in Communications* 21(3): 281–302.
2. Paulraj A & Papadias C (1997) Space-time processing for wireless communications. *IEEE Signal Processing Magazine* 14(6): 49–83.
3. Paulraj A, Nabar R & Gore D (2003) *Introduction to Space-Time Wireless Communications*. Cambridge University Press, Cambridge, UK.
4. Bolcskei H, Gesbert D, Papadias C & der veen AJV (2006) *Space-Time Wireless Systems: From Array Processing to MIMO Communications*. Cambridge University Press, Cambridge, UK.
5. Kaiser T, Bourdoux A, Boche H, Fonollosa J, Andersen J & Utschick W (2005) *Smart Antenna: State of the Art*. Hindawi Publishing Corporation, New York, USA.
6. Telatar IE (1995) Capacity of multi-antenna Gaussian channels. Tech. rep. Bell Laboratories Internal Tech.Memo, pp. 1–28.
7. Foschini GJ & Gans MJ On limits of wireless communications in a fading environment when using multiple antennas. *Wireless Personal Communications Kluwer Academic Publishers* 6: 311–335.
8. Winters J (1987) On the capacity of radio communication systems with diversity in a Rayleigh fading environment. *IEEE Journal on Selected Areas in Communications* 5(5): 871–878.
9. Paulraj AJ & Kailath T (Patent 5345599, 2004) Increasing capacity in wireless broadcast systems using distributed transmission/directional reception. .
10. Foschini G (1996) Layered space-time architecture for wireless communication in a fading environment when using multi-element antennas. *Bell Systems Technical Journal* 1(2): 41–59.
11. Foschini GJ, Golden GD, Valenzuela RA & Wolniansky PW (1999) Simplified processing for high spectral efficiency wireless communication employing multi-element arrays. *IEEE Journal on Selected Areas in Communications* 17(11): 1841–1852.
12. Golden GD, Foschini CJ, Valenzuela RA & Wolniansky PW (1999) Detection algorithm and initial laboratory results using V-BLASTspace-time communication architecture. *IEE Electronics Letters* 35(1): 14–16.
13. Raleigh GG & Cioffi JM (1998) Spatio-temporal coding for wireless communication. *IEEE Transactions on Communications* 46(3): 357–366.
14. Farrokhi FR, Foschini GJ, Lozano A & Valenzuela RA (2001) Link-optimal space-time processing with multiple transmit and receive antennas. *IEEE Communications Letters* 5(3): 85–87.

15. Viswanath P, Tse DNC & Anantharam V (2001) Asymptotically optimal water-filling in vector multiple-access channels. *IEEE Transactions on Information Theory* 47(1): 241–267.
16. Chuah CN, Tse D, Kahn JM & Valenzuela-02 RA (2002) Capacity scaling in MIMO wireless systems under correlated fading. *IEEE Transactions on Information Theory* 48(3): 637–650.
17. Chuah CN, Kahn JM & Tse D (1998) Capacity of multi-antenna array systems in indoor wireless environment. in: *Proc. IEEE Global Telecommunication Conference (GLOBECOM) 4*: 1894–1899.
18. Rapajic PB & Popescu D (2000) Information capacity of a random signature multiple-input multiple-output channel. *IEEE Transactions on Communications* 48(8): 1245–1248.
19. Smith PJ & Shafi M (2002) On gaussian approximation to the capacity of wireless MIMO systems. in: *Proc. IEEE International Conference on Communications (ICC)* 406–410.
20. Wittneben A (1993) A new bandwidth efficient transmit antenna modulation diversity scheme for linear digital modulation. in: *Proc. IEEE International Conference on Communications (ICC) 3*: 1630–1634.
21. Seshadri N & Winters JH (1993) Two signaling schemes for improving the error performance of frequency-division-duplex (FDD) transmission systems using transmitter antenna diversity. in: *Proc. IEEE Vehicular Technology Conference (VTC) Secaucus, USA* 508–511.
22. Tarokh V, Seshadri N & Calderbank AR (1998) Space-time codes for high data rate wireless communication: Performance criterion and code construction. *IEEE Transactions on Information Theory* 44(2): 744–765.
23. Alamouti S (1998) A simple transmit diversity technique for wireless communications. *IEEE Journal on Selected Areas in Communications* 16(8): 1451–1458.
24. Tarokh V, Jafarkhani H & Calderbank AR (1999) Space-time block codes from orthogonal designs. *IEEE Transactions on Information Theory* 45(5): 1456–1467.
25. Zheng L & Tse DNC (2003) Diversity and multiplexing: A fundamental tradeoff in multiple-antenna channels. *IEEE Transactions on Information Theory* 49(5): 1073–1096.
26. Jr. RWH & Love DJ (2005) Multi-mode antenna selection for spatial multiplexing with linear receivers. *IEEE Transactions on Signal Processing* 53(8): 3042–3056.
27. Hassibi B & Hochwald BM (2002) High-rate codes that are linear in space and time. *IEEE Transactions on Information Theory* 48(7): 1804–1824.
28. Heath RW & Paulraj A (2002) Linear dispersion codes for MIMO systems based on frame theory. *IEEE Transactions on Signal Processing* 50(10): 2429–2441.
29. Peled A & Ruiz A (1980) Frequency domain data transmission using reduced computational complexity algorithms. in: *Proc. IEEE International Conference on Acoustics, Speech, and Signal Processing (ICASSP) 80*: 964–967.
30. Cimini LJ (1985) Analysis and simulation of a digital mobile channel using orthogonal frequency division multiplexing. *IEEE Transactions on Communications* 33(7): 665–675.
31. LeFloch B, Alard M & Berrou C (1995) Coded orthogonal frequency division multiplex. *ieepr* 83: 982–996.
32. van Nee R & Prasad R (2000) *OFDM for Wireless Multimedia Communications*. Artech House, London, UK.
33. Boelskei H, Gesbert D & Paulraj AJ (2002) On the capacity of OFDM-based spatial multiplexing systems. *IEEE Transactions on Communications* 50(2): 225–234.
34. Boelskei H & Paulraj AJ (2001) Space-frequency codes for broadband fading channels. in: *Proc. IEEE International Symposium on Information Theory (ISIT) Washington DC, USA* 219.
35. Boelskei H, Gesbert D & Paulraj AJ (2002) On the capacity of OFDM-based spatial multiplexing systems. *IEEE Transactions on Communications* 50(2): 225–234.

36. Sampath H, Talwar S, Tellado J, Erceg V & Paulraj A (2002) A fourth-generation MIMO-OFDM broadband wireless system: Design, performance, and field trial results. *IEEE Communications Magazine* 40(9): 143–149.
37. Tujkovic D, Juntti MJ & Latva-aho M (2002) Space-time turbo coded modulation: Design and applications. *EURASIP Journal on Applied Signal Processing* 2002(3): 236–248.
38. Boelcskei H, Borgmann M & Paulraj AJ (2003) Impact of the propagation environment on the performance of space-frequency coded MIMO-OFDM. *IEEE Journal on Selected Areas in Communications* 31(3): 427–439.
39. Liu Z, Xin Y & Giannakis GB (2002) Space-time-frequency coded OFDM over frequency selective fading channels. *IEEE Transactions on Signal Processing* 50(10): 2465–2476.
40. Su W, Safar Z, Olfat M & Liu K (2003) Obtaining full-diversity space-frequency codes from space-time codes via mapping. *IEEE Transactions on Signal Processing* 51(11): 2905–2916.
41. Shao L, Roy S & Sandhu S (2003) Rate-one space frequency block codes with maximum diversity gain for MIMO-OFDM. 2: 809–813.
42. Bolcskei H, Borgmann M & Paulraj A (2003) Impact of the propagation environment on the performance of space-frequency coded MIMO-OFDM. *IEEE Journal on Selected Areas in Communications* 21(3): 427–439.
43. IEEE Standard 802.16eD11 IEEE standard for local and metropolitan area networks part 16: Air interface for fixed and mobile broadband wireless access systems: Amendment for physical and medium access control layers for combined fixed and mobile operation in licenced bands.
44. Sayed AH & Yousef NR (2003) Wireless location. in: *Wiley Encyclopedia of Telecommunications* J. Proakis Ed. New York: Wiley.
45. Location-based services: Finding their place in the market. .
46. Zhao Y (2002) Standardization of mobile phone positioning for 3G systems. *IEEE Communications Magazine* 40(7): 108–116.
47. Hightower J & Borriello G (2001) Location systems for ubiquitous computing. *IEEE Computer Magazine* 34(8): 57–66.
48. Mauve M, Widmer J & Hartenstein H (2001) A survey on position-based routing in mobile ad-hoc networks. *IEEE Network Magazine* 15(6): 30–39.
49. Jurgen R (1991) Smart cars and highways go global. *IEEE Spectrum* 28(5): 26–36.
50. Collier W & Weiland R (1994) Smart cars, smart highways. *IEEE Spectrum* 31(4): 27–33.
51. Akyildiz IF & Wang W (2004) The predictive user mobility profile framework for wireless multimedia networks. *IEEEACM Transactions on Networking* 12(6): 1021–1035.
52. Pandey V, Ghosal D & Mukherjee B (2004) Exploiting user profiles to support differentiated services in next-generation wireless networks. *IEEE Network Magazine* 18(5): 40–48.
53. Ye J, Hou J & Papavassiliou S (2002) A comprehensive resource management framework for next generation wireless networks. 1(4): 249–264.
54. Chiu M & Bassiouni MA (2000) Predictive schemes for handoff prioritization in cellular networks based on mobile positioning. *IEEE Journal on Selected Areas in Communications* 18(3): 510–522.
55. Giordano A, Chan M & Habal H (1995) A novel location-based service and architecture. in: *Proc. IEEE International Symposium on Personal, Indoor, and Mobile Radio Communications (PIMRC)* 2: 853–857.
56. Hashemi H (1991) Pulse ranging radiolocation technique and its application to channel assignment in digital cellular radio. in: *Proc. IEEE Vehicular Technology Conference (VTC)* 1: 675–680.
57. Narasimhan R & Cox D (1998) A handoff algorithm for wireless systems using pattern recognition. in: *Proc. IEEE International Symposium on Personal, Indoor, and Mobile Radio Communications (PIMRC)* 1: 335–339.

58. Revision of the commissions rules to ensure compatibility with enhanced 911 emergency calling systems, RM-8143. .
59. Yu K, Saarnisaari H, Montillet JP, Rabbachin A, Oppermann I & Abreu G (2006) UWB localization. in: Shen S, ed, Ultra-Wideband Wireless Communications and Networks Wiley.
60. Oppermann I, Stoica L, Rabbachin A, Shelby Z & Haapola J (2004) UWB wireless sensor networks: UWEN—a practical example. *IEEE Communications Magazine* 42(12): 527–532.
61. Torrieri DJ (1984) Statistical theory of passive location systems. *IEEE Transactions on Aerospace and Electronic Systems* AES-20(2): 183–198.
62. Sun G, Chen J, Guo W & Liu KJR (2005) Signal processing techniques in network-aided positioning. *IEEE Signal Processing Magazine* 22(4): 12–23.
63. Jr. JC & Stüber GL (1998) Subscriber location in CDMA cellular networks. *IEEE Transactions on Vehicular Technology* 47(5): 406–416.
64. Gustafsson F & Gunnarsson F (2005) Mobile positioning using wireless networks. *IEEE Signal Processing Magazine* 22(4): 41–53.
65. Gezici S, Tian Z, Giannakis GB, Kobayashi H, Molisch AF, Poor HV & Sahinoglu Z (2005) Localization via ultra-wideband radios. *IEEE Signal Processing Magazine* 22(4): 70–84.
66. Smith JO & Abel JS (1987) Closed-form least-squares source location estimation from range-difference measurements. *IEEE Transactions on Acoustics Speech and Signal Processing* ASSP-35(12): 1661–1669.
67. Sakagami S, Aoyama S, Kuboi K, Shirota S & Akeyama A (1992) Vehicle position estimates by multibeam antennas in multipath environments. *IEEE Transactions on Vehicular Technology* 41(1): 63–68.
68. Cong L & Zhuang W (2002) Hybrid TDOA/AOA mobile user location for wideband CDMA cellular systems. *IEEE Transactions on Wireless Communications* 1(3): 439–447.
69. Jr. JC & Stüber GL (1998) Overview of radiolocation in CDMA cellular systems. *IEEE Communications Magazine* 36(4): 38–45.
70. Molisch AF, Steinbauer M, Toeltsch M, Bonek E & Thom RS (2002) Capacity of MIMO systems based on measured wireless channels. *IEEE Journal on Selected Areas in Communications* 20(3): 561–569.
71. Miao H & Juntti M (2005) Space-time channel estimation and performance analysis for wireless MIMO-OFDM systems with spatial correlation. *IEEE Transactions on Vehicular Technology* 54(6): 2003–2016.
72. Miao H & Juntti M (2003) Data aided MMSE channel estimation for MIMO-OFDM system. in: Proc. International Workshop on Multi-Carrier Spread-Spectrum (MC-SS) Munich, Germany 211–218.
73. Miao H & Juntti M (2004) Spatial signature and channel estimation for wireless MIMO-OFDM system with spatial correlation. in: Proc. IEEE Workshop on Signal Processing Advances in Wireless Communications (SPAWC) Lisboa, Portugal 522–526.
74. Miao H & Juntti M (2004) Space-time MMSE channel estimation for MIMO-OFDM system with spatial correlation. in: Proc. IEEE Vehicular Technology Conference (VTC) 3: 1806–1810.
75. Miao H, Yu K & Juntti M (2006) Positioning for NLOS propagation: Algorithms derivation and cramer-rao bounds. in: Proc. IEEE International Conference on Acoustics, Speech, and Signal Processing (ICASSP) Toulouse, France 5 pages, CD-ROM.
76. Miao H, Juntti M & Yu K (2006) 2-d unitary ESPRIT based joint AOA and AOD estimation for MIMO system. in: Proc. IEEE International Symposium on Personal, Indoor, and Mobile Radio Communications (PIMRC) Helsinki, Finland 5 pages, CD-ROM.

77. Miao H, Yu K & Juntti M (2007) Positioning for NLOS propagation: Algorithms derivation and cramer-rao bounds. *IEEE Transactions on Vehicular Technology* xx(x): to appear.
78. Miao H & Juntti M (2005) Bit error probability of STBC-OFDM system over correlated MIMO channels with channel estimation errors. in: *Proc. IEEE International Symposium on Personal, Indoor, and Mobile Radio Communications (PIMRC)* Berlin, Germany 5 pages, CD-ROM.
79. Yu K, Bengtsson M & Ottersten B (2005) MIMO channel models. in: Kaiser T & etal, eds, *Smart Antenna: State of the Art* Hindawi Publishing Corporation 271-292.
80. Parsons JD *The Mobile Radio Propagation Channel*. Pentech Press, London.
81. Pahlavan K & Levesque A (1995) *Wireless Information Networks*. John Wiley and Sons, New York, USA.
82. German G, Spencer Q, Swindlehurst L & Walenzuela R (2001) Wireless indoor channel modelling: Statistical agreement of ray tracing simulations and channel sounding measurement. in: *Proc. IEEE International Conference on Acoustics, Speech, and Signal Processing (ICASSP)* 4: 2502-2504.
83. Martin CC, Winters JH & Sollenberg NR (2000) Multiple-input multiple-output MIMOradio channel measurements. in: *Proc. IEEE Vehicular Technology Conference (VTC)* Tokyo, Japan 774-779.
84. McNamara DP, Beach MA, Karlsson P & Fletcher PN (2000) Initial characterisation of multiple-input multiple-output MIMO channels for space-time communication. in: *Proc. IEEE Vehicular Technology Conference (VTC)* 3: 1193-1197.
85. Shiu D, Foshini GJ, Gans MJ & Kahn JM (2000) Fading correlation and its effect on the capacity of multi-element antenna systems. *IEEE Transactions on Communications* 48(3): 25-29.
86. Kay SM (1993) *Fundamentals of Statistical Signal Processing: Estimation Theory*. Prentice-Hall, Englewood Cliffs, NJ, USA.
87. Kermoal JP, Schumacher L, Pedersen K, Mogensen PE & Frederiksen F (2002) A stochastic MIMO radio channel model with experimental validation. *IEEE Journal on Selected Areas in Communications* 20(6): 1211-1226.
88. Yu K, Bengtsson M, Ottersten B, McNamara D, Karlsson P & Beach M (2004) Modeling of wideband MIMO radio channels based on NLOS indoor measurements. *IEEE Transactions on Vehicular Technology* 53(3): 655-665.
89. Molisch AF (2004) A generic model for MIMO wireless propagation channels is macro- and microcells. *IEEE Transactions on Signal Processing* 52(1): 61-71.
90. Abdi A & Kaveh M (2002) A space-time correlation model for multielement antenna systems in mobile fading channels. *IEEE Journal on Selected Areas in Communications* 20(3): 550-560.
91. Byers G & Takawira F (2004) Spatially and temporally correlated MIMO channels: Models and capacity analysis. *IEEE Transactions on Vehicular Technology* 53(3): 634-643.
92. Yu K, Bengtsson M, Ottersten B, McNamara D, Karlsson P & Beach M (2002) A wideband statistical model for NLOS indoor MIMO channels. in: *Proc. IEEE Vehicular Technology Conference (VTC)* Birmingham, Ala, USA 370-374.
93. Sayeed AM (2002) Deconstructing multiantenna fading channels. *IEEE Transactions on Signal Processing* 50(10): 2563-2579.
94. Weichselberger W, Herdin M, Ozcelik H & Bonek E (2006) A stochastic MIMO channel model with joint correlation of both link ends. *IEEE Transactions on Wireless Communications* 5(1): 90-100.
95. Gesbert D, Boelskei H, Gore D & Paulraj A (2002) Outdoor MIMO wireless channels: Models and performance prediction. *IEEE Transactions on Communications* 50(12): 1926-1934.
96. Spencer QH, Jeffs BD, Jensen MA & Swindlehurst AL (2000) Modeling the statistical time and angle of arrival characteristics of an indoor multipath channel. *IEEE Journal on Selected Areas in Communications* 18(3): 347-360.

97. ANSI/IEEE Standard 802.11,1999 Edition (R2003) Information technology - telecommunications and information exchange between systems - local and metropolitan area networks - specific requirements part 11: Wireless LAN medium access control (MAC) and physical layer (PHY) specifications.
98. 3rd Generation Partnership Project (3GPP); Technical Specification Group Radio Access Network Spatial channel model for Multiple Input Multiple Output (MIMO) simulations (3G TR 25.996 version 6.1.0 (release 6)). Tech. rep. 3rd Generation Partnership Project (3GPP).
99. Viberg M (2005) Direction-of-arrival estimation. in: Kaiser T & etal, eds, *Smart Antenna: State of the Art* Hindawi Publishing Corporation 321–341.
100. Krim H & Viberg M (1996) Two decades of array signal processing research – the parametric approach. *IEEE Signal Processing Magazine* 13(3): 67–94.
101. Trees HLV (2002) *Optimal Array Processing*. John Wiley, Canada.
102. Capon J (1969) High-resolution frequency-wavenumber spectrum analysis. *Proceedings of the IEEE* 57(8): 1408–1418.
103. Schmidt RO A signal subspace approach to multiple emitter location and spectral estimation. Ph.D. thesis Stanford University Stanford, CA, USA.
104. Schmidt RO (1986) Multiple emitter location and signal parameter estimation. *IEEE Transactions on Antennas and Propagation* 34(3): 276–280.
105. Xu W & Kaveh M (1996) Comparative study of the biases of MUSIC-like estimators. *Signal Processing Elsevier Publishing Company* 50(1-2): 39–55.
106. Rao BD & Hari KVS (1989) Performance analysis of root-MUSIC. *IEEE Transactions on Acoustics Speech and Signal Processing* 37(12): 1939–1949.
107. Roy R & Kailath T (1989) ESPRIT — estimation of signal parameters via rotational invariant techniques. *IEEE Transactions on Acoustics Speech and Signal Processing* 37(7): 984–995.
108. Haardt M & Nossek J (1995) Unitary ESPRIT: How to obtain increased estimation accuracy with a reduced computational burden. *IEEE Transactions on Signal Processing* 43(5): 1232–1242.
109. Stoica P & Sharman K (1990) Maximum likelihood methods for direction-of-arrival estimation. *IEEE Transactions on Acoustics Speech and Signal Processing* 38: 1132–1143.
110. Viberg M, Ottersten B & Kailath T (1991) Detection and estimation in sensor arrays using weighted subspace fitting. *IEEE Transactions on Acoustics Speech and Signal Processing* 39: 2436–2449.
111. Fessler J & Hero A (1994) Space-alternating generalized expectation-maximization algorithm. *IEEE Transactions on Signal Processing* 42(10): 2664–2677.
112. Li J, Zheng D & Stoica P (1997) Angle and waveform estimation via RELAXE. *IEEE Transactions on Aerospace and Electronic Systems* 33(3): 1077–1087.
113. Ziskind I & Wax M (1988) Maximum likelihood localization of multiple sources by alternating projection. *IEEE Transactions on Acoustics Speech and Signal Processing* Vol. 36(10): 1553–1560.
114. Pelin P (2001) A fast minimization technique for subspace fitting with arbitrary array manifolds. *IEEE Transactions on Signal Processing* 49(12): 2935–2939.
115. Peressini AL, Sullivan FE & Jr. JJU (1988) *The Mathematics of Nonlinear Programming*. Springer, New York, USA.
116. Fleury BH, Tschudin M, Heddergott R, Dahlhaus D & Pedersen KI (1999) Channel parameter estimation in mobile radio environments using the SAGE algorithm. *IEEE Journal on Selected Areas in Communications Wireless Communication Series* 17(3): 434–450.
117. van der Veen A, Vanderveen M & Paulraj A (1998) Joint angle and delay estimation using shift-invariance techniques. *IEEE Transactions on Signal Processing* 46(2): 405–418.
118. Steinbauer M, Molisch AF & Bonek E (2001) The double-directional radio channel. *IEEE Transactions on Antennas and Propagation* 43(4): 51–63.

119. Pesavento M, Mecklenbrauker CF & Bohme JF (2002) Double-directional radio channel estimation using MD-RARE. in: Proc. Annual Asilomar Conference on Signals, Systems and Computers 1: 594–598.
120. Meyr H, Moeneclaey M & Fechtel SA (1997) Digital Communication Receivers: Synchronization, Channel Estimation and Signal Processing. John Wiley and Sons, New York, USA.
121. Leus G & van der Veen AJ (2005) Channel estimation. in: Kaiser T & etal, eds, Smart Antenna: State of the Art Hindawi Publishing Corporation 293–319.
122. Dong M & Tong L (2002) Optimal design and placement of pilot symbols for channel estimation. IEEE Transactions on Signal Processing 50(12): 3055–3069.
123. Rousseaux O, Leus G, Stoica P & Moonen M (2005) Gaussian maximum likelihood channel estimation with short training sequences. IEEE Transactions on Wireless Communications 4(6): 2945–2955.
124. Talwar S, Viberg M & Paulraj A (1996) Blind separation of synchronous co-channel digital signals using an antenna array: I. algorithms. IEEE Transactions on Signal Processing 44(5): 1184–1197.
125. Moulines E, Duhamel P, Cardoso JF & Mayrargue S (1995) Subspace methods for the blind identification of multichannel FIR filters. IEEE Transactions on Signal Processing 43(2): 516–525.
126. Abed-Meraim K, Loubaton P & Moulines E (1997) A subspace algorithm for certain blind identification problems. IEEE Transactions on Information Theory 43(2): 499–511.
127. Tong L & Zhao Q (1999) Joint order detection and blind channel estimation by least squares smoothing. IEEE Transactions on Signal Processing 47(9): 499–509.
128. Ding Z (2000) Linear predictive algorithms for blind multichannel identification. in: Giannakis GB, Hua Y, Stoica P & Tong L, eds, Signal Processing Advances in Wireless and Mobile Communication: Trends in Channel Estimation and Equalization 1: 179–210.
129. de Carvalho E & Slock DTM (2000) Carmer–Rao bounds for semi-blind, blind and training sequence based channel estimation. in: Giannakis GB, Hua Y, Stoica P & Tong L, eds, Signal Processing Advances in Wireless and Mobile Communication: Trends in Channel Estimation and Equalization 1: 211–254.
130. van de Beek JJ, Edfors O & Sandell M (1995) On channel estimation in OFDM systems. in: Proc. IEEE Vehicular Technology Conference (VTC) 2: 815–819.
131. Edfors O, Sandell M, van de Beek JJ, Wilson S & Börjesson P (1998) OFDM channel estimation by singular value decomposition. IEEE Transactions on Communications 46(7): 931–939.
132. Li Y, Cimini LJ & Sollenberger NR (1998) Robust channel estimation for OFDM systems with rapid dispersive fading channels. IEEE Transactions on Communications 46(7): 902–915.
133. Li Y & Sollenberger NR (1999) Adaptive antenna arrays for OFDM systems with cochannel interference. IEEE Transactions on Communications 47(2): 217–229.
134. Li Y, Seshadri N & Ariyavisitakul S (1999) Channel estimation for OFDM systems with transmitter diversity in mobile wireless channels. IEEE Journal on Selected Areas in Communications 17(3): 461–471.
135. Li Y, Winters JH & Sollenberger NR (2002) MIMO-OFDM for wireless communications: Signal detection with enhanced channel estimation. IEEE Transactions on Communications 50(9): 1471–1477.
136. Li Y (2002) Simplified channel estimation for OFDM systems with multiple transmit antennas. IEEE Transactions on Communications 1(1): 67–75.
137. Xie Y & Georghiades CN (2003) Two EM-type channel estimation algorithms for OFDM with transmitter diversity. IEEE Transactions on Communications 51(1): 106–115.
138. Lu B, Wang X & Li YG (2002) Iterative receivers for space-time block coded OFDM systems in dispersive fading channels. IEEE Wireless Communications 1(2): 213–225.

139. Stoica P & Besson O (2003) Training signal design for frequency offset and frequency-selective channel estimation. *IEEE Transactions on Signal Processing* 51(11): 1910–1917.
140. Fragouli C, Dhahir N & Turin W (2003) Training-based channel estimation for multiple-antenna broadband transmissions. *IEEE Transactions on Wireless Communications* 2(2): 384–391.
141. Kotecha JH & Sayeed AM (2004) Transmit signal design for optimal estimation of correlated MIMO channels. *IEEE Transactions on Signal Processing* 52(2): 546–557.
142. Barhumi I, Leus G & Moonen M (2003) Optimal training design for MIMO-OFDM systems in mobile wireless channels. *IEEE Transactions on Signal Processing* 51(6): 1615–1624.
143. Larsson EG & Li J (2001) Preamble design for multiple-antenna OFDM-based WLANs with null subcarriers. *IEEE Signal Processing Letters* 8(11): 285–288.
144. Yousef NR, Sayed AH & Jalloul LMA (2003) Robust wireless location over fading channels. *IEEE Transactions on Vehicular Technology* 52(1): 117–126.
145. Hata M (1980) Empirical formula for propagation loss in land mobile radio services. *IEEE Transactions on Vehicular Technology* 29(3): 317–325.
146. Gustafsson F, Gunnarsson F, Bergman N, Forsslund U, Jansson J, Karlsson R & Nordlund PJ (2002) Particle filters for positioning, navigation and tracking. *IEEE Transactions on Signal Processing* 50(2): 425–437.
147. Dennis Jr. JE & Schnabel RB (1987) *Numerical Methods for Unconstrained Optimization and Nonlinear Equations*. Society for Industrial and Applied Mathematics.
148. Urruela A & Riba J (2004) Novel closed-form ML position estimator for hyperbolic location. in: *Proc. IEEE International Conference on Acoustics, Speech, and Signal Processing (ICASSP)* 2: 149–152.
149. Gustafsson F & Gunnarsson F (2003) Positioning using time-difference of arrival measurements. in: *Proc. IEEE International Conference on Acoustics, Speech, and Signal Processing (ICASSP)* 6: 553–556.
150. Cong L & Zhuang W (2005) Nonline-of-sight error mitigation in mobile location. *IEEE Transactions on Wireless Communications* 4(2): 560–573.
151. Xiong L (1998) A selective model to suppress NLOS signals in angle-of-arrival AOA location estimation. in: *Proc. IEEE International Symposium on Personal, Indoor, and Mobile Radio Communications (PIMRC)* 1: 461–465.
152. Chen P (1999) A nonline-of-sight error mitigation algorithm in location estimation. in: *Proc. IEEE Wireless Communications and Networking Conference (WCNC)* 1: 316–320.
153. Cong L & Zhuang W (2001) Non-line-of-sight error mitigation in TDOA mobile location. in: *Proc. IEEE Global Telecommunication Conference (GLOBECOM)* 1: 680–684.
154. Al-Jazzar S, Caffery J & You H (2002) A scattering model based approach to NLOS mitigation in TOA location systems. in: *Proc. IEEE Vehicular Technology Conference (VTC)* 2: 861–865.
155. Wylie MP & Wang S (2001) Robust range estimation in the presence of the nonline-of-sight error. in: *Proc. IEEE Vehicular Technology Conference (VTC)* 1: 101–105.
156. Venkatraman S, Caffery J & You HR (2002) Location using LOS range estimation in NLOS environments. in: *Proc. IEEE Vehicular Technology Conference (VTC)* 2: 856–860.
157. Wong KD & Cox DC (2000) A pattern recognition system for handoff algorithms. *IEEE Journal on Selected Areas in Communications* 18(7): 1301–1311.
158. Wang S & Green M (2000) Mobile location method for nonline-of-sight situation. in: *Proc. IEEE Vehicular Technology Conference (VTC)* Boston, USA 608–612.
159. Thomas NJ, Cruickshank DGM & Laurenson DI (2001) Calculation of mobile location using scatterer information. *IEE Electronics Letters* 37(19): 1193–1194.
160. Wan Q, Yang W & Peng Y (2004) Closed-form solution to mobile location using linear constraint on scatterer. *IEE Electronics Letters* 40(14): 883–884.

161. Swindlehurst AL (1998) Time delay and spatial signature estimation using known asynchronous signals. *IEEE Transactions on Signal Processing* 46(2): 449–462.
162. Bresler Y & Macovski A (1986) Exact maximum likelihood parameter estimation of superimposed exponential signals in noise. *IEEE Transactions on Acoustics Speech and Signal Processing ASSP-34*(5): 1081–1089.
163. Zoltowski M, Haardt M & Mathews C (1996) Closed-form 2-D angle estimation with rectangular arrays in element space or beamspace via unitary ESPRIT. *IEEE Transactions on Signal Processing* 44(2): 316–328.
164. ETSI BRAN - HIPERLAN type 2; physical layer. Tech. rep. European Telecommunications Standards Institute (ETSI).
165. Stoica P & Nehorai A (1989) MUSIC, Maximum Likelihood, and Cramer-Rao Bound. *IEEE Transactions on Acoustics Speech and Signal Processing* 37(5): 720–741.
166. Shan T.J, Wax M & Kailath T (1985) On spatial smoothing for direction-of-arrival estimation of coherent signals. *IEEE Transactions on Acoustics Speech and Signal Processing* 33: 806–811.
167. Uysal M & Georgiades CN (1999) Effect of spatial fading correlation on performance of space-time codes. *IEE Electronics Letters* 37: 181–183.
168. Siwamogsatham S & Fitz MP (2002) Robust space-time codes for correlated fading channels. *IEEE Transactions on Signal Processing* 50(10).
169. Shamain P & Milstein LB (2002) Performance of space-time spreading with correlated fading and channel estimation. in: *Proc. IEEE International Conference on Communications (ICC)* 3: 1630–1634.
170. Safar Z & Liu KJR (2003) Performance analysis of space-time codes over correlated Rayleigh fading channels. in: *Proc. IEEE International Conference on Communications (ICC)* 5: 3185–3189.
171. Femenias G (2004) BER performance of linear STBC from orthogonal designs over MIMO correlated Nakagami-m fading channels. *IEEE Transactions on Vehicular Technology* 53(2): 307–317.
172. Hochwald BM, Marzetta TL & Papadias CB (2001) A transmitter diversity scheme for wideband CDMA systems based on space-time spreading. *IEEE Journal on Selected Areas in Communications* 19(1): 48–60.
173. ETSI Broadband radio access networks (BRAN); HIPERLAN type 2; physical (PHY) layer. Tech. rep. European Telecommunications Standards Institute (ETSI).
174. Asztely D (1996) On antenna arrays in mobile communication systems: Fast fading and GSM base station receiver algorithms. Tech. rep. IR-S3-SB-9611, Royal Inst. Technol., Stockholm, Sweden.
175. Golub GH & Loan CFV (1996) *Matrix Computations*, 3rd edn. The Johns Hopkins University Press, Baltimore.
176. Kailath T & Chun J (1994) Generalized displacement structure for block-Toeplitz, Toeplitz-block, and Toeplitz-derived matrices. 15(1): 114–128.
177. Verdú S (1998) *Multiuser Detection*. Cambridge University Press, Cambridge, UK.

Appendix 1 Proof of (156)

The autocorrelation of the k th subcarrier of the CFR $\tilde{h}_{i,j}[k]$ can be described as

$$\begin{aligned} \mathbb{E} \left(\tilde{h}_{i,j}[k] \tilde{h}_{i,j}[k]^* \right) &= \mathbb{E} \left(\mathbf{F}_K^L(k, :) \mathbf{h}_{i,j} \mathbf{h}_{i,j}^H \mathbf{F}_K^L(k, :)^H \right) \quad (\text{A1.206}) \\ &= \sum_{l=0}^{L-1} \sigma_l^2 = 1. \end{aligned}$$

The covariance between the k th subcarriers of the CFR $\tilde{h}_{i,p}[k]$ and $\tilde{h}_{i,q}[k]$ can be expressed as

$$\begin{aligned} \mathbb{E} \left(\tilde{h}_{i,p}[k] \tilde{h}_{i,q}[k]^* \right) &= \mathbb{E} \left(\mathbf{F}_K^L(k, :) \mathbf{h}_{i,p} \mathbf{h}_{i,q}^H \mathbf{F}_K^L(k, :)^H \right) \quad (\text{A1.207}) \\ &= \sum_{l=0}^{L-1} (\boldsymbol{\Sigma}_{\mathbf{h}_i[l]})_{p,q}. \end{aligned}$$

Due to the independence of transmit antennas, the covariance between the k th subcarriers of the CFR $\tilde{h}_{i,p}[k]$ and $\tilde{h}_{j,q}[k]$ can be expressed as

$$\mathbb{E} \left(\tilde{h}_{i,p}[k] \tilde{h}_{j,q}[k]^* \right) = \mathbb{E} \left(\mathbf{F}_K^L(k, :) \mathbf{h}_{i,p} \mathbf{h}_{j,q}^H \mathbf{F}_K^L(k, :)^H \right) = 0. \quad (\text{A1.208})$$

In that the estimation error $\xi_{i,j}[k]$ is independent of the ideal CFR $\tilde{h}_{i,j}[k]$, the covariance matrix $\boldsymbol{\Sigma}_{\mathbf{h}[k]}^{\Delta}$ in (156) follows from the (A1.206), (A1.207) and (A1.208).

Appendix 2 Derivation of the LS Algorithm in the General Scenario

As mentioned in Section 5.3.1, there are two cases where (159) does not hold, due to the nonexistence of the slope k . This happens if and only if

$$\sin\theta_{\text{T}} + \sin\theta_{\text{R}} = 0. \quad (\text{A2.209})$$

Because the range of θ_{T} and θ_{R} is $[0, 2\pi)$, the solutions of (A2.209) are described as

$$|\theta_{\text{T}} - \theta_{\text{R}}| = \pi, \quad (\text{A2.210})$$

$$\theta_{\text{T}} + \theta_{\text{R}} = 2\pi. \quad (\text{A2.211})$$

It is interesting to note that (A2.210) corresponds to the LOS case as illustrated in Fig. A-34. Therefore, (A2.210) implies a new method of identifying the LOS path. It is obvious that the possible region of the MS in the LOS case is a point with the coordinates as follows

$$\begin{aligned} \hat{x}_{\text{LOS}} &= x_{\text{f}} + \mathfrak{d}\sin\theta_{\text{R}}, \\ \hat{y}_{\text{LOS}} &= y_{\text{f}} + \mathfrak{d}\cos\theta_{\text{R}}. \end{aligned} \quad (\text{A2.212})$$

(A2.211) corresponds to the possible region which is a line parallel to the y -axis; this is illustrated in Fig. A-35, when the possible region becomes

$$\hat{x}_{\perp} = x_{\text{f}} - \mathfrak{d}\sin\theta_{\text{T}}. \quad (\text{A2.213})$$

We assume that N_{f} paths consist of N_1 LOS paths, N_2 NLOS paths from which the derived possible regions are lines with slopes of finite values and N_3 NLOS paths from which the derived possible region are lines parallel to the y -axis, $N_{\text{f}} \geq N_i \geq 0, i = 1, 2, 3$. The LS based position estimate $(\hat{x}_{\text{LS}}, \hat{y}_{\text{LS}})$ of the MS considering this general case can be derived as

$$\begin{aligned} (\hat{x}_{\text{LS}}, \hat{y}_{\text{LS}}) &= \underset{(x,y)}{\operatorname{argmin}} \sum_{i=1}^{N_1} ((x - \hat{x}_{\text{LOS}i})^2 + (y - \hat{y}_{\text{LOS}i})^2) \\ &\quad + \sum_{i=1}^{N_2} (k_i x + b_i - y)^2 + \sum_{i=1}^{N_3} (x - \hat{x}_{\perp i})^2, \end{aligned} \quad (\text{A2.214})$$

where $(\hat{x}_{\text{LOS}i}, \hat{y}_{\text{LOS}i}), i = 1, 2, \dots, N_1$ and $\hat{x}_{\perp i}, i = 1, 2, \dots, N_3$ can be calculated from (A2.212) and (A2.213), respectively. We define the objective function as

$$\mathcal{O}(x, y) = \sum_{i=1}^{N_1} ((x - \hat{x}_{\text{LOS}i})^2 + (y - \hat{y}_{\text{LOS}i})^2) + \sum_{i=1}^{N_2} (k_i x + b_i - y)^2 + \sum_{i=1}^{N_3} (x - \hat{x}_{\perp i})^2, \quad (\text{A2.215})$$

the LS solution $(\hat{x}_{\text{LS}}, \hat{y}_{\text{LS}})$ of (A2.214) can be obtained by

$$\hat{x}_{\text{LS}} = \frac{\partial \mathcal{O}(x, y)}{\partial x} = 0, \quad (\text{A2.216})$$

$$\hat{y}_{\text{LS}} = \frac{\partial \mathcal{O}(x, y)}{\partial y} = 0. \quad (\text{A2.217})$$

It can be derived that

$$\frac{\partial \mathcal{O}(x, y)}{\partial x} = x \sum_{i=1}^{N_2} k_i + y(N_1 - N_2) + \sum_{i=1}^{N_2} b_i - \sum_{i=1}^{N_1} \hat{y}_{\text{LOS}i}, \quad (\text{A2.218})$$

$$\frac{\partial \mathcal{O}(x, y)}{\partial y} = x(N_1 + N_3 + \sum_{i=1}^{N_2} k_i^2) - y \sum_{i=1}^{N_2} k_i + \sum_{i=1}^{N_2} k_i b_i - \sum_{i=1}^{N_1} \hat{x}_{\text{LOS}i} - \sum_{i=1}^{N_3} \hat{x}_{\perp i}. \quad (\text{A2.219})$$

We denote

$$G = \begin{vmatrix} \sum_{i=1}^{N_2} k_i & N_1 - N_2 \\ N_1 + N_3 + \sum_{i=1}^{N_2} k_i^2 & -\sum_{i=1}^{N_2} k_i \end{vmatrix}, \quad (\text{A2.220})$$

$$E = \begin{vmatrix} \sum_{i=1}^{N_1} \hat{y}_{\text{LOS}i} - \sum_{i=1}^{N_2} b_i & N_1 - N_2 \\ \sum_{i=1}^{N_1} \hat{x}_{\text{LOS}i} + \sum_{i=1}^{N_3} \hat{x}_{\perp i} - \sum_{i=1}^{N_2} k_i b_i & -\sum_{i=1}^{N_2} k_i \end{vmatrix}, \quad (\text{A2.221})$$

$$F = \begin{vmatrix} \sum_{i=1}^{N_2} k_i & \sum_{i=1}^{N_1} \hat{y}_{\text{LOS}i} - \sum_{i=1}^{N_2} b_i \\ N_1 + N_3 + \sum_{i=1}^{N_2} k_i^2 & \sum_{i=1}^{N_1} \hat{x}_{\text{LOS}i} + \sum_{i=1}^{N_3} \hat{x}_{\perp i} - \sum_{i=1}^{N_2} k_i b_i \end{vmatrix}. \quad (\text{A2.222})$$

According to Cramer's Rule, the LS solution $(\hat{x}_{\text{LS}}, \hat{y}_{\text{LS}})$ can be calculated from

$$\begin{aligned} \hat{x}_{\text{LS}} &= \frac{E}{G}, \\ \hat{y}_{\text{LS}} &= \frac{F}{G}. \end{aligned} \quad (\text{A2.223})$$

(A2.223) shows that the LS based position estimate of the MS takes all the propagation paths including LOS paths and NLOS paths into account.

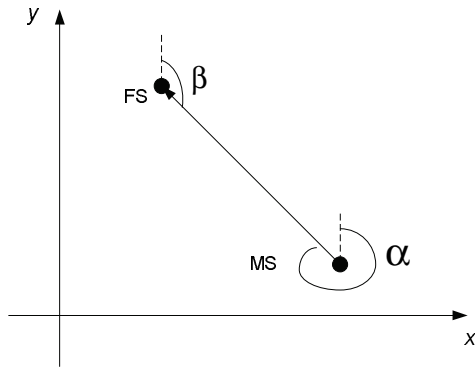
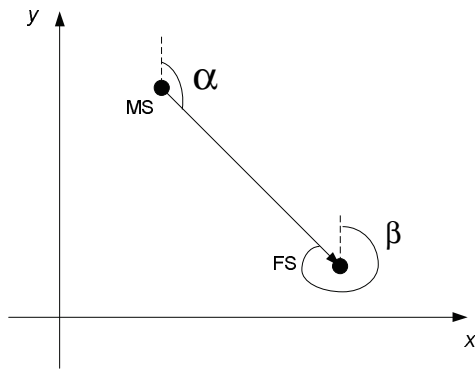
(a) $\theta_T - \theta_R = \pi$ (b) $\theta_R - \theta_T = \pi$

Fig. A-34. The LOS case.

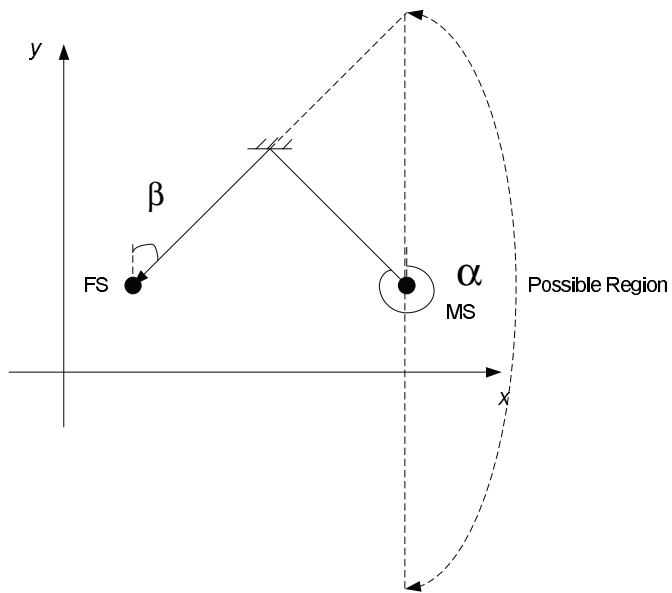


Fig. A-35. Possible region: a line parallel to the y -axis.

254. Heino, Jyrki (2006) Harjavallan Suurteollisuuspuisto teollisen ekosysteemin esimerkkinä kehitettäessä hiiliteräksen ympäristömyönteisyyttä
255. Gebus, Sébastien (2006) Knowledge-based decision support systems for production optimization and quality improvement in the electronics industry
256. Alarousu, Erkki (2006) Low coherence interferometry and optical coherence tomography in paper measurements
257. Leppäkoski, Kimmo (2006) Utilisation of non-linear modelling methods in flue-gas oxygen-content control
258. Juutilainen, Ilmari (2006) Modelling of conditional variance and uncertainty using industrial process data
259. Sorvoja, Hannu (2006) Noninvasive blood pressure pulse detection and blood pressure determination
260. Pirinen, Pekka (2006) Effective capacity evaluation of advanced wideband CDMA and UWB radio networks
261. Huuhtanen, Mika (2006) Zeolite catalysts in the reduction of NO_x in lean automotive exhaust gas conditions. Behaviour of catalysts in activity, DRIFT and TPD studies
262. Rautiainen, Mika (2006) Content-based search and browsing in semantic multimedia retrieval
263. Häkkinen, Jonna (2006) Usability with context-aware mobile applications. Case studies and design guidelines
264. Jari Heikkilä ja Jouni Koiso-Kanttila (toim.) (2007) Patinoituu ja paranee—Moderni puukaupunki -tutkijakoulu 2003–2006
265. Suikki, Raija (2007) Changing business environment—effects of continuous innovations and disruptive technologies
266. Harri Haapasalo & Päivi Iskanius (Eds.) (2007) The 1st Nordic Innovation Research Conference—Finnkampen
267. Pikka, Vesa (2007) A Business Enabling Network. A case study of a high-tech network; its concepts, elements and actors
268. Noora Ervasti, Anna-Elina Pietikäinen, Eva Wiklund, Maarit Hiltunen ja Esa Vesmanen (2007) Yksilölliset toiveet asuntotuotannossa
269. Fabritius, Tapio (2007) Optical method for liquid sorption measurements in paper

Book orders:
OULU UNIVERSITY PRESS
P.O. Box 8200, FI-90014
University of Oulu, Finland

Distributed by
OULU UNIVERSITY LIBRARY
P.O. Box 7500, FI-90014
University of Oulu, Finland

S E R I E S E D I T O R S

A
SCIENTIAE RERUM NATURALIUM
Professor Mikko Siponen

B
HUMANIORA
Professor Harri Mantila

C
TECHNICA
Professor Juha Kostamovaara

D
MEDICA
Professor Olli Vuolteenaho

E
SCIENTIAE RERUM SOCIALIUM
Senior Assistant Timo Latomaa

E
SCRIPTA ACADEMICA
Communications Officer Elna Stjerna

G
OECONOMICA
Senior Lecturer Seppo Eriksson

EDITOR IN CHIEF
Professor Olli Vuolteenaho

EDITORIAL SECRETARY
Publications Editor Kirsti Nurkkala

ISBN 978-951-42-8410-6 (Paperback)

ISBN 978-951-42-8411-3 (PDF)

ISSN 0355-3213 (Print)

ISSN 1796-2226 (Online)

